Ph.D.Thesis

The primary relaxation in glass-forming liquids

An empirical investigation of dielectric data

Albena Ivanova Nielsen

Supervisor: Jeppe C. Dyre

*Danish National Research Foundation Centre "Glass and Time",
IMFUFA, Department of Science, Systems and Models,
Roskilde University, Denmark*

February 27, 2009

Abstract in english

The focus in this study is on the high frequency decay of the relaxation in terms of the "minimum slope" of the α dielectric loss vs. the loss peak frequency in log-log plot. The analysis is kept model-independent in an attempt to perform an unbiased conclusion.The dielectric data collection consist of measurement for 53 liquids at ambient pressure and high pressure (isothermal conditions) data sets for 10 liquids. The data are provided from different groups and supplemented by new measurements. The main conclusion is: the most frequently observed minimum slope is close to $-1/2$, corresponding to approximate $\sqrt{t}$ dependence of the dielectric relaxation function at short times. The study encloses an investigation of possible correlations between minimum slopes and: 1) Temperature quantified via the loss-peak frequency; 2) How well an inverse power law fits data above the loss peak; 3) Degree of time-temperature superposition for data at ambient pressure; 4) Loss-peak half width, and stretching exponent; 5) The phenomenological classification in A and B type liquids; 6) Deviation from non-Arrhenius behavior; 7) Loss strength; 8) Temperature pressure co-invariance of the spectral shape along isochrones (pressure-temperature superposition the same relaxation time) . The result is: minimum slopes close to $-1/2$ correlates to the listed in the first three and the very last points, which indicates a special status of liquids with minimum slopes close to $-1/2$. Concerning the last points only fairly insignificant correlations are found with the exception of large-loss liquids, which have minimum slopes that are numerically significantly larger than $1/2$ and loss peak widths that are significantly smaller than those of most other liquids. We conclude that – excluding large-loss liquids – approximate $\sqrt{t}$ relaxation appears to be a generic property of the α relaxation of organic glass formers. There are some secondary conclusions: The large loss liquids are typically A-type. Besides this purely descriptive classification in two types do not give some new insight, since there is no correlation to other than the shape parameters of the relaxation process. The high pressure study shows that the model independent minimum slope as a shape parameter captures phenomena that are reported for the different liquids like the pressure-temperature superposition. There is indication that it captures hidden beta processes

Abstract in danish

I denne afhandling er hovedfokus retted mod den højfrekvente henfald i relaksationsprocesset beskrevet ved hældningskoefficienten i saddelpunktet af grafen af den dielektriske α tab vs. frekvensen ved maksimale i dobbelt logaritmisk plot. Samlingen af dielektriske data består af målinger af 53 væsker ved atmosfærisk tryk og af 10 væsker ved højt tryk. Nogle data var målt specielt for denne studie, mens den største del var leveret af forskellige forsknings grupper. Hoved resultatet fra den model frie analyse er, at det oftest observerede koefficient er ca. $-1/2$ som er ensbetydende med $\sqrt{t}$ tidsafhængighed af relaksationsfunktionen ved korte tider. Studiet indbefatter undersøgelse af mulig korrelation mellem minimum hældningen og 1) dens temperaturafhængihed; 2)hvor godt tangenten med denne koefficient fitter i punktet; 3) hvor godt tid temperatur superposistionen er opfyldt 4)Det halve brede i halve højde af relaksationen og "stretching exponent"; 5) Væskeopdelingen i type A og B 6)hvor non-Arrhenius er dynamikken 7)amplituden af af tabet 8) Temperatur tryk invarinsen af den spektrale form langs ischroner. Konklusionen af dette er følgende ad 1)-3) viser sig at værdien $-1/2$ er specielt. ellers i forhold til de restende punkter ar kun en lille eller ingen sammenhæng dog med undtagelse af dise der har et tab med relative høj amplitude, som også viser sig til være relativt smalle. På baggrund af dette kan man konkludere at $\sqrt{t}$-relaksationen er et generel egenskab ved viskøse væsker. De sekundære resultater er: De mest dissipative væsker er A-type, men ellers får man ikke nogen indsigt i væskers dynamik ved at opdele dem i de to typer. Hojtryksmålingerne viser at den modeluafhænginge hældningskoefficient indfanger fænomener, der er observeret ved ændring aftryk . Der er indikation for at, det indfanger skjulte sekundere processer.

3

Contents

Chapter 1
Introduction

We are surrounded by objects made of amorphous materials, i.e., materials that are microscopically are disordered like a liquid, but macroscopically appear solid like crystals. These disordered materials are easy to obtain - just by cooling a liquid sufficiently quick bypassing the material's melting point. When the now supercooled liquid is cooled further down it become more viscous until certain temperatures at which we can not detect any flow. The same vitrification phenomenon will be observed if the same liquid is compressed until it densifies. The obtained material state is a glass. Technologically this vitrification process is utilized in order to produce on different forms condensed matter such as systems of organic, inorganic simple molecular liquids and metallic systems. The glassy state is easy to obtain especially by cooling. However a theoretical explanation of the mechanism that governs this phenomena is still missing in spite of the big scientific effort.

The relaxation of the systems consists of processes that appears on different time scales. The dominant and slowest structural relaxation process of a glassforming liquid is the so-called α process. The α process defines the liquid's relaxation time. The α relaxation slows down or the structural relaxation time grows concurrently with temperature decrease and with compression.

To classify and to describe the rich phenomenology of the dynamics and the relaxation process a number of phenomenological models are used. The most employed parameters which characterize a glassformer are its stretching exponent β_{KWW} and its fragility m. The first measures the non exponentiality of the relaxation process described by a stretched exponential and implies a high-frequency power-law loss varying with frequency as $f^{-\beta_{KWW}}$. The latter measures how much the temperature dependence of the liquid's average relaxation time $\langle \tau(T) \rangle$, deviates from the Arrhenius equation at the glass transition. Theoreticians make attempts to incorporate these two quantities in or obtain as result of models, while the experimentalists try to link the two concepts, the

stretched exponential together with the fragility. In this way one will correlate the "three nons": the non-Arrhenius temperature dependence of the relaxation time, the deviation from simple exponential decay in the linear response regime to perturbations from the equilibrium state, and the nonlinearity of that response to thermodynamic perturbations. The liquids has been divided in different categories depending on the two parameters. Somehow this counteract the observation that all liquids appears to be glassformers. The vitrification is a generic property and hence one will expect that the structural relaxation should be ruled by the same simple mechanism. The first step torward formulation of a model or a theory is to point out what is the generic in the observed phenomena.

The scope of this study is to analyze a big number of experimental data in order to find the most general property of the structural relaxation.

The focus of the empirical investigation here is a model-independent description of the high frequency flank , i..e. the short-time (high-frequency) relaxation properties, of the α relaxation process at different temperature and pressure. I test possible correlations to other properties, including stretching exponential β_{KWW} and fragility m, the amplitude of the dielectric loss, the width of the relaxation and a conjecture stated in a paper from 2001 [110]. Therein Niels Boye Olsen, Tage Christensen and Jeppe Dyre showed that the high frequency slope of the dielectric loss for a group of materials tends to be $-1/2$ if the spectral shape is temperature invariant (time-temperature superposition (TTS))

A way to study the structural changes and motions is to study the relaxation processes after subjecting the liquid to a perturbation. The most easy way to monitor the phenomenology during the vitrification is by dielectric spectroscopy. Dielectric relaxation spectroscopy provides information about the collective rotation of the dipoles in the liquid. The complex permittivity is experimentally well defined and the most accessible of all constitutive quantities.The experimentalmeasure method is easy and precise and can covers a broad band of frequencies, thus the dielectric data are the most abundant.

A data collection was gathered, in all more than 100 data sets. Part of the data are own measurements and the biggest part of the data were kindly provided from different working groups Some of the data **are measured** and some were kindly **provided** from the Rössler group (Bayreuth, Germany) the Loidl-Lunkenheimer group (Augsburg, Germany) and the Paluch group (Katowice, Poland) (See for more information in Table A.1) and my co-workers in Glass and Time group Niels Boye Olsen, Kristine Niss and Bo Jakobsen. Most of the dielectric frequency scans are measured at ambient pressure and varying temperature.The remaining spectra are taken at isothermal conditions, while the vitrification process is controlled by high pressure.

The present report is structured as follows:

Chapter 2 gives an introduction to concepts that are necessary for understanding the investigation - the glass transition phenomenology, including a short introduction to the theoretical background of the linear dielectric experiment. The α relaxation and the phenomenological fitting function parameters like the stretched exponential and the model-independent minimum slope are presented mostly in terms of the temperature dependence.

The experimental technique and the experimental setup are described in the Chapter 3.

The analysis is divided in two. Chapter 4 contains the ambient pressure data, data selection, the minimum slope and the test of the stated conjecture and possible correlations. The high pressure data and results are described in Chapter 5. This chapter is devoted mostly to investigation whether the minimum slope is a quantity which is sufficient to describe and capture different phenomena as temperature pressure superposition at given relaxation times.

Chapter 6 presents some final remarks regarding the different scenarios of the shape of the relaxation spectra during the vitrification in terms of minimum slope. A connection between the isobaric and isothermal minimum slopes and some recent results from computer simulations is established. Last an short-handed list of scientific questions are presented.

Chapter 2
Vitrification of liquids and dielectric spectroscopy

This chapter is an introduction to the concepts that are fundamental for navigate into the topics supercooled liquids, glass transition and dielectric spectroscopy and hereby we present the dielectric response function which is the dynamical variable that is studied in this work. There is a big number of reviews and books that present the concepts. For this reason the presentation in the following will be relatively short and be restricted only to concepts and descriptions that are needed later on in this work. There is a number of reviews but there also books books by Böttcher and Bordewijk [12, 13],Dont [33], Richert and Blumen [128] and Kremer and Schönhals [83] that present the basic phenomena concerning the glass transition and linear responce and dielectric spectroscopy.

2.1   Phenomenology of relaxations in glass-forming liquids

If a liquid is cooled below the melting point sufficiently quickly T_m, the material enters a *supercooled liquid* state. This state is *metastable but in equilibrium* and with higher energy than the corresponding crystal (at the same temperature). With further supercooling of the liquid below the melting point, a glass is formed when the viscosity reaches values of $\eta = 10^{12}$ Pa.s that are typical for a solid body, i.e. the state is characterized macroscopically as crystal solid, but microscopically it is isotropic. However, in contrast to crystallization, glass formation does not involve any distinct change of the material structure during the process of solidification, and thus appears to be a purely kinetic phenomenon.

This value of the viscosity defines the *glass transition temperature T_g*. Here,

5

with temperature decreases of a few percent, viscosity increases dramatically. Molecular reorientation or *structural relaxation* timescales grow from values on the order of picoseconds in the liquid regime up to some hundreds of seconds around the glass transition temperature. At that point the structural relaxation becomes so slow (nearly frozen in) compared to the typical experimental timescale and the supercooled liquid falls out of equilibrium. The *structural alpha relaxation*, which we refer to as the slow dynamics of the system, is associated with a characteristic time known as the *structural relaxation time*[1] This is also called the alpha (α) relaxation time, τ_α or just τ. [49, 38, 5, 33, 35]. The changes in the relaxation process are monitored via macroscopic observabels, where characteristic constitutive quantities, like the density and specific heat, more or less abruptly change their temperature dependence. E.g., in calorimetric experiments the specific heat shows a pronounced step, which is most often used to define the *calorimetric glass transition temperature*. In measurements of frequency dependent dielectric constant, shear, etc, the alpha relaxation $\tau_\alpha = 100$ s is used to define the experimental glass transition temperatures of liquid during measurements but in principle it could be some other long time. These measurements result from linear relaxation experiments where the liquid in the equilibrium is subjected to perturbation (an input) and afterwards another quantity (the output) is monitored for change as the liquid reaches a new equilibrium. Under cooling the entropy and the density of the liquid change. This happens also if the liquid is compressed at given temperature [99]. The liquid densities and the characteristic alpha relaxation time also increase with increasing pressure until the structural arrest occurs at pressure P_g and temperature T_g. Thus a glassy state is obtained in isothermal conditions by compressing the liquid. In the temperature-pressure space the glass transition is just a line, the points (T_g, P_g), defined by constant relaxation time of 100 s. If some other time is used to define the glass transition then another line be found. These lines are called *isochrones* [106].

Non-Arrhenius temperature dependence

The slowing down of the molecular dynamics, the viscosity increase and the structural relaxation time follow a particular temperature dependence with cooling and compression. If one assumes that the relaxation process is due to activated processes with certain activation energy the most general way to express the the relation between the relaxation time (viscosity) and the temperature is

---

[1]Actually the structural relaxation time is an average relaxation time $< \tau(T) >$.

by the expression

$$\tau(T) = \tau_0 \exp\left(\frac{\Delta E(T)}{k_B T}\right),$$ (2.1)

where the prefactor τ_0 is the high temperature limit (at $T \to \infty$ is it order 10^{-13} s) and k_B is the Boltzmann constant while $\Delta E(T)$ is the temperature-dependent[2] activation energy [37, 80, 36] The simplest case is to assume that the relaxation time or viscosity only depends on temperature and the relaxation process is defined by one activation energy, $\Delta E(T) = E_A$ or temperature invariant activation barrier (in order to apply to a macroscopic ensemble) [38, 66]. This is referred as Arrhenius temperature dependence and for the relaxation time it is expressed by

$$\tau(T) = \tau_0 \exp\left(\frac{E_A}{k_B T}\right),$$ (2.2)

The Arrhenius law is one limit of the temperature dependence of the structural time as well as viscosity, and far from all supercooled liquids obeys it. If one plots $\log(\tau)$ as a function of $1/T$ it is clear that the slope is not constant, i.e. there is no single value for E_A, but the activation energy increases with decreasing temperature. It becomes steeper with temperature decrease, or in other words, the activation energy for the viscous flow grows continuously. The slowing down of a liquid's relaxation usually displays super-Arrhenius behavior [120]. So the equation 2.1 must be modified to describe the entire τ or η curve. Two widely-used expressions closely approximate the curves. The first is Williams-Landel-Ferry (WLF) equation [153]

$$\log(\tau) = \log(\tau_{ref}) - \frac{C_1 \left(T - T_{ref}\right)}{C_2 + T - T_{ref}}.$$ (2.3)

In this expression there is no prefactor. The constants C_1 and C_2 are normally given with respect to a reference state, i.e., temperature $T_{ref} = T_g$ (and $\tau_{ref} = \tau(T_g)$). With Equation 2.3 we have the mathematical formulation of the so-called time temperature superposition principle hence the expression gives a shift factor with respect to reference relaxation time and temperature and depends only on the temperature difference.[3] The second is the Vogel-Fulcher-Tammann (VFT) law [139, 40, 138, 41],

$$\log(\tau) = A + \frac{B}{T - T_0},$$ (2.4)

---

[2]In fact the the activation energy depends on the pressure or the density as well [107], but most concepts are developed to describe phenomena at ambient pressure with changing temperature. For simplicity ρ or P is omitted the notation.

[3]The WLF law is used in characterization of polymers.

where the parameters A, B and T_0, are material specific, or empirical, temperature invariant fitting parameters. The values of those three parameters have no physical interpretation[4] The expression gives a relatively good fit to data in some ranges and is thus widely used in describing simple molecular glass formers or extrapolating the kinetic T_g from temperature scans. The difference between the two expressions is that in Equation 2.4 there is a third fitting parameter T_0. If $T_0 \rightarrow 0$, then Arrhenius behavior is observed. However, this limit implies some unphysical consequences: if the VFT equation is rewritten as $\tau = \tau_0 \exp(CDT_0(T - T_0))$, where $B = DT_0$ in the Arrhenius limit will be zero and thus $\tau = \tau_0$ unless $D \rightarrow \infty$ [58]. When $T_0 \rightarrow T_g$, τ diverges and the curvature in the $\log(\tau)$ vs. $1/T$ plot is too big. VFT shows also a divergence of the $\tau(1/T)$ graph in T_0, but a divergence at any temperature is not necessarily expected in measurements, i.e. the relaxation time will be a finite number [52, 94]. The WLF and VFT are mathematical equivalents and based on free volume arguments [22, 23]. The Adam and Gibbs entropy model [1, 45] and the free volume model [39] are connected to these two phenomenological equations. From isotherm experiments where the pressure, P, is variable, deviation from Arrhenius law in plots of $\log(\tau)$ vs. P is observed. This indicates that the activation volume ($\Delta V = RT(d \log(\tau))(dP)$) increases with pressure. Thus, simple volume-activated models are not appropriate for description of the structural time- pressure dependence.[116] However, the VFT function is paraphrased phenomenologically simply by substitution of T with P in order to describe change in relaxation time with compression

A standard way of characterizing the reduction in structural relaxation is to quantify the deviation from Arrhenius law. This is based upon the concept of *fragility* or the steepness index [3],

$$m \equiv \frac{d \log(\tau)}{d \left(\frac{T_g}{T}\right)}\Big|_{T=T_g}. \tag{2.5}$$

m indicates how temperature affects the relaxation time from $\tau_g = 100s$ at T_g to phonon frequencies at 10^{-14} s in the limit of $T \rightarrow \infty$.

The strong limit regains Arrhenius (strong liquid) behavior at a slope $m = \log(\tau_g/\tau_0) = 16$, whereas extremely fragile behavior displays $m = 200$. The steepness index depends on the choice of τ_g and τ_0. Besides this, m is evaluated in T_g which depends on the cooling rate of the liquid. However, fragility is widely used to characterize the glass formers. As a measure of the degree of non-Arrhenius behavior we used the "*activation energy temperature index*"[5], $I_{\Delta E}$,

---

[4]However, in the phenomenological free volume models [22, 23] T_0 is defined as temperature at which the free volume is zero.

[5]This index is also called Olsen index.
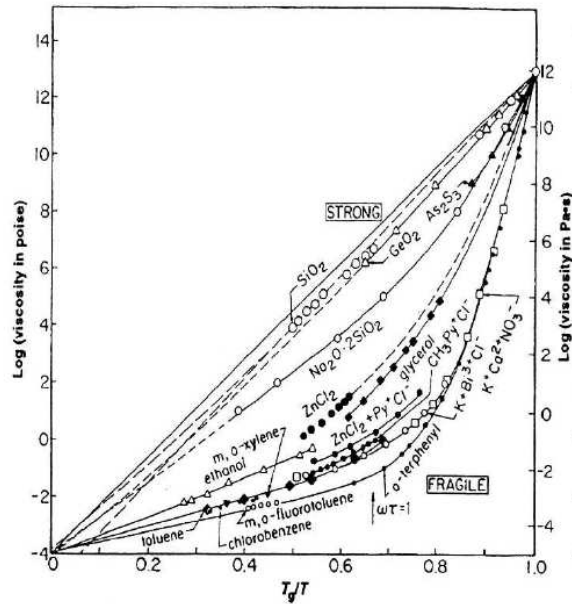
Figure 2.1: The so-called Angell plot is the logarithm of the viscosity versus the inverse temperature normalized by the glass transition temperature T_g. Glass formers where $\tau(T)$ approximately follows an Arrhenius law Equation 2.2 are called strong (the straight line with slope $\log(\tau_g/\tau_0)$). As the curvature of the concave curve gets closer to one, the deviation from Arrhenius behavior increases, i.e. the liquid is more fragile. The figure is taken from [3].

defined [135, 36, 52] as the logarithmic temperature derivative of the activation energy:

$$I_{\Delta E}(T) = -\frac{d \ln \Delta E(T)}{d \ln T}. \tag{2.6}$$

Here the activation energy $\Delta E(T)$ is defined by writing[6] $\tau_\alpha(T) = \tau_0 \exp(-\Delta E(T)/k_B T)$ with $\tau_0 = 10^{-14}$ s. The temperature index $I_{\Delta E}$ reflects the extent of deviation from Arrhenius behavior at any given temperature with values $I = 0$ for Arrhenius behavior (at high temperatures) and up to $I = 13$ for the most fragile systems. In particular, when evaluated at T_g this quantity relates to m as follows:

$$m = \log\left(\frac{\tau(T_g)}{\tau_0}\right)(I_{\Delta E}(T_g) + 1) = 16(I_{\Delta E}(T_g) + 1), \tag{2.7}$$

if $\tau(T_g) = 100$s and $\tau_0 = 10^{-14}$s. As it is pointed out in [52] the temperature index quantifies the activation-energy temperature dependence in a way that is independent of the unit system. In other words, the changes that can be observed are given directly by the relative changes. At every temperature $I_{\Delta E}$ gives the percentage increase in the activation energy as the temperature is lowered by 1%. If the only experimental variable is temperature, then thermal energy and volume effects are interwoven. Pressure change induces density variation, and the effect of the volume contribution to the relaxation timescale changes can be separated out. Then the fragility concept Equation 2.7 is reformulated as isobaric fragility (T-effect at different constant pressures) that is dependent on isochor fragility [105]. There appears to be insufficient evidence that fragility is a fundamental quantity [105, 98]. In this work the concept of the "activation energy temperature index" is used to describe the departure of a liquid's structural relaxation from Arrhenius behavior in measurements at ambient pressure.

Non-exponential relaxation

As already mentioned, structural relaxation is seen when linear experiments are performed. The way the liquid relaxes toward a new equilibrium after disturbance depends on whether the system, figuratively speaking, 'remembers' its past after the input is applied the system. If a memoryless system is subjected to a Heaviside step input then it undergoes an instantaneous rebalancing to the new equilibrium seen in the output response. In viscous liquids the response will be delayed. The output or the response function of harmonic input will

---

[6]From this relation the energy $\Delta E(T) = (\ln \tau(T) - \ln \tau_0) - T$

be also frequency dependent. Equilibrium behavior appears at low frequencies whereas instantaneous contributions to relaxation is seen at high frequencies. The simplest frequency dependent relaxation process is exponential or Debye relaxation. Real viscous liquids relax to equilibrium in a non-Debye way. The origin of the non-exponentiality is not theoretically explained.[21, 5]

There are two mechanisms that can give raise to nonexponential relaxation: the so called heterogeneous and the homogeneous limits. The heterogeneous limit is based on construction whereas the nonexponential relaxation is expressed in terms of a distribution of correlation times, representing relaxation contributions from different subsets to the overall average that the systems constitute. Subensembles or subdomains relax exponentially but with individually different relaxation times. In this case the non-Debye average relaxation stems from the fact that it is an average.[126, 21].

On the other hand is the homogeneous limit, in which all parts of the ensemble have non-exponential relaxation function and contributes equally and identically to the total average ensemble and the dynamics is intrinsically non-exponential.

Or in other words the liquid structure is homogeneous but the dynamics are heterogeneous. This means that different parts of the liquid move in different ways at a given time.[126, 21]. So experimentally (and in a molecular dynamic simulation) this limits the ability to identify the region of molecules whose dynamics are distinguishable from the ensemble [10].

2.2 Dielectric dynamics

Dielectric Susceptibility

The dielectric susceptibility is the most accessible quantity experimentally. Usually it is measured in the frequency domain by monitoring the frequency (time) dependent polarization response, $\bar{\mathbf{P}}(t)$, due to permanent and induced dipoles in a dipolar material after an external electric field (small) perturbation, $\bar{\mathbf{E}}(\mathbf{t})$. The polarization depends on the dielectric susceptibility, $\bar{\chi}$. Via the linear response theory[7] and the fluctuation-dissipation theorem (FDT) is possible to connect the macroscopic and microscopic dynamics. In the following isotropic media are assumed for simplicity and thus the vector and tensor notation will be omitted.

---

[7]The general formulation is as follows: If an equilibrated system is pertubated by changing the conditions then the systems relaxation toward a new equilibrium with time can be described by a time dependent output observable $\mathcal{O}(t)$. The perturbation is called the input ($\mathcal{I}(\mathrm{t})$)

Dynamic susceptibility response

The polarization of a dielectric liquid, placed in a electric field, is due to two processes. The first one is due to the induced dipole moments due instantaneous redistribution of the charges in the single molecule. This process of relaxation happens at times in the vicinity of 10^{-14} s and is noted $P_\infty = \varepsilon_0 \chi_\infty E(t)$. The second polarization process, P_{or}, is the reorientation of the permanent dipoles along the electric field [8].

If the electric field is constant $E(t) = E_0$, no dynamics will occur and the polarization is determined by the static susceptibility $P_{or} = \varepsilon_0(\chi_s - \chi_\infty)E_0 = \varepsilon_0 \Delta\chi E_0$. The partial orientation of the dipoles is due to molecular motion and thus governs/determines the dielectric response. The polarization at curtain time depends on the changes of the electric field for all times in the past ($t' \leq t$) then time dependent response can be expressed by:

$$P_{or} = \qquad P(t) - P_\infty(t) \qquad (2.9)$$

$$= \varepsilon_0 \Delta\chi \int_{-\infty}^{t} \phi(t - t')E(t')dt' \qquad (2.10)$$

$$= \varepsilon_0 \Delta\chi \int_0^\infty \phi(t')E(t - t')dt',$$

where ϕ is the memory function and expresses how the system remembers its past. The memory function or the response function has mathematically to obey to physical conditions – No orientational polarization response should be observed before an input is applied, i.e. the response function is zero for $t < 0$, and at equilibrium the polarization will decay to zero. The static limit has to be obtained and thus ϕ has to be normalized as follows:

$$\int_0^\infty \phi(t)dt = 1. \qquad (2.11)$$

The input is the electrical field $E(t)$ and can have different time dependence. If the electrical field is a Heaviside step function (corresponds a switching off the field at time $t = 0$), by Kubo's identity [84] ($\phi(t) = -\dot{\Phi}(t)$) one obtains:

$$P_{or} = \varepsilon_0 \Delta\chi \int_{-\infty}^{t} \phi(t')E(t - t')dt' = \varepsilon_0 \Delta\chi \int_0^t \phi(t')dt' = \varepsilon_0 \Delta\chi E_0 \Phi(t). \qquad (2.12)$$

---

[8]In fact every dipole "feels" also an additional, effective field, E_{local}. It is induced from the surroundings polarized dipoles. Let the external electric field be constant and the dipole's surrounding be a homogeneously polarized and determined by the static susceptibility, χ_s. The effective local field can be calculated for a cavity into this media and one arrives to the expression for the Lorentzian local field,

$$E_{local} = \frac{\chi_s + 3}{3}E_0. \qquad (2.8)$$

In equilibrium $\Phi(t \to \infty) = 0$ the normalization condition is directly obtained from Equation 2.11 $\Phi(0) = 1$. These results are for the time domain. If the electric field is a harmonic oscillating function, $\tilde{E} = E_0 e^{i\omega t}$ replaced into the expression 2.11 then the response will be expressed in the frequency domain as follows:

$$\tilde{P}_{or}(\omega, t) = \varepsilon_0 \Delta\chi E_0 e^{i\omega t} \int_0^\infty \phi(t - t') e^{i\omega(t-t')} d(t - t') . \tag{2.13}$$

Generally the linear output oscillates with the same frequency as the input and

$$\tilde{P}(\omega, t) = \varepsilon_0 \tilde{\chi}(\omega) \tilde{E}(\omega, t) , \tag{2.14}$$

where the susceptibility is a complex quantity $\tilde{\chi}(\omega) = \chi'(\omega) - \chi''(\omega)$ in the frequency domain. Thus a relation between the two response functions in the frequency respectively time domain (by using the expression 2.9) can be established:

$$\frac{\tilde{\chi}(\omega) - \chi_\infty}{\Delta\chi} = \int_0^\infty \phi(t) e^{i\omega(t)} d(t) . \tag{2.15}$$

If one uses the dielectric permittivity instead of the susceptibility $\tilde{\varepsilon}(\omega) = \tilde{\chi}(\omega) + 1$. then the complex dielectric displacement can be found $\tilde{D}(\omega, t) = \varepsilon_0 \tilde{E}(\omega, t) + \tilde{P}(\omega, t) = \varepsilon_0 \tilde{\varepsilon}(\omega) \tilde{E}(\omega, t)$

Molecular dynamics

The linear response is directly related to the local fluctuations in an equilibrated system. In the case of the macroscopic polarization in the thermodynamic equilibrium, polarization fluctuates with an (ensemble) average value $\langle \bar{P}_{or} \rangle = 0$. The fluctuations can be described by a two time correlation function $C_{PP}(t)$, which $C_{PP}(t = 0) = 1$ and $C_{PP}(t \to \infty) = 0$.

$$C_{PP}(t) = \langle \bar{P}_{or}(0) . \bar{P}_{or}(t) \rangle \tag{2.16}$$

The *Fluctuation Dissipation Theorem* [84, 15] states that in the linear response regime the response of a system to an external perturbation is determined by the same molecular relaxation mechanism that also controls the statistical equilibrium fluctuations within the system.

$$\frac{d\Phi(t)}{dt} = \frac{1}{k_B T} \frac{d}{dt} \langle \bar{P}_{or}(0) . \bar{P}_{or}(t) \rangle . \tag{2.17}$$

By Fourier transformation the correlation function is presented in the frequency domain

$$C_{PP}(\omega) = \frac{1}{2\pi} \int_{-\infty}^\infty C_{PP}(t) e^{-i\omega t} dt \tag{2.18}$$

13

On a microscopical level the orientational polarization $\bar{P}_{or}$ is due to the net sum of all dipole moments $\bar{\mu}_i$ in the system,

$$\bar{P}_{or} = \frac{1}{V} \sum_{i=1}^{N} \bar{\mu}_i(t), \tag{2.19}$$

with volume V containing N dipoles. The orientational polarization in a given volume is just the sum of all dipole moments in the volume

2.3 Phenomenological responce functions

The primary α-process

The structural relaxation time is associated with a maximum of the so called *primary or α relaxation* that is observed in the *dissipation (loss, absorption or imaginary) part* of the response functions in the frequency domain. The primary relaxation appears as the dominant relaxation process, also referred to as *loss peak* and its maximum is located at frequency, $\omega_{max} = 2\pi f_{max}$ that corresponds to the relaxation time τ_{α}. The nonexponentiality is expressed in the shape of the relaxation like a deviation from single dipole relaxation process, described by Debye relaxation function in the frequency domain as the complex permittivity $\tilde{\varepsilon}$

$$\tilde{\varepsilon}(\omega) - \varepsilon_{\infty} = \frac{\Delta\varepsilon}{1 + i\omega\tau_{\alpha}},$$

and in the time domain it is expressed as

$$\phi(t) = e^{-\left(\frac{t}{\tau_{\alpha}}\right)}$$

where τ quantifies the relaxation time scale. Observations show large deviations from the Debye relaxation. In the frequency domain the primary relaxation is an asymmetrically broadened peak. Therefore a measure of this deviation is used to characterize the response, i.e., the spectral dissipation shape [29]. There are a number of phenomenological fit functions that are used to describe the shape but here a few selected relaxation functions are used. The chosen functions are these that show a low frequency decay of one. At low frequencies (long times) there is time for the molecules to rearrange in the supercooled liquid or the liquid flows.

Kohlrausch-Williams-Watts

The deviation from an exponential relaxation pattern is commonly observed as a correlation function following the Kohlrausch-Williams-Watts (KWW) decay law [82, 152]

$$\phi(t) = \exp\left[-\left(\frac{t}{\tau_{KWW}}\right)^{\beta_{KWW}}\right],$$

where τ_{KWW} is the averaged relaxation time and $0 < \beta_{KWW} < 1$ represents the extent of dispersion or deviation from a single time constant. β_{KWW} is called the stretching exponent. It is generally accepted that the larger the fragility, the lower is β_{KWW} [11, 147]; in fact based on experiment a quantitative relation between m and β_{KWW} has been suggested [11]. According to this picture all values between 0 and 1 for the stretching exponent can occur, depending on the fragility.

Cole-Davidson

In literature characterizing a given liquid response, a β-stretching exponent fitted using the phenomenological Cole-Davidson (CD) response function is often used. The CD function is in the frequency domain and was introduced in 1950 by Cole and Davidson [26, 27]

$$\tilde{\varepsilon}(\omega) - \varepsilon_\infty = \frac{\Delta\varepsilon}{(1 + i\omega\tau_{CD})^{\beta_{CD}}} \tag{2.20}$$

The imaginary part of this expression produces an asymmetrically broadened peak with power laws at both sides of the maximum ω_{max}:

$$\varepsilon''(\omega) \propto \begin{array}{ll} \omega^{-\beta}, & \omega > \omega_{max} \\ \omega, & \omega < \omega_{max} \end{array}$$

The minimum slope

From observations of different master curves the following can be stated more or less generally: If there are changes to the shape of the loss, these are mainly due to changes of the slope of the high frequency part. Thus, one can expect the same information about the spectral shape of the loss by looking only at the high-frequency part of the relaxation. No models or assumptions about the nature of the relaxation process (whether well distinguishable α and β or a Johari–Goldstein-wing or some secondary internal relaxation process) are used to define the slope. The minimum slope is already defined and used in literature (see e.g. [110]), as the local minima, α_{min}, of the values for the slope of the high frequency wing in log-log plot, or the double logarithmic derivative:

$$\alpha = \frac{d\log\varepsilon''}{d\log f}. \tag{2.21}$$

Since the second-order derivative is by definition zero at the inflection point (at frequency $f_{\alpha_{min}}$) where the slope is minimal, the linear tangent approximation works particularly well here. This means that the approximate power-law description $\varepsilon'' \propto f^{\alpha_{min}}$ gives a good representation of the loss over a considerable frequency range. Thus if, for instance, the minimum slope α_{min} is close to $-1/2$, then to a good approximation $\varepsilon'' \propto 1/\sqrt{f}$ for $f \gg f_{max}$ over several decades. In the time domain this corresponds to $\sqrt{t}$ relaxation being a good approximation of the relaxation function over several decades of time shorter than the mean relaxation time.

Time temperature superposition

Time temperature or frequency temperature superposition [9] (TTS) is an empirical relationship between the time (frequency) and temperature dependent properties of (some) supercooled liquids. The basis for this relationship is the existence of a connection between the temperature and the characteristic structural time, and the spectral shape of the linear response function of the liquid.

At lower temperatures, the relaxation process slows. If the liquid under investigation obeys TTS, then the dissipations measured at different temperatures in the frequency domain have similar shape, i.e., temperature shifts only the time scale of the response, without modifying the shape of the susceptibility or correlation function. In these cases, the dissipation curves can be exactly superimposed into a master curve by shifting the curves horizontally along the frequency axis as well vertically normalized by the process' strength. This can be formulated mathematically as follows: The frequency-dependent relaxation response function $\chi(\omega, T)$ obeys TTS if a function $\phi(\tau(T)\omega)$ exists that describes the temperature independent relaxation shape (the master curve shape) with temperature dependent (scaled) relaxation time $\tau(T)$, and temperature dependent relaxation process strength $\phi_0(T)$ such[110]

$$\chi(\omega, T) = \phi_0(T)\phi(\tau(T)\omega).$$

Many investigations show that TTS is not always fulfilled, due to secondary relaxation processes [5, 110]. Generally because of the changes in the entropy and the energy TTS is also not fulfilled when the system is out of equilibrium[10] [83, p.125]. However in many cases there is, to some extent, an implicit assumption that TTS is fullfilled for the primary relaxation at least close to T_g. For example, when one investigates correlation between KWW stretched exponential and the

---

[9]TTS is also called time-temperature superposition principle

[10]Though there is an investigation that shows that TTS is obeyed if the scaling factor is aging-time dependent [111, To be published]

fragility where relaxation spectra at T_g are not always available, then the temperature is estimated from VFT fit and β_{KWW} is fitted to curves above T_g. The same situation occurs when Ngai's coupling model [154, 97, 102] is used to predict relaxation times for the α or β relaxation – An extreme case is to use sub T_g measurement to read off a τ_{beta} and β_{KWW} from spectra where the main loss peak is in the window and use this to estimate a τ_α given τ_β. Based on broad band relaxation spectra of the EW liquids Rössler states the conjecture: if the relaxation at high temperatures in the stable liquid regime and at low (in vicinity of 0 K) are characterized by the same β_{KWW} then α relaxation should at intermediate temperatures also have a temperature independent spectral shape. [130]

High pressure dielectric spectra along the isochrones show another kind of superposition that is only determined by the relaxation time. Different combinations of p and T can result in the same relaxation dynamics for the same τ or liquids' primary relaxation obeys the temperature-pressure superposition at the same relaxation times. This is also called τ_{alpha} and β_{KWW} co-invariance of changing the thermodynamic conditions via T and P or $\beta_{KWW}\alpha_{min}(f_{max} = const, T, P) = const$. In this thesis this is called isochron temperature pressure superposion (ITPS) [99, 107, 56, 115, 121, 77, 115, 95, 98].

A stronger condition can be formulated, namely, time temperature pressure superposition (TTPS) where $\beta_{KWW}\alpha_{min}(f_{max}, T, P) = const$ for all relaxation times and thermodynamic conditions. This general invariance is found for supercooled and -compressed salol limited of course to the accessible experimental window [25].

It is not obvious when a single master dispersion curve is enough to describe the relaxation at all temperatures (and pressures). Olsen, Christensen and Dyre asked the question the other way round – What is common for liquids that obey TTS [110]?

Their investigation [110] gave rise to the conjecture: if the α-process obeys time temperature superposition, then the frequency dependence of the high-frequency α-relaxation decays with the universal exponent $-\frac{1}{2}$ or in mathematical symbols,

$$TTS \Longrightarrow \varepsilon''(\omega) \propto \omega^{-\frac{1}{2}}, \ \omega < \omega_{max}.$$

The conjecture was not only based on experimental observations only but also on models (See in article for references)

Secondary processes

The phenomenology we see with dielectric spectroscopy over 16-19 decades is complex. Besides the primary relaxation processes there are different faster

secondary processes. The temperature and pressure induced slowdown of the dynamics of these processes alternates, i.e. they have different sensitivity to thermodynamic conditions. The fastest process, the Boson peak, is observed in 1 THz range (See e.g.[92]) and is not subject to the work here.

Other secondary processes, the *β processes*, appear at widely different time scales and they are liquid specific. The way these secondary processes manifest in the frequency spectra depends on the bifurcation between the α and the β processes. Distinguishable features, for example loss peak, high frequency shoulder or just an additional high-frequency wing also called *excess wing* (EW) can be seen. Generally the primary process slows down quicker than the secondary, thus a merging temperature can be identified. Today it is recognized that one loss spectra can encompass more than one secondary process.

The origin of these processes is not explained apart from β processes that are due to *intramolecular* motions, where parts of the molecules relax.

Experiments on liquids of small rigid molecules led Johari and Goldstein to the conclusion that the observed secondary relaxations are due to *intermolecular* mobility. These *Johari-Goldstein* (JG) processes were ascribed heterogeneity in the spatial structure where local and highly mobile regions in the glass "islands of mobility" relax relatively quickly.[71, 72, 68, 69, 70]. There has been a discussion about the origin (see in e.g. [142, 140, 141]) and how to identify the true JG process ever since. [97, 73, 102, 77]

Some controversy exists regarding the microscopical origin of the JG beta processes and what the *excess wing* (EW) really is. The ongoing discussion revolves around whether EW is a generic feature of the primary relaxation [85, 32], or whether EW is nothing else than JG process, where the high-frequency part is *not* dominated by high frequency α relaxation.[59, 32, 83]

Dielectric measurements of liquids with secondary relaxation process above 1 Hz at relatively high temperatures show an excess relaxation, while under T_g a well-revealed β process can be detected. Scaling of the dispersion data in the high frequency minimum that appears between the α and β processes shows TTS around the minimum, but if the liquid is cooled further from a certain temperature (α and β processes separate) TTS is violated. These observations are interpreted as: no changes in the EW happens i.e. they have the same slope; and thus, EW features[11] of the α process. The slope of this linear segment (in log-log plot) is approximately to -0.2. [14, 42, 91, 86, 85].

Rössler group suggest a phenomenological classification of the liquids in type A and B [85]. Type A are those that have relaxation where there is no clear

---

[11]The phenomenological argument for EW is that it slows down in unison with the structural relaxation, i.e. the two processes have the almost the same relaxation time and therefore EW is somehow linked to α relaxation.

(slow) secondary process but a EW is observed. The B-type liquids' absorption spectra are characterized with resolved β process. This classification is qualitative and depends on experimental window width, and measuring procedures. Three (still qualitative) characteristics of liquids with a wing have now been developed, based on observation of the linear part between the primary and secondary processes seen in the dispersion curve of a number of liquids like Glycerol.

When a glass is subjected to annealing then the structure begins to relax toward equilibrium, i.e. the structural relaxation slows down, while β relaxation time remains virtually unaffected[12] These low temperature ageing experiments showed that EW reveals into one or two β processes. This indicates that EW is just an way of interaction of α and JG process. [112, 90, 101, 88, 89, 143, 133, 148]

At high pressure measurements temperature governs the magnitude of the β process while the compression somehow affects the local minimum between the primary and secondary relaxations and the β peak is better resolved, i.e, this indicates that its shape is described with a CC exponent that is bigger than at ambient pressure. When the liquid is squeezed then the structural process slows down while the secondary process is relatively pressure insensitive. There are a number of cases where EW evolve in one or two β processes. [78, 76, 122, 87, 54]

The secondary (well-revealed) relaxation is usually modelled by a symmetric Cole-Cole function [24]

$$\tilde{\varepsilon}(\omega) - \varepsilon_\infty = \frac{\Delta\varepsilon}{1 + (i\omega\tau_{CC})^{\beta_{CC}}} \tag{2.22}$$

DC conductivity

Sometimes in dielectric loss spectra an additional relaxation process, *DC conductivity*, can be detected at low frequencies. The DC conductivity is caused by translational motion of small (mobile) ions. The ions are possibly impurities in the liquids. However they are present in almost every polar liquid, whereas the a process is partially related to reorientation of the entire molecules. If a frequency-independent conductivity assumed then the DC conductivity contribution to the complex permittivity is [89, 148]

$$\epsilon''_{DC} = \frac{\sigma_{DC}}{\omega\epsilon_0},$$

---

[12]In dispersion plots it looks like the τ_β is temperature dependent, but this can be the effect of the high frequency flank. If one takes just the simple additive model to combine the primary and secondary relaxation, it is easy to see that this can be due to linear translation of the β process up to the line that corresponds to the high frequency part.

where the vacuum permittivity is $\epsilon_0 = 8.854.10^{-12} A.s(V.m)^{-1}$). Since the DC conductivity recovers a translational motion its correlation with the α relaxation is observed and discussed in terms of the Debye-Stokes-Einstein equation that relates the rotational correlation time with viscosity $\tau = 4\pi\eta$.

In dielectric spectra is observed that the DC conductivity "follows" the same temperature depends as the primary relaxation but often from some temperature the translational and the rotational motions decouples with temperature decrease [81, 112]. This can detected from the change in the temperature-dependence of the low frequency minimum which appears between the DC conductivity line and the low frequency flank of the primary relaxation. It is not clear what exactly causes the decoupling. In many cases the coupling can be observed when the temperatures are lower than the temperature where α and β processes merge. [111]

Chapter 3
Measurement Technique

3.1   Experimental setup

Some of the data in this thesis were measured especially for this study at four different experimental setups in laboratories at universities in Roskilde, Tempe and Katowice. These four setups will be described here in separated sections.

Almost all the measured glass-formers are moderate-viscosity liquids at room temperature. Every liquid is listed on the end of the relevant section with chemical name, purity and abbreviation and details in the particular preparation procedure. If nothing else is noted, chemicals were purchased from Sigma-Aldrich Chemical Company and used as acquired. The raw data spectra are shown in Appendix **??**.

The setup at Roskilde is the most detailed in regard to systematic errors and thermal equilibration of the sample. These issues, in common with errors arising from commercial measuring devices, volume changes of the tested liquid upon cooling etc. are the same/valid for the other setups but not necessarily repeated. A voltage U is applied on a capacitor with the liquid. This induces an electric field between the capacitor plates and the liquid is polarized (P) and charge displacement (D) gives rise to electric current[1] (I) in the circuit. In terms of linear response theory the macroscopic electric field is the input and the displacement field is the output. The dielectric relaxation at every frequency can be defined using the measured capacitance $\tilde{C}(\omega)$ of the filled capacitor by using the equation

$$\tilde{C}(\omega) = \frac{A}{d}\varepsilon_0\tilde{\varepsilon}(\omega) \;\Leftrightarrow\; \tilde{\varepsilon}(\omega) = \frac{\tilde{C}}{C_{geo}}\,, \tag{3.1}$$

---

[1]It is easy to show for a Heaviside step voltage input that $P(t) \propto D(t) \propto \int I(t)dt$).

where the vacuum permittivity $\varepsilon_0 = 8.8541878176.10{-}12$ $A^2s^4kg^{-1}m^{-3}$ and C_{geo} is geometric capacitance. The electrode area A has to be much bigger than the distance between the electrodes d in order to ensure a homogeneous field over the sample. In all experimental frequency domain setups measuring at frequencies less than 1 kHz is a technical challenge [2]

Roskilde University Setup, (RU setup)

The setup at Roskilde University is described in [63, 62].

The general setup is described as follows. The dielectric scan covers the frequency range from 10^{-3} Hz up to 10^6 Hz. Capacitances were measured with an HP 3458A multimeter in the range $10^{-3} - 10^2$ Hz in conjunction with a HP 4284A Precision LCR-meter at frequencies in the range $10^2 - 10^6$ Hz. The two apparatus were connected to the measurement cell via a mechanical switch at 100 Hz (between the two frequency ranges). The switchbox is software-controlled and automatically changes the connection between the capacitor to the various instruments in succession. In this way, a relatively broad frequency spectrum of 1 mHz up to 1 MHz can be obtained with one measurement only.

The LCR meter is a commercial one and measures the complex capacitance directly, while the output data from the multimeter setup are taken indirectly and depend on a reference measurement (more about the multimeter is in the coming section). The multimeter measurements were performed on a home-built setup consisting of a voltage divider (described below) with the multimeter in combination with a homebuilt arbitrary wavefunction generator [62]. The measurement cell is a multilayered gold-platen capacitor with empty capacitance 71 pF (See in Fig. 3.1). There are 22 plates and the distance between is less than 1 mm. The sample substances have to be prepared as a capacitor. The dielectric cell here is suitable only for glass-forming materials that are liquids with relatively low viscosity at or somewhat above room temperature.

The condensator with the liquid is mounted on a holder and placed into the cryostat. The temperature of the sample is controlled by a homebuilt nitrogen-cooled cryostat with an absolute accuracy on the temperature under 0.2 K and a temperature stability less than 20 mK. The sample chamber is subjected to a stream of cold N_2-gas, and heated to temperatures between 100 K and 320 K. The cooling rate must be sufficiently large, especially in temperature ranges

---

[2]If measurements are performed in the frequency domain then the applied voltage is complex with frequency ω and $\tilde{I}(\omega) = \tilde{U}(\omega)/\tilde{Z}(\omega) = \tilde{U}i\omega\tilde{C}(\omega)$ (Z is the impedance and C is the capacitance). The applied voltages must be small in order to keep the linearity condition. Let $\omega = 0.1$ Hz and, sinusoidal voltage $U = \sin(\omega t)$ V. The typical sample capacitance is $C = 0.1\ \mu F$, then $I = i0.1Hz100pF1\sin(0.01mathrmHzt) = i1\sin(0.01t)$ pF. This current is too small to be detected with ease.

Figure 3.1: The multilayered gold-plated capacitor (geometric capacitance around 71 pF) used for measurements at Roskilde University setup

where the tendency to crystallize is enhanced. In some cases it may be necessary to perform the measurements after heating the sample up to melting temperature and directly cooling it to the measurement temperature at a fast rate. This is done by pouring liquid nitrogen directly in the cryostat chamber that is cooled down to the necessary temperature and placing the sample holder in the chamber. In this way a cooling rate in order of 100 K/sec is obtained. Another advantage with the procedure is to keep the reactive oxygen out of the chamber. [63]

The multimeter measurements

As mentioned the induced currents in a capacitance after a voltage excitation are of order of pA at low frequencies is an instrumental challenge. In this setup a special part of the setup is constructed [62].

The multimeter setup is based on a voltage divider. The generator produces low-frequency ($10^{-3} - 10^2$ Hz) sinusoidal input signals with voltages that are reproducible within 10 ppm [62]. The input voltage U_{in} is therefore known and the output voltage U_{out} over a component Z_0, consisting of parallel connected known capacitor and resistor with $C_0 = 10$ nF and $R_0 = 100$ MΩ, is measured. The ratio between the input and the output voltage is used to find the unknown sample complex capacitance $\tilde{C}_x$ (the impedance $\tilde{Z}_x = \frac{1}{iw\tilde{C}_x}$)
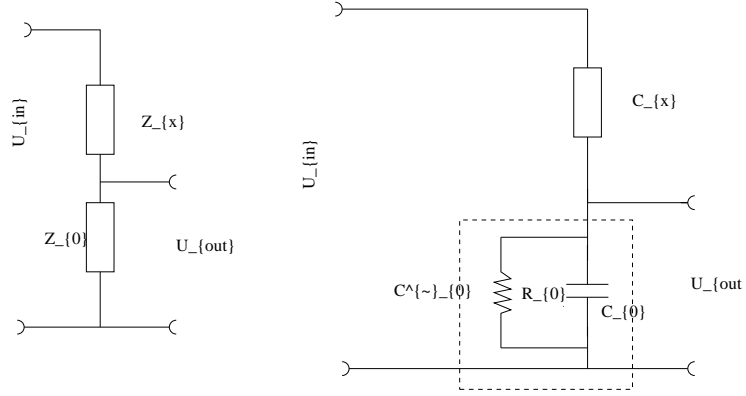
Figure 3.2: Schematic illustration of (a) the measurement experiment and (b) the dielectric reference experiment. The capacitance C_0 and the resistance R_0 are components basically taken to reduce the noise from the multimeter inside capacity and the netsuplay at low frequencies.

$$\frac{U_{out}}{U_{in}} = \frac{\tilde{Z}_0}{\tilde{Z}_x + \tilde{Z}_0} \quad \Rightarrow \quad \tilde{Z}_x = \left(\frac{U_{in}}{U_{out}} - 1\right)\tilde{Z}_0$$

$$\Rightarrow \quad \tilde{C}_x = \tilde{C}_0 \frac{U_{out}}{U_{in} - U_{out}}, \tag{3.2}$$

where the complex capacitance $\tilde{C}_0 = C_0 + (iwR_0)^{-1}$. Thus, the above equation is equivalent to

$$\tilde{C}_x = \left(C_0 + \frac{1}{iwR_0}\right)\frac{U_{out}}{U_{in} - U_{out}}. \tag{3.3}$$

The complex voltage quotient in this expression is obtained from the Fourier transformed (Fast Fourier Transformation) time dependent voltages,

$$\tilde{\alpha}(w) = \frac{\mathcal{F}(U_{out})}{\mathcal{F}(U_{in}) - \mathcal{F}(U_{out})}. \tag{3.4}$$

Thus, the determed sample capacitance is in the frequency domain. In reality the known resistor and capacitor, i.e., complex capacitance $\tilde{C}_0$, are partially frequency dependent. The exact value $\tilde{C}_0$ at every frequency is obtained in a calibration measurement. The components R_0 and C_0 are chosen so that

$R_0C_0 >> 2 \cdot 10^{-2} sec$ (50 Hz) in order to reduce the noise from the supply net. The internal capacitance of the multimeter is about $1pF$ which is insignificant compared to $C_0 = 10nF$. Nonetheless, all wirings and electrical connections in the setup comprise a complex impedance which affects the precision of the measurement, especially at low frequencies. In addition, nominal values of the known components are not given to the necessary precision needed for calculation. All this is captured in a calibration procedure. The calibration of $\tilde{C}_0$ is done by a reference measurement where the unknown complex capacitance $\tilde{C}_x$ is interchanged with a known capacitor. The measurement is performed with the dielectric measurement cell as reference cell. This measurement is done with the capacitor and the measurement cell holder, so the resistance and the capacitance due the wiring and the connections is taken in account. Unavoidable leak currents are modelled by a resistance $10^{16}\Omega$. In this way as many as possible artifacts are included in $\tilde{C}_0$.

Systematic errors

Approximately one decade away from each end ends of the frequency window of the commercial LCR-meter, systematic errors can be seen. While systematic, they can change with the time or after restarting the LCR-meter. The errors are not of major importance in the real part, but in the imaginary part of the dielectric response signals manifest themself as nicks in the loss spectra. Bellow 1 Hz the errors decrease the factual imaginary part whereas at the highest frequencies they cause an increase with frequency. The errors are reproducible and are seen in all frequency spectra. Due to variations in magnitude the errors can be only partly eliminated direct subtraction of the dielectric spectrum of the empty measurecell from the response data. Thus, a nick around $100Hz$ can be seen in almost all data from this setup. The exact value of the geometrical capacitance C_{geo} for the measure cell can change due to geometric temperature dependence. The exact value at different temperatures is not known but it is assumed that is nearly frequency independent. Measurements for frequencies less than 100 Hz are partially captured in the calibration that is performed at low temperature, within the usual working temperature interval. Filling the sample cell is a potential source of error. Loading of the cell is done by exploiting the capillary effect which causes the liquid to fill the space between the electrodes. The supercooled liquid volume 'creeps' compared with the volume of the normal liquid. In consequence the effective electrode area is less than assummed and hence a smaller $\tilde{\varepsilon}$ is calculated. There are no corrections for this in C_{geo} and this will affect only the absolute value of the dielectric response. Another error can occur concerning dielectric cell with rigid geometry. Close to the glass transition temperature large temperature changes can result in the formation

of cracks inside the highly viscous liquid or in the separation from one of the electrode surfaces due to mechanical stress. This can be detected in the spectra as sudden jumps in the real and the imaginary part of the dielectric response.

Aging and thermal process

The experimental procedure involves two relaxation times – the structural relaxation time and the thermal relaxation time. The reproducibility of the data depends on whether the system is able to equilibrate i.e. to stay at a given temperature for sufficient time.

The structural or Maxwell relaxation time is due to relaxation processes or molecular motion in the equilibrating system that occurs just after temperature jump. Sample thermal relaxation time for a temperature change $\Delta T = 1K$ is defined as:

$$\tau_T = \frac{l^2}{D},\tag{3.5}$$

where l is the dimension of the sample and D is the thermal diffusion specific constant for the liquid. The dielectric cell is plated with gold which is a good thermal conductor. Thus it is negligible in the estimation of the thermal diffusion time. The typical thermal diffusion constant value for liquids is of the order of 10^{-6} and l is around 10^{-3} m. Hence, $\tau_T = 1000$ s or roughly 20 min per 1 K jump. Therefore, a wait of at least half an hour followed temperature changes of $2K$ in the cryostat. An easy check of the thermal equilibration of the sample is to make several measurements of the relaxation at given temperature. The routine in the Roskilde is to do two successive measurements at every temperature with a time interval corresponding to the time needed for a frequency scan, i.e., from a couple of hours up to eleven hours. If the spectral shape of the two measurements deviates, then the last measurement was assumed to represent the true equilibrated liquid. To minimize the arbitrary random errors dielectric constant value at every measure frequency the average of 250 periods at each frequency.. The following liquids were measured on this setup: 1,3 propandiol (98%, 13PD), 1,2 propandiol (99%, Merk, PG), dibutyl phthalate (98%, DBP), diethyl phthalate (97%, DEP) and Isoeugenol ($\geq$ 98%, Fluka). All these chemicals are liquids with low viscosity at room tempearture. They were cooled in the cryostat starting from room temperature. D-Panthenol ($\geq$ 98%) is a rather viscous liquid at room temperature. The melting point is not known. It is, in fact, in the supercooled liquid state and ages/vitrifeys under storage in a refrigerator. The sample and the capacitor were heated very carefully up to 299 K. Higher temperature causes chemical decomposition where one of the products is pantothenic acid. The measurement spectra is dominated by DC-conductivity. Salicylsalicylic acid (99%, SSA), and D(-)sorbitol (99%, AppliChem, Sor) are crystals

at room temperature. They were melted in an oven, placed in the heated-up (melting temperature) capacitor and subsequently cooled to room temperature. D(-)sorbitol was melted at 390 K for four hours and SSA at 419 K for one hour.

Arizona State University Setup

The dielectric setups at Arizona State University measure in the frequency domain. (See for more in [125, 149]) The technical problem with weak electrical signal at low frequencies in measurements in the frequency domain is solved here by using a Mestec DM-1360 trans-impedance amplifier which is basically a current-to-voltage converter[3] The electrical circuit for the setup and Mestec DM-1360 are presented in Figure 3.3. The measuring device is a gain-phase analyzer Solartron SI-1260. The sine generator output is connected to the sample capacitor and the converter in series. The gain-phase analyzer connects the generator output to the two voltage inputs of the analyzer (Shown in Figure 3.3 on the right) and thus measures their amplitudes and signal phases relative to the generator frequencies. The converter circuit is presented in Figure 3.3 right. The components $R_0 = 10$ GV and $C_0 = 10pF$ respectively damp output signal noise at high frequencies. The capacitances in the amplifier $C_i = 100$ pF and the resistors $R_i = 10(i+1)$ V for all $i = 1, 2, \ldots 9$, constitute the feedback circuit for a fast electrometer-type OpAmp. The amplifier output voltage $U_out(\omega) = I(\omega)/Y_f$, where Y_f is the feedback admittance (almost frequency independent) and $I(\omega)$ is the input current that comes from the measure cell. From the nominal values of the components one finds the admittance $Y_f = R_0^{-1} + i\omega C_0 + \Sigma \left(R_i + (i\omega C_i)^{-1} \right) \right)^{-1}$ but as in the previous setup a reference measurement of the empty capacitor gives the reference admittance Y_r which is used to calculate the sample admittance Y_s,

$$Y_s(\omega) = Y_r(\omega)\frac{U_r}{U_s}, \tag{3.6}$$

where U_r and U_s are the output from the converter and the voltage over the sample.

The gain-phase analyzer Solartron SI-1260 measures in the range $10^{-4} - 10^7$ Hz. In the measurement presented here, the amplitude of voltage was 2 V at the measurements done on ASU Setup1 and with amplitude 1 V - at ASU Setup2. The number of measurement frequencies per decade was 8 and they were logarithmically spaced.

---

[3]The device converts small currents to measurable voltages over the entire frequency range.
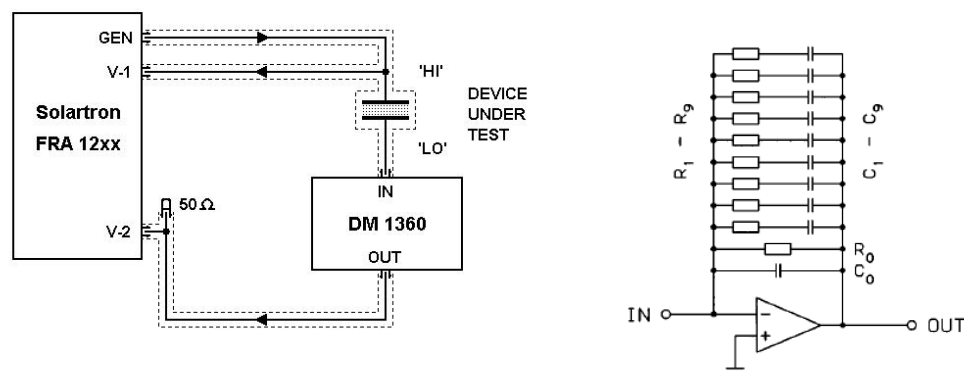
Figure 3.3: Left the principal presentation of the electrical part of the ASU setups. On the right is the circuit of Mestec DM-1360 is a current-to-voltage converter developed and used in the setups at ASU. From [125].

ASU Setup1

The basic setup is described in Refs. [125, 50, 60]. This setup is used for measuring liquids with relatively low glass transition temperatures. The sample cell (shown in Figure 3.4) was placed directly on a temperature-controlled plate in an evacuated He-refrigerator cryostat (Leybold RDK 6-320) driven by a Cool Pak 6200 compressor. The temperature control is provided by a Lakeshore 340 temperature controller. In order to measure the temperature inside the cryostat there are two calibrated DT-470-CU diodes: One attached to the base plate; The other diode is in contact with the upper part of the measure cell. These two diodes give input to the temperature controller. The difference in the temperatures of the plate and the top of the dielectric cell is less than 0.025 K when the measurements are performed. The temperature stability for this cryostat is within 5 mK and the accuracy ± 0.5 K. To avoid thermal transport from the environment to the measure cell into the vacuum cryostat, the wires connecting the electrodes and the electrical measure apparatus are in thermal contact with the stage on which the measure cell is mounted.

The measure cell is presented in Figure 3.4). The cell consists of two electrodes that are held at fixed distance from each other by two sapphire windows, which are mounted in a frame. The electrodes are made of stainless steel and are with a diameter of 18 mm. The distance between the electrodes is 100 μm. Due to the material properties the brass frame provides thermal contact between the
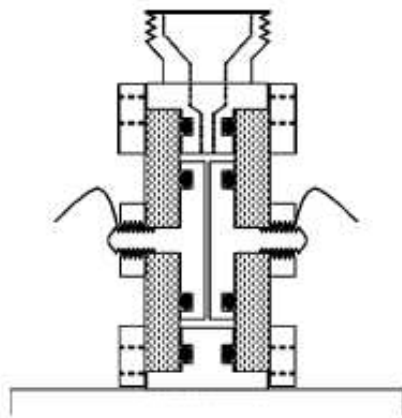
Figure 3.4: Schematic presentation of the capacitor used for measurements into the He-cooled cryostat. From [137][]

liquid and the cryostat. The geometric capacitance is measured to $C_0 = 17.32$ pF (slightly changed to $17.58\,pF$ after resembling and cleaning) with a loss of magnitude $\tan \delta = 0.3.10^{-5}$. The cell is filled up with sample liquid to the edge of the frame. In this way it is ensured that there is liquid between the electrodes when the liquid shrinks under cooling. A reference spectra was made with the empty cell as reference, but only once because of the rigid construction and robust geometric capacitance. The liquids were supercooled in the cryostat chamber. Because of the relatively low cooling rate, around 1.5 K/min, 5 minutes was used for temperature stabilization after a temperature step. A further 10 minutes were allowed before starting measurements. The following liquids were measured on this setup: 2-methyltetrahydrofuran (99.1%, *distilled*, MTHF), methyl-*m*-toluate (98%, Avocado Research Chemicals Ltd., MMT) and n-propyl-benzene (99%, nPB). All the chemicals are liquids at room temperature and were injected directly into the measure cell.

ASU Setup2

The measuring cell, which has an empty-cell capacitance of 55.63 pF, consists of two steel disc electrodes of diameter 20 mm separated by six $50\,\mu$m thick Teflon strips. The strips were placed radially. The electrodes with the liquid and the spacers were placed in a holder. The holder provides electrical and thermal contact (see in Figure 3.5). The holder with the cell was placed inside a standard nitrogen-gas cooled cryostat where temperature was stabilized and

Screw, the part underneath
is spring loaded

Wires, electrical connection

Electrodes with liquid and spacers
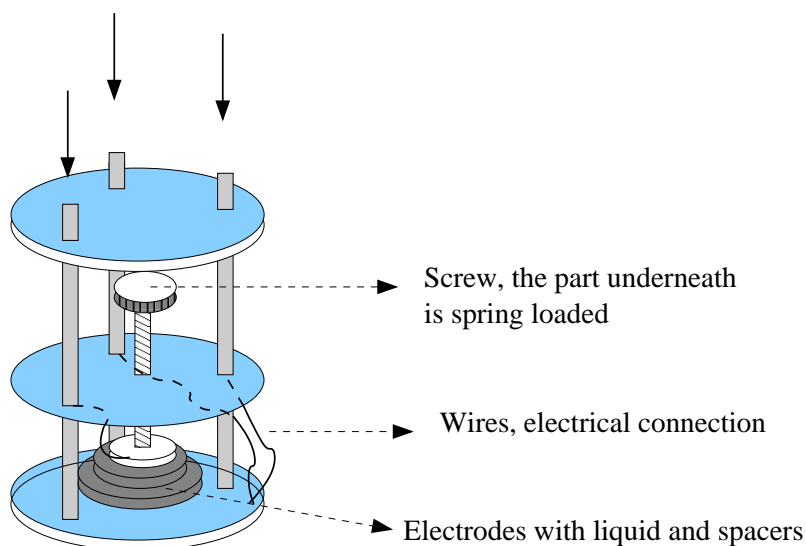
Figure 3.5: Schematic presentation of the electrode holder used for measurements into the ASU Setup2. The two electrodes are placed in the lower part of the holder and are fixed by a screw. The lower end of the screw is attached via a loaded spring to a plate that provides the electrical contact with the one electrode. The spring-loaded plate ensures that the Teflon spacers and the liquid are not squeezed while the screw is tightened and that the stress-field on the Teflon ring is temperature insensitive.

measured by a Novocontrol Quatro controller. The stability of the temperature reading is better than 0.05 K.

The empty sample capacitor in the measure cell was used as reference in order to calibrate the frequency-dependent trans-impedance $Z(\omega)$ of the amplifier and to compensate for capacitor holder inductance, capacitance and resistance. The following liquids were measured on this setup: N-ε-methyl-caprolactam (99%, nMC, Fig. **??**), dipropylene glycol dimethyl ether ($\geq$ 98%, DPGDME, Fig.**??**), di-*iso*-butyl phthalate (99%, DisoBP, Fig. **??**) and 2-ethylhexylamine ($\geq$ 98%, 2EHA, Fig. **??**). 2EHA's spectra shows a shoulder at low frequencies, that had not been observed at previous measurements. This is a dielectric fingerprint of eventual chemical decomposition. The mixture of old and new components show a new dynamics – here double loss peak. Tetramethyltetraphenyltrisiloxane (DC704, Dow Corning 704® diffusion pump fluid) was also measured on at this setup, but it turned out that the cell was not appropriate for this liquid. The liquid wetted all the surfaces no matter how carefully

the sample was prepared and obtained dielectric spectra did not contained any meaningful information.

High pressure setup - Silesian University

The high pressure dielectric data are obtained from the Paluch group. The setup principal is described in [132]. On the same experimental setup the high pressure measurements of DC704 are measured by the author in the laboratory at Silesian University, Katowice, Poland. For high-pressure measurements a pressure system constructed by Unipress (High Pressure Research, Poland) is used. The liquid was placed in a special home-made parallel capacitor (See in Fig. 3.7, presented latter in the text.). The pressure chamber is basically a cylinder closed from both sides (See in the lower figure in Figure 3.6). From the top a pressure stopper is mounted (screwed in). This serves as a measure cell holder. Coaxial wires which provide the electrical connection between the sample cell and the measuring device go through the stopper. The sample was soldered to the electrical connections inside the pressure chamber. An impedance analyzer was connected to the external electrical connections via a BNC (Bayonet-Neill-Concelman) type coax connector. The dielectric permittivity of the capacitor with the sample was measured with Novo-Control GmbH Alpha dielectric spectrometer with a range $10^{-2} - 10^7$ Hz. From the bottom part a pipe coil that circles the high-pressure chamber is connected to a thermostatic bath which cools the chamber by a liquid flow, i.e. a temperature stabilization and control within 0.1 K is achieved by means of a thermostatic liquid flowing from the thermostatic bath and circulating through the pipe coil and back to the bath. Both the chamber and the thermostatic coil are thermally insulated from the environment. The temperature was set manually from the thermostat-bath control panel, and the temperature inside the chamber was measured by and was noted before and at the end of a frequency scan. From the bottom side of the pressure chamber a capillary is connected which allows the pressure medium to flow inside and out of the chamber. The compression on the sample is exerted by a pressure-transmitting liquid that is 'injected' via a hydraulic press (See in Fig. 3.6 the hydraulic connections are marked with dashed lines). In the hydraulic press the pressure-transmitting liquid is pressurized (by use of a piston) and transmitted via capillary to the pressure chamber. A valve ensures that no back flow of transmitting liquid occurs. The valve furthermore separates the liquid in hydraulic press from the chamber. To ensure full separation the valve is closed and one can change the pressure inside the press without causing a pressure change inside the pressure chamber. This allows one to fill up the piston with pressure-transmitting liquid. [4] Inside the valve is a sensor that gives input to a pressure meter that gives the pressure inside the capillary which is connected to the pressure chamber. Since it is in direct contact with the electrical

---

[4]The chamber volume is larger than the piston volume. If the chamber is totally empty then, with advantage, a pressure-transmitting liquid can be poured into the chamber.

impedance analyser

F [Hz], C [pF], R [Ω]

pressure metre

MPa

hydraulic press

PC

high-pressure chamber

T[K]

tensometric sensor

liquid bath

valve

Wires to measure device

Pressure chamber

Sample cell

Thermostating jacket with circulating cooling liquid

Capillary for pressure transmitting fluid
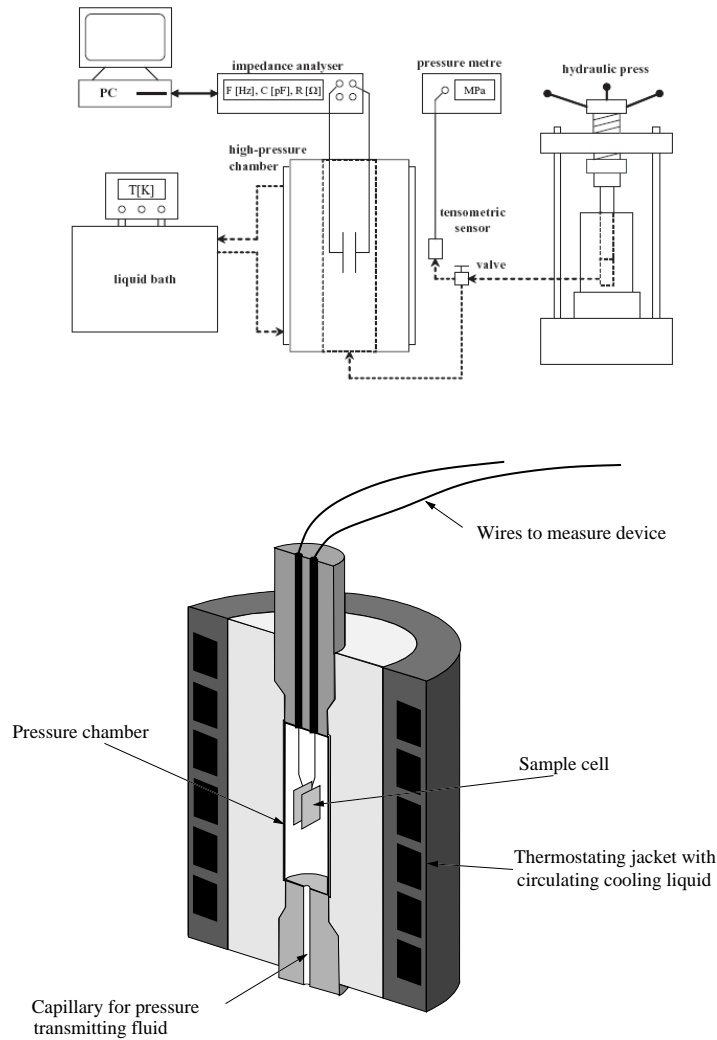
Figure 3.6: Upper: Schematic presentation of the high pressure setup at Silesian University, Katowice, Polland. Hydraulic connections are denoted by dashed lines and electrical connections by solid lines. From [132]. Lower: Scematic scetch of the insulated pressure chamber with dielectric sample cell. The separation of the sample cell and the transmitting liquid is not on sketch.

connection to the capacitor electrodes and is object to compression and cooling, the pressure-transmitting liquid must have some qualities. It has to be nonpolar, noncorrosive to metal, and maintain a low viscosity at low temperatures and high pressures.Thus, one it is necessary to know the glass transition line (p_g, T_g) for it in order to avoid that it solidify itself. The transmitting liquid is a silicon oil (consisting of perflourinated alkanes) and is suitable for measurements at pressures up to 1.8 GPa and temperatures close to room temperature. If measurements at higher pressures and lower temperatures must be performed then the silicon oil can be mixed with alkanes such as heptane. Since the capacitor with the sample is embedded in the pressure-transmitting liquid, it is physically separated by a thin Teflon film that acts like a flexible membrane. The simplest parallel-plate capacitor used for the high pressure dielectric measurements is shown in Figure 3.7(a). An analogue to the capacitor used for measurements at ASU setup but without a holder. It consists of two round stainless steel electrodes with diameter of 20 mm separated by one 0.1 mm thin Teflon ring. The sample liquid is placed into the Teflon ring and the two plates are wrapped in Teflon film and hereby sealed and afterwards mounted inside a stiff Teflon ring with a thickness that corresponds to the hight of the two plates. This ring serves as a frame or holder for the electrodes and ensures that the pressure-transmitting liquid does not squeeze the sample liquid in radial direction and shear it. The plates are mounted to the electrical connections with screws. This construction is suitable for measurements of samples of relatively polar liquids or chemicals that are crystals at room temperatures and has to be melted into the capacitor. One measurement of DC704 was performed with this capacitor, but it is not suitable for measurements of this liquid because of the relatively low dipole moment of the molecule and a pressure insensitive DC contribution to the loss was observed. Furthermore the sealing does not necessary provide good insulation due to DC704 quality as silicon pump oil with very low surface tension. The dielectric scans included the theses are made with the second home-made capacitor, which is shown in Figure 3.7.

This capacitor consist of two parallel parts of the steel cylinder, separated by Teflon strips[5] and kept together by two Teflon rings (not drawn on the schematic presentation in Figure 3.7(b). The capacitor is placed inside a Teflon barrel filled up with the sample liquid and connected to the pressure stopper. This measure cell needs much more sample liquid than the previous one but is better separated from the pressure medium.

The experimental procedure for high pressure dielectric scans at isothermal

---

[5]In some measurements spacers made of a more rigid material than Teflon such as quartz can be used, but the problem with this is that it can be crushed and, besides, quartz has ion conductivity by its self [150].
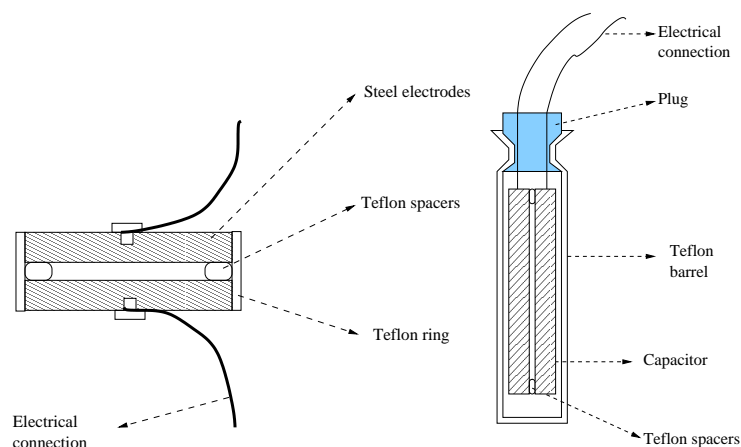
Figure 3.7: The capacitors used for the high pressure dielectric measurements. (a) Parallel-plate capacitor with Teflon ring as spacer. This cell is wrapped in Teflon film i order to separate the sample liquid from the pressure-transmitting liquid (b) Parallel-plate capacitor encapsulated by a Teflon container. The container is tightly closed.

conditions for DC704 is as follows: Firstly the sample was compressed at room temperature to 40-50 bars above the wished pressure. The valve was closed. With compression the temperature in the chamber rises. It was thus necessary to wait two-three hours in order for the temperature in the high pressure chamber to stabilize.

A dielectric frequency swap was started from the PC. The temperature and pressure were noted at beginning and end of the scan.

After measurement ceased the pressure in the chamber was slowly raised manually. This was done in two steps: Firstly before opening the valve an overpressure in the capillary and the press is ensured. This is done to avoid a pressure drop when the pressure-transmitting liquid flows back driven by the difference of the pressure on the both sides of the valve. One side is at the pressure in the chamber and the other is at atmospheric pressure. The second step is to increase the pressure slowly. Afterwards it was again necessary to wait for thermal equilibration before taking a measurement. To ensure that the sample was in true thermal equilibrium the dielectric response was monitored at short frequency intervals until the data curves were on top of each other. Then the scan was started. The procedure was repeated with pressure changes of around 100 bars until the desired number of scans at different pressures were obtained. All the high pressure measurements at different temperatures are done with the

same sample.

The temperature was decreased. This resulted in a pressure drop which was convenient, because the relaxation at the new T, P-point had loss peak frequencies close to high frequency part of the scan window.[6]

The system that is temperature controlled consists of the sample liquid, the condenser, the Teflon membrane and the pressure-transmitting liquid. The system is relatively big and thus the thermal relaxation time is relatively long. Besides, the waiting time for equilibration depends on the temperature rate of the thermostatic bath, the temperature inside the chamber and the pressure change rate. The thermal insulation of the system causes the temperature rise, when pressure is increased. The temperature change depends on the pressure difference. If one wants the isothermal condition maintained then the compression rate must be so low that the rate of the resulting temperature rise is comparable to the thermostatic cooling rate. When the pressure-transmitting liquid flows into the chamber it is at room temperature. Thus in this way one imports heat into the system if the experiment is performed at lower temperatures. The effect of this heat can be countered by employing a slow, but time-consuming compression process. So long as one is dealing with an equilibrium metastable liquid the lack of ideal isothermal conditions should not give rise to considerable structural re-arrangement due to the decreased viscosity of the sample liquid caused by the temperature rise. However it is necessary to squeeze the sample slowly and continually in order to avoid breakage in the Teflon membrane which separates the sample and pressure-transmitting liquid. The origin of DC-conductivity in the relaxation spectra is the charge carriers (ions) of impurities in the sample liquids. Thus, sudden qualitative change in the DC-conductivity contribution to the imaginary dielectric relaxation indicates that the Teflon film or container has broken.

On the same sample measurements were performed on DC704 at $T = 253$K $p \in [6; 2460]$ bar, $T = 263$K $p \in [1333; 2404]$ bar and $T = 283$K $p \in [2559; 2404]$ bar. The measuring took weeks and the liquid stayed at a specified temperature and pressure for 13 hours with no observed changes to the spectral shape. Thus, no breakage in container appeared under the measurements. In this setup 2,3-epoxypropyl phenylether was also measured, but it crystallized. When determining the complex ε'' it is assumed that the geometric capacitance of the measure cell is nearly constant. However Teflon contracts at low temperatures, and in addition the Teflon spacers can be deformed mechanically under compression and become thinner. This results in an decrease in the distance between the electrodes or a change in the actual value of the empty capacitance. This can be seen clearly in plots of the real part of of the dielectric constant as

---

[6]It is also possible to perform a procedure, where the pressure is decreasing.

a change in the value of the low and high frequency limits of the real dielectric response, ε_s respectively ε_∞. Changes in spacer thickness of 0.01 μmIn give a relative change of ε_s changes of 1%. The problem cannot be solved by a reference measurements, because the compression induced distance change depends on the viscosity of the liquid as well.

Chapter 4
Data analysis

4.1 Data choice

The aim of this work was to find trends in the shape of the primary relaxation that are general for glass-forming liquids. Thus great care has been taken to make an unbiased procedure for the analysis and selection of data. (In this section I will describe the choices that were made to ensure this.)

The library of dielectric data sets includes data for organic liquids, plastic crystals and polymers. However, the nature of glass transition is different for these materials, and thus some exclusions prior to the analysis was made: Polymers were omitted from the analysis because the polymer glass transition is not a liquid-glass transition and the primary relaxation observed in polymers is a segmental relaxation. Plastic crystals were excluded because their primary relaxation is due to orientational degrees of freedom of translationally ordered molecules [4] rather than a structural relaxation. No prior selection based on chemistry was made with one exception: all simple monohydroxy alcohols were excluded because these liquids exhibit a (strong) Debye like peak in dielectric spectroscopy (slower than the genuine α structural) which is not related to the calorimetric glass temperature or the structural relaxation [144, 61, 146].

The 87 remaining data sets, are measured on different experimental setups and therefore they differ in frequency-windows and in number of measurement points per decade. To make meaningsful comparison of the information extracted from the raw data, one important assumption is made: Namely, all measurements are done on thermally equilibrated systems and experimental setups with the nearly same absolute temperature calibration.
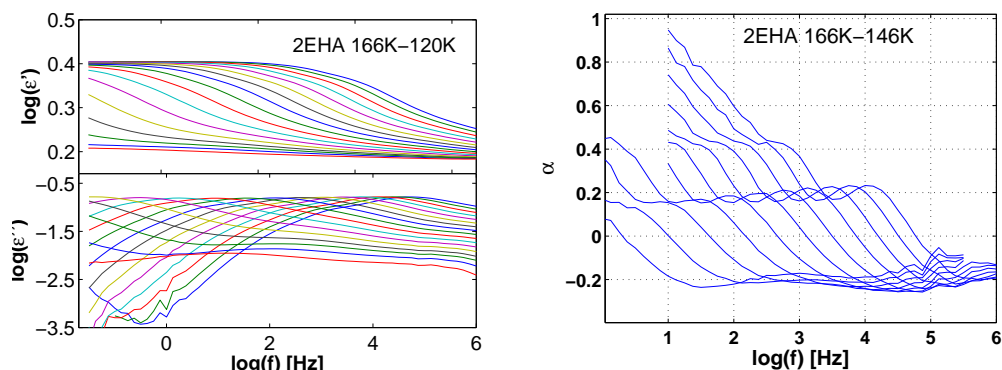
Figure 4.1: 2-ethyl-hexyl-amine dielectric scan made on ASU Setup2. It is clear that the shoulder on the low-frequency is due to chemical degradation especially this is well seen in the slope.

Multiple data sets for the same liquid

In the data base generated for this work there are multiple data set for some liquids measured by different groups. In these cases there are two possibilities: either the sets were combined (such that they compliment different frequency intervals), or one of the datasets were chosen (if the data sets covers the same temperature and frequency interval).

Both solutions are based on the the assumption also mentioned above, that the dielectric responce is measured in the equilibrated viscous liquid regime, and thus the dielectric dispersion should have the same relaxation time at one temperature (regardless of the where the data were generated).

The first option was applied only for the liquid Decahydroisoquiline (DHIQ). There were three different data sets for this liquid. One was measured by Jakobsen et al [67] (RU Setup), one was measured by Richert et al [129] (ASU Setup2) and the last was measured by the Paluch group, but unpublished. (Part of the scans from the three sets are in Fig.4.2)

From the plot in Figure 4.2 of the dielectric loss it is obvious that the data set from SU differs the most from the other two sets both in spectral shape and temperatures. There are two possible explanations for this. First of all, DHIQ chemically reacts with air and it is possible that the liquid was exposed to air that under the preparation or measurement procedure. Thus the liquid may deviate from the other two chemically. This would also explain the deviation in the shape, absolute loss amplitude and temperature dependence of the loss. The second explanation for the discrepancy is a possible difference in the ab-
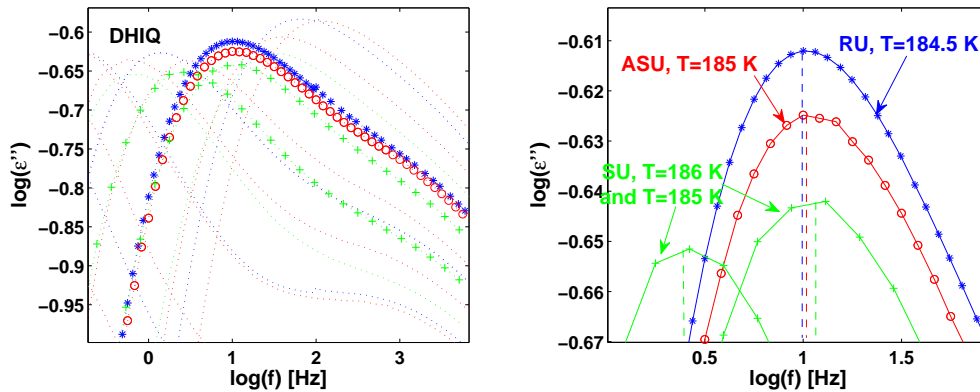
Figure 4.2: DHIQ dielectric scans from the three different datasets Jakobsen et al [67] (RU Setup, blue), from Richert et al [129] (ASU Setup2, red) and unpublished dataset from the Paluch group (SU Setup, green). The emphasized curves' loss peaks are show on the left plot. The chosen (raw data) curves have close loss peak frequencies But the temperatures are different: RU setup $T = 184.5$ K, ASU setup $T = 185$ K, and SU Setup at temperatures $T = 185$ K and $T = 186$ K. Besides this, it is air reactive.

solute temperature calibration of the three setups. DHIQ is rather fragile and in the temperature interval around 185 K the loss peak frequency changes approximately half a decade per 1 K. The temperature difference between the RU and ASU dataset is 0.5 K while the frequency distance between the maximum absorption is roughly 0.1 decades and not the expected ~ 0.25. We can conclude that the deviation in absolute temperature in these two setups is less than 0.5 K (assuming that the liquid is handled almost in the same way). Thus, suitable scans from the ASU and RU datasets complimented each other in the data analysis of DHIQ and the SU data set was discarded.

In Figure 4.2 the curves from the different dataset are presented with different number of measure points per decade – RU with 16, ASU with 13 and SU with 6 points per decade. This dissimilarity is used to state another requirement to the multiple data sets regarding the situation where two or more datasets are made in the same temperature intervals: The dataset with the densest frequency scans were chosen. No new information was obtained by weaving the sets together and solve the problem with deviations that results from different setups and procedures or systematic errors.

Selection within one data set

Prior the analysis no changes in the dielectric spectra was made like removal of points in the interesting frequency intervals. The investigation in this work is based on model free analysis by use of an automated algorithm, where the loss peak frequency, and amplitude are found, as well the minimum slope. Nummerical differentiation makes it extremely important that there be as little noise as possible. For the analysis it also crucial that the frequency scan contains a very well defined loss peak with at least 3 points on the low frequency side. Furthermore, the high frequency wing should contain enough points so that the minimum slope (explained below) is well defined. At least two temperature scans for each liquid is required for the analysis.

From the spectra measured at the RU setup we removed the points around 100 Hz because of the systematic error due to the mechanical switch and the LCR-meter. If a nick was detectable in the loss peak this scan was removed from the analysis (See in 3.1). All other data sets were used as measured, or received from the different groups. If there were two dataseries for the same chemical was chosen the series with the highest measure-points density.

Following the basic philosophy of analyzing the raw data directly, no attempts were made to subtract contributions from the DC conductivity and no attempts were made to subtract contributions from β relaxation(s). This procedure is fundamental for the approach of this work. Thus while one may argue what is the correct way of compensating for these and possibly other interfering effects in order to isolate the "true" α process, it should be much easier to reach consensus regarding the raw data themselves and their properties.

4.2 Minimum slope

If we recall, the minimum slope, α_{min} was defined as the minimum value of the slope in the log-log plot of the dielectric dispersion frequency scans at frequencies higher that the loss peak frequency. The slope is given by $\alpha = (d \log \varepsilon'')/(d \log(f))$. Since data are discrete quantities, a numerical differentiation gives the slope

$$\alpha = \frac{\Delta \log(\varepsilon_i'')}{\Delta \log(f_i)} \tag{4.1}$$

Figure 4.3 presents three examples of the high-frequency dielectric constant scans and the corresponding slopes at different temperatures for a particular liquids DPGDME, $T = 139$ K.

The slope is zero at the loss peak frequency f_{max}. The high frequency dispersion has a negative slope and thereby in the interval of the slope values, among
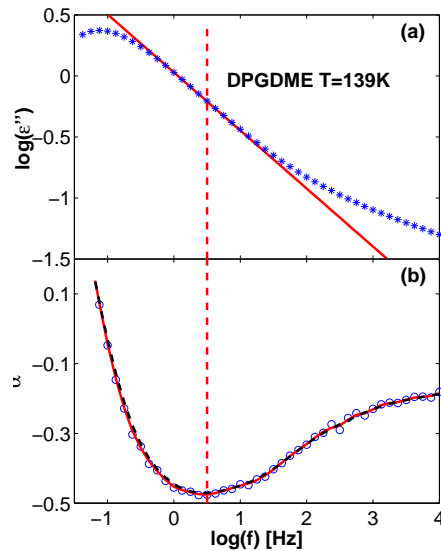
Figure 4.3: An examples of the dielectric loss frequency spectrum in double logarithmic plot (the upper panels) and the double logarithmic slope, α, obtained from numerical point-by-point differention dipropylene glycol dimethyl ether (DPGDME) at $T = 139$ K

which the minimum slope α_{min} is, are only negative numbers. To ensure that the minimum slope is defined at the inflection point at true minimum in the slope curve is needed. Thus, corresponding slopes some of the dissipation curves in the high frequency part of the sets are removed from the analysis if they were cutted of the edge of the experimental window before at least three-four points shows an increase in the slope values. In this way some of spectra at the highest temperature are removed from many datasets.

As we can see in Fig. 4.3 the quality of the data varies in how noisy they are. If the noisy data are omitted the left data collection suddenly shrinks notable. Like a compromise between the data quality and number of liquids in the analysis a smoothing, more precisely an averaging, procedure was applied to the slope data. The procedure is kept rather simple – the new set of slope consisted of points that each is an average over two neighboring points. If the numerical derivative is still too noisy, the smoothing procedure is applied to the averaged data. The number of iteration varies but it is kept under ten. This number is decided because after more averages the curves changes noteworthy.

On Figure 4.3 is shown the result of different number of times the average procedure was applied. As a means to increase the reliability of the α_{min} estimate we applied averaging. Thus the noise in the numerical derivative was reduced by using a simple routine that averages over two neighboring points (compare with Fig. 4.3(b)). The number of times this averaging procedure was applied varied with the data set, but was always kept below ten. For the data in Fig. 4.3(b), for instance, a double iteration of the averaging routine was used, but as an illustration the black dashed line shows the result if averaging was instead applied ten times. If averraging ten times changes α_{min} more than 0.01, the data set was discarded. Subsequent applications of the smoothing procedure result in numerically slightly smaller values of the minimum slope, but this is never a serious problem. If the resulting curve after a maximum of ten averagings was still too noisy, the frequency scan was discarded.

Moreover, data sets were only included if there is so little noise in the resulting slopes, that data allow for a determination of α_{min} with two significant digits. These selection criteria imply that several frequency scans at high temperatures, as well numerous noisy data sets, were omitted from the data analysis.

This procedure left a total of 53 liquids of an initial collection of 84 liquid. The number of frequency scans (temperature) for each liquid varies between 2 and 17. Altogether 347 minimum-slope values that are in the interval from -0.751 up to -0.101.

The result is shown in Figure 4.4. The histograms shows the minimum slope distribution for the 53 liquids in two histograms of different resolutions. Or, what part of the α_{min}-observations lays in different partitions of interval of α_{min} $- [-1; 0]$. The subinterval width in Figure 4.4 (a) is with length of 0.1 while in (b), is 0.5. Each minimum -slope observation was divided by the number of scans, that the particular liquid participates into the analysis, N (takes value from 2 up to 17), and the total number of liquids, ($n = 53$). In this way all observations are weighted and the hight of the bars gives the proportion of minimum-slopes values within a subinterval.

Both histograms shows a prevalence of minimum slopes around $-1/2$. Almost the half of the all liquids have minimum slopes between -0.6 and -0.4. Even in the subinterval from -0.525 to -0.475 are double as many liquids as in the second most well represented α_{min}-subinterval $[-0.475; -0.425]$. Until now nobody reported such prevalence of the value that corresponds to a dielectric relaxation function with $\omega^{-1/2}$ or $\sqrt{t}$. The natural question, that one can ask is, what is the significance of this result? Is it related to the primary process?
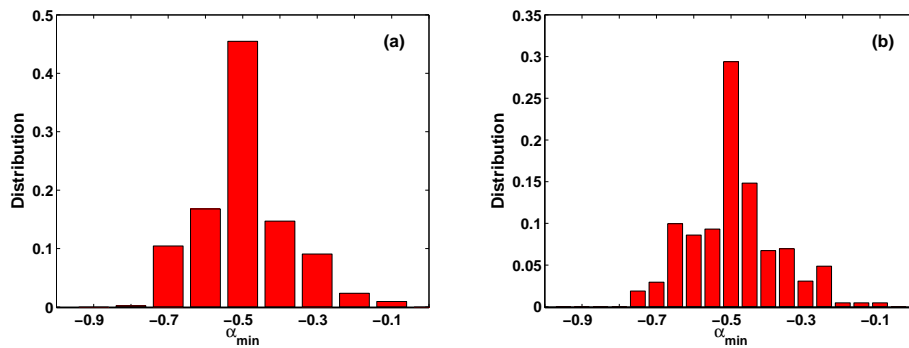
Figure 4.4: (a) Histogram of the minimum slope distribution for all included dielectric data for the 53 liquids, using subinterval width of 0.1. The most frequently observed values of α_{min} lies between -0.45 and -0.55. This implies prevalence of approximate $\sqrt{t}$ relaxation. (b) Histogram of the same data but the observation α_{min} subintervals have length of 0.05. Almost one third of the minimum slopes are between -0.525 and -0.475. Since the number of α_{min}-values is different (from 2 to 17), in both histograms in order to give all liquids equal weight, each minimum slope value was given the weight $1/N$ if the liquid in question has N spectra included in the analysis.

Minimum slope as a shape parameter of the α high frequency relaxation?

As already described in section 2.3 the dynamics in the relaxation processes is very complex, since often the relaxation is consisting of several process, which merge and separate depending on their time scales of and the way they slow down with temperature decrease. The influence of the secondary process on the spectral shape of the primary relaxation can be significant. The minimum slope concept does not need any assumptions concerning how α and β processes interact, if a excess wing is a β process, etc. but it intrinsicly contains informa-
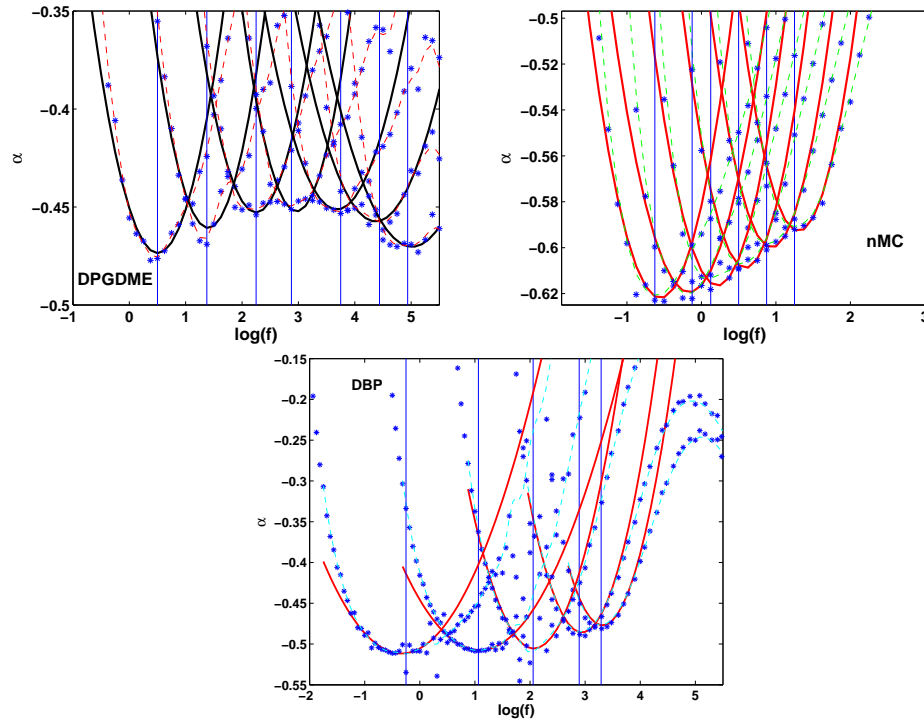
Figure 4.5: Illustration of the procedure where the thirdth derivative is estimated from the second order polynomial (red full drawn curve) through point $[f_{\alpha_{min}}, \alpha_{min}]$ (marked by the vertical straight line) of the averaged slope data (dashed line). The stars are the points from the point-by-point numerical differentiation of the dielectric dissipation in log-log plot. The examples are Dipropylenedimethyl Glycoldimethylether (DPGDME, right), n-Methylcaprolactam (nMC, left) and Dibutyl Phthalate (DBP,lowest)

tion about the β process. The inflection point $f_{\alpha_{min}}$ is just the place where the one process takes over. But if the separation between the two processes is big enough then the minimum slope estimates the high frequency decay of the of primary process.

In order to investigate if the slope $\alpha = -1/2$ describes, one can analyze the range of the frequency region around the inflection point $\log f_{\alpha_{min}}$, where the tangent with slope α_{min} gives a good approximation of the high frequency relaxation, i.e. if $\varepsilon''(\omega) \propto 1/\sqrt{\omega}$ is the generic high-frequency α behavior, while deviations comes from interference of other relaxation processes.

To get this information mathematically one can use a simple function analysis of the double logarithmic dielectric dissipation, $H(f) = \log \varepsilon''(\log(f))$. The functions are smooth and around $\log(f_{\alpha_{min}})$. By Taylor's thirdth order approximation for the imaginary part as function of $\log(f)$ in the neighborhood of $a = \log(f_{\alpha_{min}})$ gives:

$$
\begin{aligned}
H(x) &= H(f_{\alpha_{min}}) + H^{(1)}(f_{\alpha_{min}})(\log(f) - a) + \frac{H^{(2)}(f_{\alpha_{min}})}{2!}(\log(f) - a)^2 \\
&\quad + \frac{H^{(3)}(f_{\alpha_{min}})}{3!}(\log(f) - a)^3 \\
&= H(f_{\alpha_{min}}) + \alpha_{min}(\log(f) - a) + \frac{H^{(3)}(f_{\alpha_{min}})}{6}(\log(f) - a)^3, \qquad (4.2)
\end{aligned}
$$

where the first derivative $H^{(1)}(f_{\alpha_{min}}) = \alpha_{min}$ and second order derivative $H^{(2)}(f_{\alpha_{min}}) = 0$ by definition of the inflection point. By Taylors Theorem α_{min} the best approximation is the tangent through the inflection point at $\log(f_{\alpha_{min}})$, if the reminder $\frac{H^{(3)}(f_{\alpha_{min}})}{6}(\log(f) - a)^3$ is negligible.[1] Or with other words the frequency range

---

[1] In fact the same art of unction analysis we can get from the graph of the double logarithmic slope of the dielectric dissipation, α. The functions are smooth and around $\log(f_{\alpha_{min}})$ are the values bigger than or equal to α_{min}. By Taylor's second order approximation for the slope as function of $x = \log(f)$ in the neighborhood of $a = \log(f_{\alpha_{min}})$ gives:

$$
\begin{aligned}
\alpha(x) &= \alpha(a) + \alpha^{(1)}(a)(x - a) + \frac{\alpha^{(2)}(a)}{2!}(x - a)^2 \\
&= \alpha_{min} + \frac{\alpha^{(2)}(a)}{2}(x - a)^2,
\end{aligned}
$$

where the first derivative is $\alpha(a)^{(1)} = 0$ per definition of the inflection point. By Taylors Theorem α_{min} is the best approximation in the neighborhood of $\log(f_{\alpha_{min}})$ if the reminder $\frac{\alpha^{(2)}(a)}{2}(x - a)^2$ is negligible, or just if $\alpha^{(2)}(a) \to 0$.

of $\omega^{-1/2}$ relaxation grows if $H^{(3)}(f_{\alpha_{min}}) \to 0$. The smaller this number is, the better is the inverse power-law fit.

The thirdth derivative one recognizes as the curvature of the graph the double logarithmic slope of the dielectric dissipation, α, in $\log(f_{\alpha_{min}})$

$$\kappa = \frac{1}{R} = \frac{\left|\alpha^{(2)}\right|}{(1 + (\alpha^{(1)})^2)^{3/2}} = \left|\alpha^{(2)}\right|, \tag{4.3}$$

where $\alpha^{(1)} = H^{(2)}(\log(f_{\alpha_{min}})) = 0$ and $\left|\alpha^{(2)}\right| = H^{(3)}(\log(f_{\alpha_{min}}))$. This gives a solution to problems with noise when a numerical point-by-point differentiation of the slope α is made: The curve around $\log(f_{\alpha_{min}})$ is approximated with a second order polynomial (see for several examples in Figure 4.5). The number of points in the fitting interval depended on the measured point density and on the symmetry of the neighborhood of this frequency; we used between five and seven points in the fitting intervals and is kept constant for all curves within one liquid data set when the MatLab routine was applied.

Figure 4.6(a) shows the result of the investigation in the plot $\left|H^{(3)}\right|$ versus α_{min}. We note two things. First, there is no clear tendency that the power-law approximation works particularly well for liquids with minimum slopes close to $-1/2$. However, there is a tendency indicated by dashed lines that, conversely, if one requires the power-law approximation to work well, minimum slopes tend to be fairly close to $-1/2$. To summarize, this confirms a special status associated with liquids with $\alpha_{min} \cong -1/2$.

The temperature dependence of $\left|H^{(3)}\right|$ indicates that a majority of the liquids' relaxations decreases with temperature fall (see in Figure)4.6(b)). These dielectric dissipation scans have one or two fast secondary processes above 10 Hz. when the scan is taken under the α-β merging temperature the two processes separates. This is captured by the curvature in the slope graph. It is obvious that it flatters with time scale separation of the primary and secondary processes. Unfortunately the noise in the estimated values of $\left|H^{(3)}\right|$ makes impossible a firm conclusion. Thus the information from the thirdth derivative has to be compared with the temperature dependence of the minimum slope.
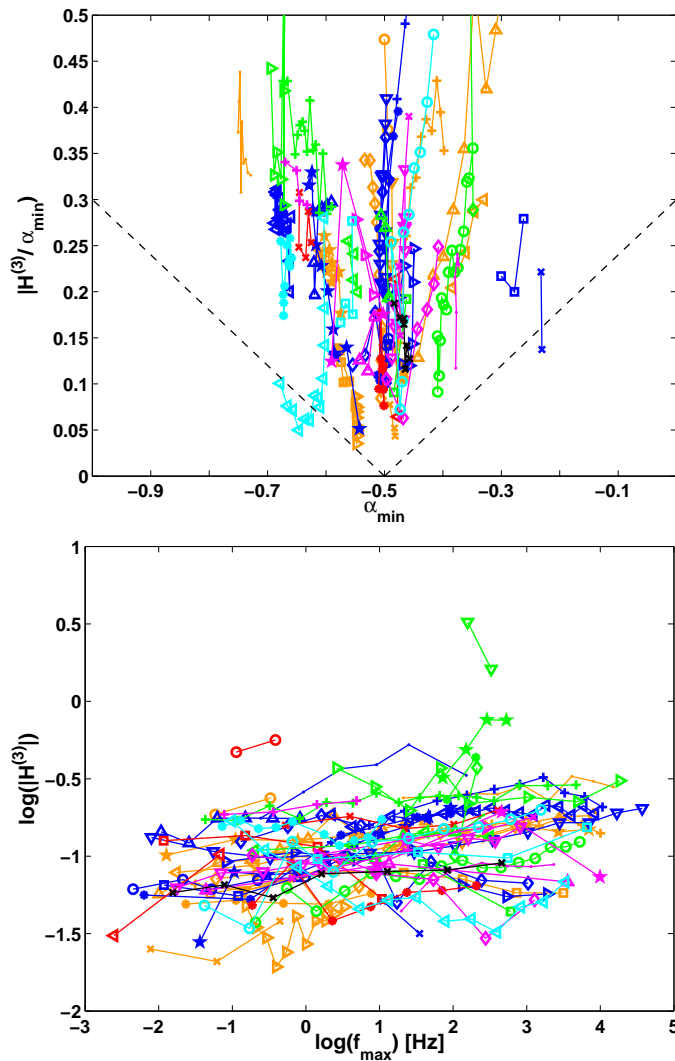
Figure 4.6: A measure of how well the inflection point inverse power-law approximation applies ($\left|H^{(3)}\right|$) plotted versus minimum slope (the upper plot). The black dashed lines are guides for the eye. Every liquid data set is presented with the color and symbol listed in table A.1. And $\left|H^{(3)}\right|$ versus the loss peak frequency that gives implicit the temperature dependence (the lower plot). With a few outliers there is a tendency that liquids where the inverse power-law approximation applies particularly well have minimum slopes α_{min} close to $-1/2$, as well the main trend is that the curvature decreases with cooling the liquid.
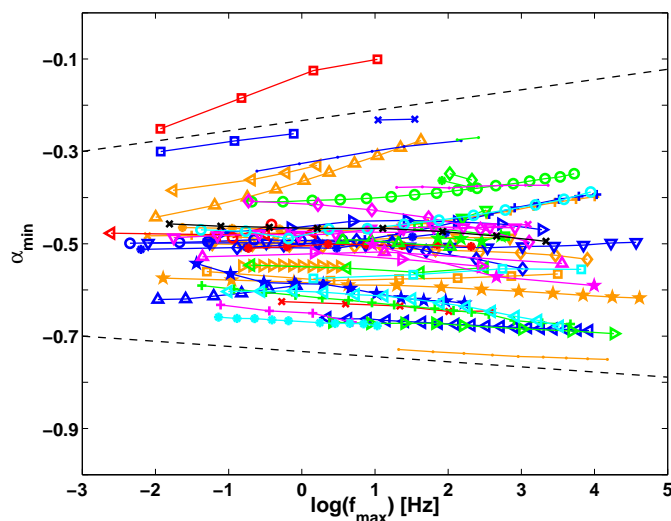
Figure 4.7: Plot of the minimum slope α_{min} versus loss peak frequency f_{max}. There is a tendency that minimum slopes approach $-1/2$ as temperature is lowered; the dashed lines are drawn as guides to the eye.

An eventual α-β time scale separation can be detected mostly as a decrease in α_{min}-values for minimum slopes at high temperatures that are above -0.5. This it can be seen in Figure 4.7, where the minimum slope is plotted against the loss peak frequency, f_{max} for liquids' relaxation with well defined β process. Since all dissipation loss spectra are within the same frequency interval, to plot a given quantity as function of the loss peak $f_{max} = f_{max}(T)$ is a convenient way to express the temperature dependence of the quantity in order to compare the evolution of it with temperature change without scaling procedures.

Figure 4.7 shows the results in the investigation of the minimum slope changes upon cooling. Minimum slopes are only weakly temperature dependent, but there is a tendency (with some exceptions) that liquids with minimum slopes numerically larger than $1/2$ have minimum slopes that decrease numerically as temperature is lowered, whereas for liquids with minimum slopes numerically smaller than $1/2$, $|\alpha_{min}|$ tends to increase or the loss peak increases. The dashed lines in the figure are drawn to indicate this overall tendency.

If one looks into the data a more complex world is appearing because the minimum slope is intrinsic connected to the secondary processes.

From a certain frequency nearly a constant minimum slope values are observed for the following liquids: 2-methyltetrahydrofuran (MTHF, blue $\triangledown$),
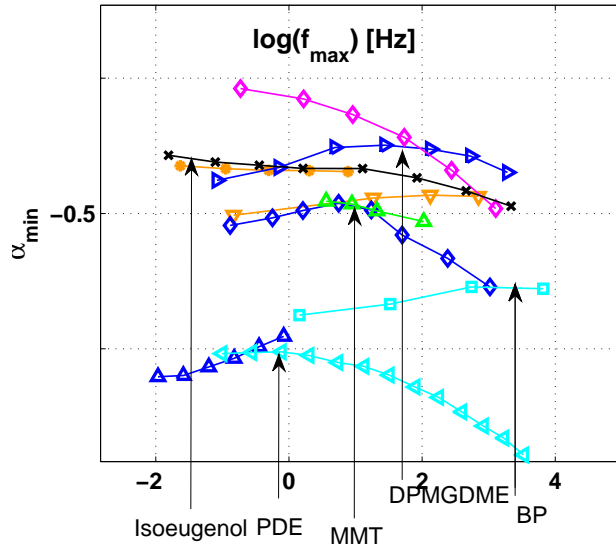
Figure 4.8: An excerpt from the plot in Figure 4.7, where the minimum slope $\alpha_{min}(f_{max})$ shows a maximum. This maximum can be explained as the merging of the α_{min} and a loss peak of a secondary process with relatively low magnitude, i.e. $f_{\alpha_{min}} = f_{max}^{\beta}$. The relaxation time for the β dispersion is marked by arrows to the respective α_{min} curves.

DBP (blue $*$), DEP (blue $\circ$), DOP (orange $\diamond$), 5-polyphenyl-ether (PPE, red $*$), tetraphenyl-tetramethyl-trisiloxane (DC704 red $\triangleleft$), triphenyl phosphite(TPP $\times$) and 4-methyl-heptane (4MH, green $\star$). The slope of these liquids is close to $-1/2$. They all have either a β relaxation loss peaks above 10^5Hz or no beta relaxation is observed within the experimental window.

The liquids with well revealed secondary process with relatively high amplitude like 4,7,10-trioxatridecane-1,13- diamine(TOTDD $0.33; 0.38$ $\triangleleft$) toluene-pyridine mixture (TolPyr, $\triangle$), sorbitol (blue $\square$) and DHIQ (red $\square$), as well as Xylitol ($\bullet$), 3-methylheptane (3-MH, green $\bullet$), TODDA ($\triangleleft$) shows an decrease in the alpha minimum value when the system dynamics slows down.

For some glass formers like methyl-m-toluate MMT (blue $\diamond$) α_{min} increases above $-1/2$, but eventually approaches $-1/2$ as temperature is further decreased. This presumably reflects the merging of α and low-intensity β processes that one observes for scans at temperatures below T_g. MMT has a secondary process in the range $10 - 100$ Hz (see in Appedix **??**) In Figure 4.8 some liquids' α_{min} which have a high frequency, hidden secondary relaxations are

plotted. For example a β process around 10 Hz is rapported for dipropylene-dimethylglycol-dimethylether [48] (DPGDME ▷), 0.1 Hz for phenolphthalein-dimethylether (PDE ◁) [74] and 10^4 Hz for Benzophenone (BP □) [90]. In the raw data spectra in the appendix **??** some of the liquids have a detectable β processes like nPB 10^4 Hz (all frequencies are marked in the same figure). The minimum slope monotonic changes indicate low intensity β processes.

Some hidden intermidate β process are recognized like an increase followed by decrease in the α_{min}. The frequency where α_{min}-maximum probably corresponds to $f_{\alpha_{min}} = f_{max}^{\beta}$ (f_{max}^{β} is the loss peak frequency of the secondary process).

This phenomenon is also observed for glassformers with $|\alpha_{min}| > 1/2$ PG (blue ◁), nMC (blue △ there are two secondary processes with f_{max}^{β} (around 100 Hz and 0.1 Hz, respectively) and propylene carbonate (PC, red ×). This liquids' α_{min} values are not graphed in Figure 4.8

In summary, there is a tendency that minimum slopes to slowly approach $-1/2$ as temperature is lowered. It would be interesting to have lower temperature observations, but it is not realistic in the foreseeable future to extend observations to significantly lower temperatures and frequencies to get an insight in the further dissipation shape evolution. The minimum slope decreases with temperature, but if there is an intermediate low intensity β process then it is detected from a small maximum in the α_{min}. When the β relaxation loss peak is passed by the inflection point then the minimum slope decrease again. The β process induced curvature in the α_{min} depends on the magnitude of the secondary process. The high intensity secondary relaxations affect mostly α_{min}.

How does minimum slope relate to the shape parameters determined from fitting functions?

In order to compare the found minimum slopes and the shape parameters of two of the most used fit functions (CD and KWW) one need another shape parameter, namely the width of dispersion spectra or more precisely the width a half loss peak in decades.

Half width at half loss peak

As allready mentioned the spectral shape is characterized by a low frequency decay with slope one. Besides, the low frequency part of the dissipation is not compensated for the DC contribution. Thus in order to be able to make a comparison between the fitting functions and the experimental relaxation spectra. For this reason the width at half dispersion maximum is redefined as follows: the *half width at half loss peak*, $W_{1/2}$, as the number of decades of frequency from
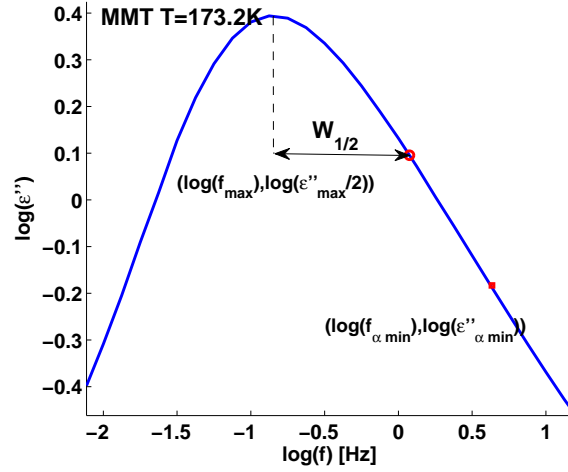
Figure 4.9: The half width at half maximum in decades is marked at the dielectric relaxation for the liquid methyl-*m*-toluate (MMT).

the loss peak frequency to the right of the loss peak frequency until the loss is halved (if $f_{1/2} : \varepsilon''(f) = \varepsilon''_{max}/2$ then $W_{1/2} = \log(f_{1/2}/f_{max})$) This is illustrated at Figure 4.9.

To give some information about the deviation of the relaxation from single exponential function, this number is normalized with respect to the half Debye width on log scale, $W_{D/2} = W_D/2 = \log(2 + \sqrt{3}) \approx 0.571$. Thus, the normalized half width at half loss peak (HWHM) is defined as follows:

$$w_{1/2} \equiv \frac{W_{1/2}}{W_{D/2}}. \tag{4.4}$$

In most experiments the primary relaxation is wider than Debye. Therefore, $w_{1/2}$ is always above unity. The Debye like spectral shape is charactered with HWHM is close to one ($w_{1/2} \to 1$). All the experimental HWHM temperature dependence is presented in Fig. 4.10 ($w_{1/2}$ versus f_{max}). The widths vary between 1.2 and 3.0 with the exception of DHIQ (red □) that has one spectrum with $w_{1/2} = 4.0$. The overall tendency to reach torward one value observed in the temperature dependence of minimum slope is not mirrored into the temperature induced changes in the widths. The reason for this leis probably in the description range of HWHM. In Figure 4.9 the half loss peak is above the inflection point, i.e., captures only changes relatively close to the maximum or the curvature of the primary relaxation. Thus describes part of the loss graph

53
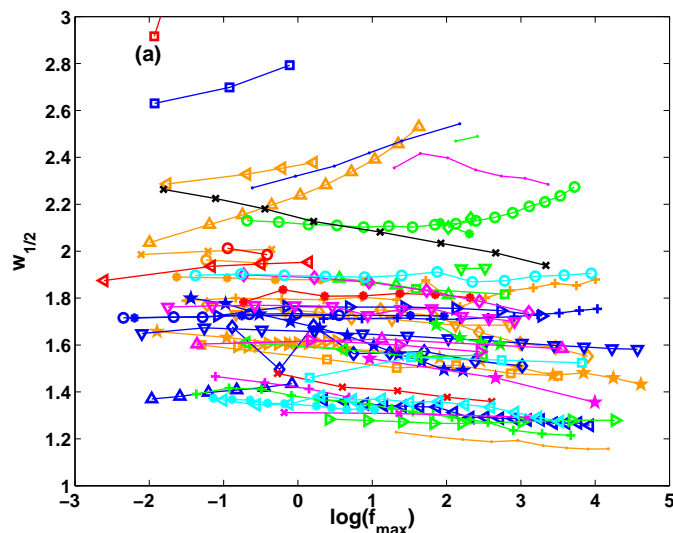
Figure 4.10: Normalized width $w_{1/2}$ plotted versus loss peak frequency, the latter quantity providing a convenient measure of temperature. The width generally changes with temperature and only in some cases becomes almost constant as the temperature is lowered.

where the relaxation at different temperatures is well described by a master curve. Liquids with almost Debye dissipation have nearly same normalized widths ($1 < w_{1/2} < 1.5$ in Fig. 4.10); these liquids are: PC, ethylene glycol (EG, magenta +), 13PD (orange •), butyronitrile (But, green +) and dibutylammonium formide (DBAF, green ▷) – all liquids with strong hydrogen(nitrogen) bonding. These liquids, as it will be pointed out later, have relatively high loss peak magnitude and relatively similar shape. However in this well defined bunch of relatively narrow HWHM also salol (magenta ×) belongs. This liquids dispersion have minimum slopes close to $-1/2$. The glassformer nMC (blue △) data points that the width narrows as $T \rightarrow T_g$.

Comparison

All the found experimental and KWW and CD functions HWHM values and the corresponding minimum slopes are plotted in Figure 4.11. There must be some correlation between the experimental α_{min} and $w_{1/2}$ as it the case for the shape of the fitting functions: If the minimum slope is numerically small, the width must be large and vice versa. In Fig. 4.11(a) one indeed finds such a

correlation between α_{min} and $w_{1/2}$. This is especially apparent for liquids with α_{min} at the boundaries of the α_{min} interval.

Thus significant variations of $w_{1/2}$ with minimum slope appears for materials with very broad relaxation shape like sorbitol (blue □) and DHIQ (red □) – liquids with high-intensity secondary process, as well as Xylitol (●), 3-methylheptane (3MH, green ●), TODDA (◁).

Sucrose benzoate's (SB, green ○) width narrows in the same way, but below some temperature it again begins to grow while the minimum slope gets smaller. This may indicate interference from underlying low-intensity β relaxation process (there is an additional well-resolved β-process above 1 MHz).

In this figure one sees the lack of equivalence between the two fitting functions. For the same widths corresponds to different exponents such $\beta_{CD} < \beta_{KWW}$. The minimum slope lie mainly in-between the CD and KWW lines. However the CD function is closest to the experimental values. This indicates the tendency in the result of fitting with KWW – β_{KWW} is fitted only close to the maximum of the dissipation. Thus is not surprising that one can assumes that TTS is obeyed for a much wider temperature range than it is in the reality.

If we focus on minimum-slopes between -0.4 and -0.6 (Fig. 4.11(b)), however, there is a significant spread in the values of normalized widths and no strong correlation between $w_{1/2}$ and α_{min}. For the glass former for example MMT (blue ◇) the two quantities are, from some temperature on, almost constant with $\alpha_{min} \in [0.493; 0.503]$ and $w_{1/2} \in [1.495; 1.684]$. Isoeugenol (black ×) has the same behavior as nMC, the loss peak broadens, but minimum slope is close to $-1/2$. Other examples of this are DOP (orange ◇), DEP (blue ○), and PPE (red *). For some cases like for DisoBP (blue +) and DC705 (orange ○) α_{min} changes significantly while $w_{1/2}$ stays almost constant. The reason for this is that $w_{1/2}$ does not capture deviations beyond one decade, thus it does not necessarily change when α and β processes separate as temperature decrease. In fact, the quantity $w_{1/2}$ rarely includes the contributions near by the inflection point where the minimum slope is determined.
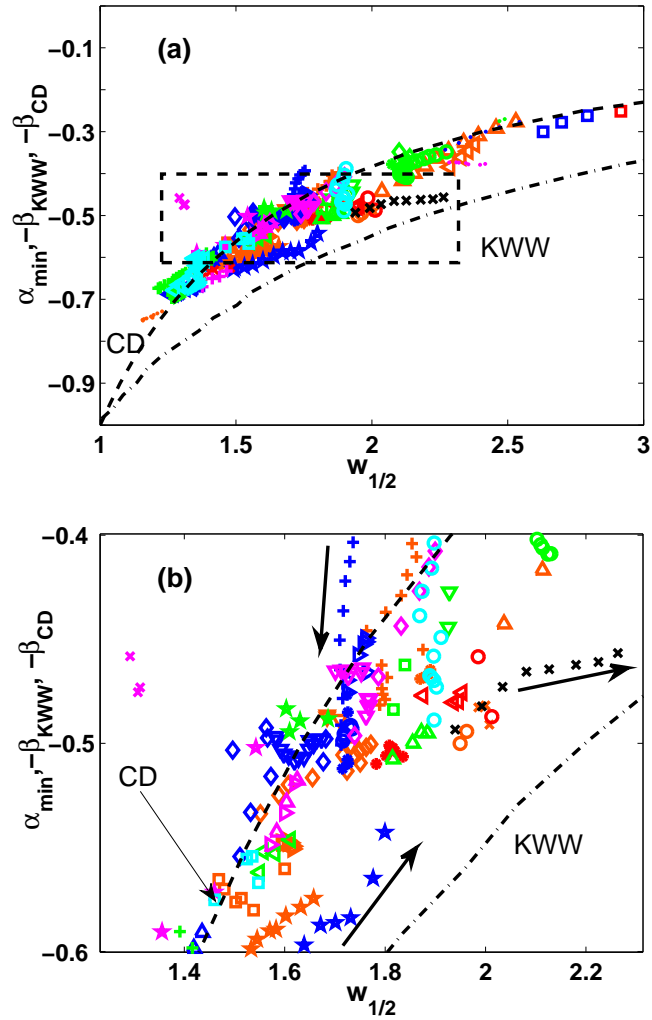
Figure 4.11: (a) Normalized half width at half maximum, $w_{1/2}$ versus minimum slope α_{min}. There is an overall correlation between the two measures, reflecting the fact that a numerically low value of the minimum slope forces the width to be large and vice versa. The dashed-line rectangle frames the zoom-in shown on the plot (b), $-0.6 < \alpha_{min} < -0.4$. Here we more clearly see that often minimum slopes vary whereas $w_{1/2}$ is nearly constant. In both figures the two black dashed and dash-doted curves give $-\beta_{CD}$, respectively $-\beta_{KWW}$, vs. the corresponding $w_{1/2}$. The black arrows indicate the direction of changes as temperature decreases. The values for β_{KWW} and $w_{1/2}$ for the KWW process are from [57].

4.3   Test of the conjecture: TTS $\implies \varepsilon'' \propto \omega^{-\frac{1}{2}}$

If the reader recalls in Section 2.3 the conjecture stated by Olsen and co-workers that correlates TTS with a $\omega^{-1/2}$ decay was presented. For these purpose a quantity that gives the deviation of a spectral shape from a master curve is defined in the current section.

Master curve

In order to investigate TTS one needs to normalize dielectric scans. Values for the magnitude of the dispersion and the loss peak frequency can be obtained in different ways.

The magnitude can be identified as:

- $\Delta\varepsilon = \varepsilon_s - \varepsilon_\infty$ found from the spectra of the real part ε'

- from Kramers-Kroning relation $\Delta\varepsilon = \frac{2}{\pi}\int \varepsilon''(\omega)dln\omega$

- by fitting the amplitude of α process using functions like KWW or CD

- just to pick the amplitude ε''_{max} from the dielectric dispersion plot.

The first two methods are the most stringent but difficult to obtain precisely from dielectric scans, because of the relatively narrow experimental windows as well as the limitations in the precision of the measuring technique.

The loss peak frequency can be found by:

- obtaining the average time by use of the fitting functions $(\omega\langle\tau\rangle)$

- to assume that the true relaxation time corresponds to the loss peak frequency f_{max}.

When the average structural relaxation time is used the result deviates if one uses KWW and CD fitting functions which give different relaxation times[2]:

$$\omega_{max} = \frac{1}{\langle\tau\rangle} = \left(\frac{\tau_{KWW}}{\beta_{KWW}}\Gamma\left(\frac{1}{\beta_{KWW}}\right)\right)$$

respectively,

$$\omega_{max} = \frac{1}{\tau_{CD}}\tan\left(\frac{\pi}{2(1+\beta_{CD})}\right).$$

---

[2]In the expression for KWW average relaxation time Γ denotes Gamma function, $\Gamma(x) = \int_0^\infty t^{x-1}e^{-t}dt$, for real and positive x.

The obtained master plot can point to whether TTS is valid for a given temperature-frequency loss scan. Visually one can decide the frequency or temperature range, where TTS applies. More precise information is obtained if the shape characterizing quantities' temperature dependence is investigated. Here, we approximate the validity of TTS by requiring only a temperature-invariant e.g., by evaluating the plot of the dispersion parameter β_{KWW} vs. temperature (or loss peak frequency). In this method the answer depends on the fitting frequency range. For example, in fitting with KWW function the common procedure is to fit the low-frequency flank of the data with the same of one side Fourier transformed KWW function. Thus β_{KWW} gives information about changes close to the loss peak and the low-frequency part of the relaxation. Neither method gives any precise information that can be used for comparison of changes induced from temperature variation.

Since the investigation is based on raw data analysis the master plot of the scans is obtained by normalization with respect to loss peak frequency and loss found directly from the raw data. If one assumes that close to the experimental data loss peak the data graph is symmetrical, then the loss peak values are identified by fitting a second-order polynomial to an interval of data points in double logarithmic plot, using from 5 up to 9 points around the maximum depending on the symmetry of the loss peak and the density of the measure points for the particular data set. In Figure 4.12 the chosen data points around the top are shown and the estimated second order polynomial through these. The resulting master plot is shown on the left in the figure.

TTS measure

A simple way to quantify the change in shape is to use the master plot of the dielectric dissipation. If two curves for two different temperatures do not collapse on the top of each other then the curves embrace a part with a curtain area. The area will be large if the deviation in the spectral shape is significant and vice versa - negligible deviation results in very small number.

On the master plot every dielectric loss and frequency at given temperature are normalized with the loss peak dielectric loss, ε''_{max}, and the loss peak frequency, f_{max}, respectively (Look on the left plot in Figure 4.12 and Figure 4.13). Let the normalized quantities be $\tilde{\varepsilon} = \varepsilon''/\varepsilon''_{max}$ and $\tilde{f} = f/f_{max}$. In the following, let us consider dielectric loss spectra at two neighboring temperatures, $T_j < T_{j+1}$. We define dS_j as the deviation in area between the two spectra. dS_j is sum of the difference in the values of $\log(\tilde{\varepsilon}_j)$ and $\log(\tilde{\varepsilon}_{j+1})$ at m frequencies in the normalized graphs. In Figure 4.13 $m = 13$ with $\log(\tilde{f}_1) = -0.4$ to $\log(\tilde{f}_{13}) = 2.0$ equally spaced in between with $\Delta log(\tilde{f}) = 0.2$. The values $\tilde{\varepsilon}''_j$ are
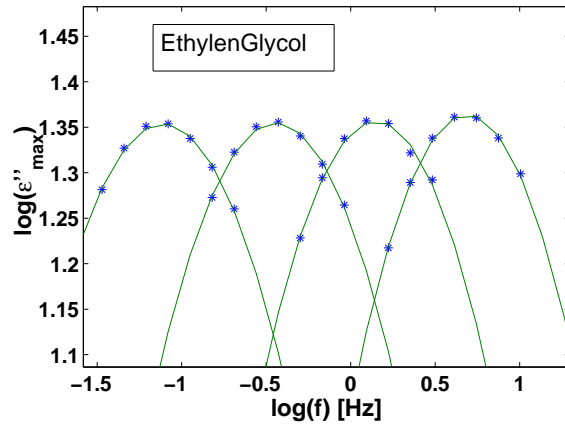
Figure 4.12: The calculation of the loss peak frequency,f_{max}, and the loss, ε''_{max}: The chosen data points are marked with stars and the curve is the estimated second order polynomial which is used to find f_{max} and ε''_{max}.
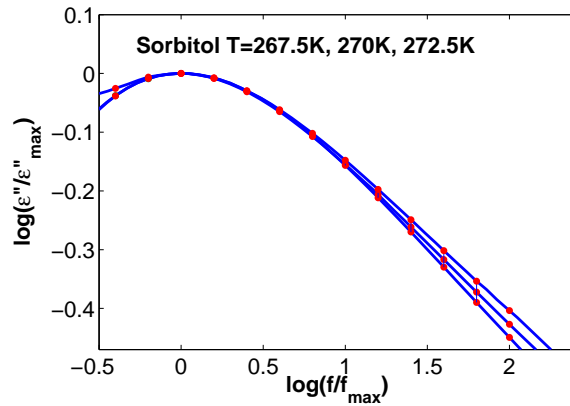
Figure 4.13: Illustration of the procedure to find the time-temperature superposition (TTS) measure. The plot is normalized data for sorbitol at three different temperatures. The red dots mark the ε''-values which are used to calculate the deviation in the dissipation shape at two nearby temperatures, i.e. the area between two temperature curves. These three scans result in two points for TTS measure Δ.

found by interpolation at every m frequency. The calculation of dS_j was made

with those 13 $\tilde{\varepsilon}$ values,

$$dS_j = \sum_{i=1}^{13} \left| \log(\tilde{\varepsilon}_{j+1}(\log(\tilde{f}_i))) - \log(\tilde{\varepsilon}_j(\log(\tilde{f}_i))) \right| \, .$$

The frequency interval $[\tilde{f}_1; \tilde{f}_{13}]$ contains the main part of the α loss peak and is asymmetric with nearly a half decade on the low-frequency side and two decades on the high-frequency side of the loss peak. There are three reasons for the determined asymmetry: This TTS measurement introduces a further constraint on the data selection, namely that only data sets with a well-defined maximum and at least half a decade of measure points on the low-frequency side of loss were included in the analysis. Furthermore, data must be quite accurate since the $\tilde{\varepsilon}$ values are found from data by linear extrapolation.

First as mentioned, in most cases the approximate low frequency slope of the relaxation is -1. The most interesting shape variation happens for frequencies higher than f_{max}.

Second, in many data sets the experimental window ends in the low-frequency part around the frequency corresponding to the glass temperature. This results in many dissipation curves ending around 0.01 Hz. In many cases the time scale separation of the α and β processes with relaxation times corresponding to high-frequencies happens at relatively low temperatures. Dissipation at temperatures close to the glass transition thus describes the tendency of changes in shape of the primary relaxation alone. Thus, it is important not to exclude these scans from the analysis.

Last, the DC conductivity often is responsible for significant spectral shape changes at low frequencies. An asymmetric interval reduces this effects.

Bearing in mind that: 1) the temperature difference between two neighbouring temperatures varies within a data set and for different set as well as 2) measurements at close temperatures trivially result in curves of closely similar shapes and temperature is connected to the loss peak frequencies TTS deviation measure Δ_j is defined as follows:

$$\Delta_j = \frac{dS_j}{d \log(f_{max,j})}, \tag{4.5}$$

where $d \log(f_{max,j}) = |\log(f_{max,j}) - \log(f_{max,j+1})|$ is the numerical difference in the loss peak in decades. Δ thus gives information about shape changes per frequency decade. Note that we need at least two frequency scans to calculate one value of the area difference and thus Δ; the TTS analysis therefore does not result in 347, but in $347 - 53 = 294$ data points.

In figure 4.14(a) all the resulting 294 data points can be seen, $\log |\Delta|$ and values of the minimum slope corresponding to the mean value of every two

neighbour temperatures. TTS is better obeyed as the value of $\log |\Delta|$ decreases. All the liquids are represented with different number of points. The population of all points on the graph does not therefore give a clear picture of the relation between TTS and α_{min}.

To emphasize the relationship between TTS and the minimum slope on figure 4.14(b), a distribution function is defined Δ that accounts for every glass-former on the graph having a different number of points. This function is constructed so it gives information about the number of materials under a certain level l, that characterise the deviation from the temperature invariance in the form of the relaxation as a function of the minimum slope

$$\Phi(\alpha_{min}, l) = \frac{\sqrt{\Lambda}}{n} \sum_{i=1}^{n} \frac{1}{N_i - 1} \sum_{j=1}^{N_i - 1} \exp\left(-\frac{\left(\alpha_{min} - \alpha_{ij}\right)^2}{\Lambda}\right) \theta(l - \log(\Delta_{ij})), \quad (4.6)$$

where α_{ij} is the minimum slope at j-th liquid and the i-th point (temperature) in the dataseries, n is the total number of all liquids, $N_j(l)$ is the number of points in j-th liquid, that are laying under the level l and are counted via θ that is a delta function

$$\theta = \begin{matrix} 1 & l \geq \log(\Delta_{i,j}) \\ 0 & l \leq \log(\Delta_{i,j}) \end{matrix}$$

The overall distribution is in 4.14(b) where the distribution includes all points that mimic the already observed distribution of minimum slope values. From Figure 4.14 one should expected that the peak of the distribution broadens much more than it observed. In other words liquids that $\alpha_{min} = -0.5$ does not obey TTS. Liquids with numerical values bigger than $1/2$ have a spectral shape that change relatively little with temperature decrease. These liquids are both the hydrogen bonding liquids like 13PD and PG and some van der Waals liquids like PC. This is in agreement with the conventional view that these liquids obey TTS. But other groups of liquids appear to behave in the same way, where liquid behaves with relatively broad spectra and low intensity of the dissipation like the alcans. The conjecture seems to hold. There are a number of liquids, showing that TTS is better fullfilled by lowering the temperature - these liquids have a minimum slope of $1/2$.
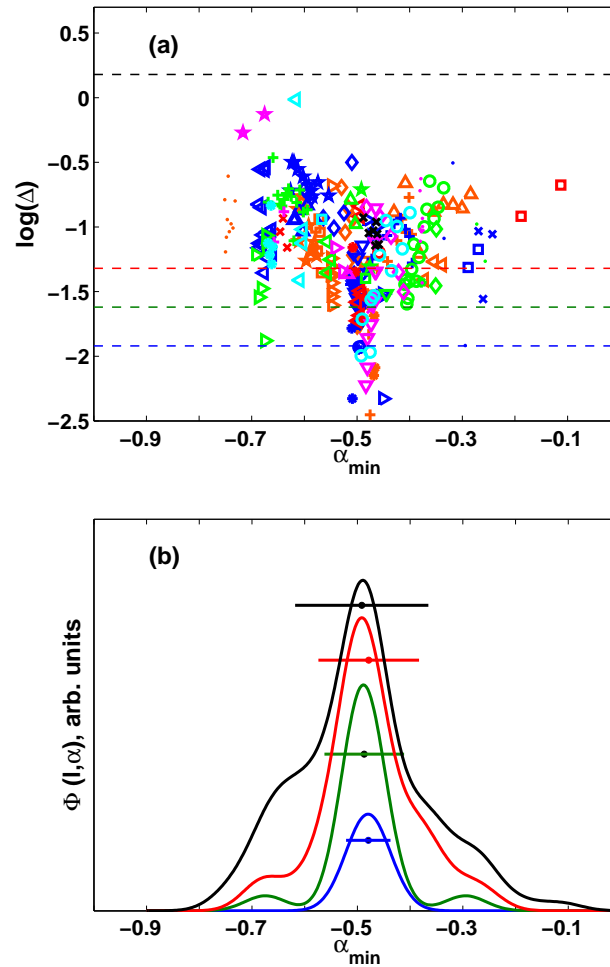
Figure 4.14: (a) Time-temperature superposition (TTS) analysis: (a) shows the measure of how well TTS applies, $\log|\Delta|$, plotted versus α_{min}. With a few outliers it is seen that the smaller $\log|\Delta|$ is (i.e., the better TTS applies) the more α_{min} tends to $-1/2$. (b) The smoothed distribution $\Phi(\alpha, l)$ of the number of measuring points (normalized to the total number of points representing a given liquid) for all liquids for which $\log|\Delta| < l$. The levels $l = -1.92; -1.62; -1.32; 0.18$ correspond to the colors blue, green, red and black, and are marked with dashed lines in (a). The four dots and vertical lines mark the mean value and variances of α_{min} for the four distributions and have the respective colours. NB! the four distribution are not normalized to the number af points associated with one level but with respect to the total number in order to include all distribution plots in one figure.
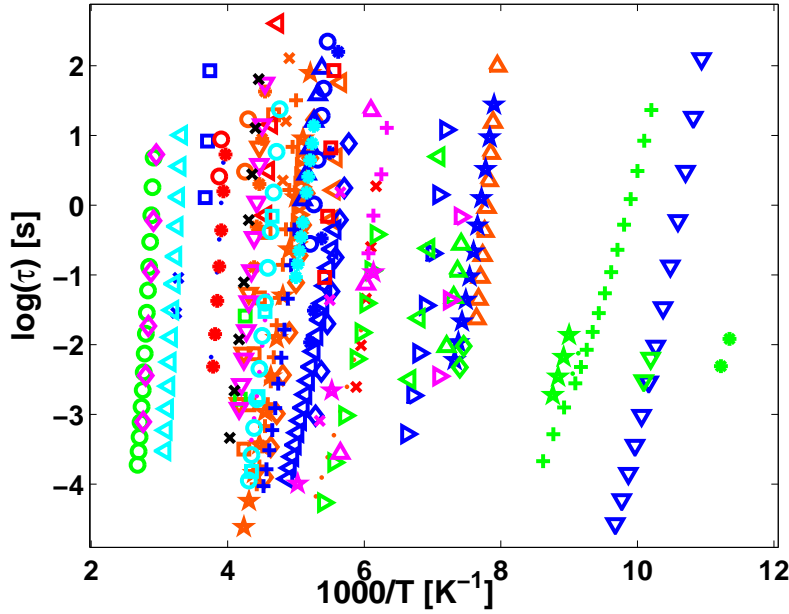
Figure 4.15: The dramatic slow down of the relaxation processes is illustrated by a plot of logarithm of the relaxation time versus the inverse the temperature scaled by 1000 for all the experimental data in this study.

The degree of non-Arrhenius behavior

In this study as a measure of the degree of non-Arrhenius behavior is used the activation energy temperature index $I_{\Delta E}$ 10 The calculation of the Olsen index is made under the assumption that the microscopical time is constant $\tau_0 = 10^{-14}$s. In the calculation of the temperature index the activation energy $\Delta E(T) = k_B T(ln(\tau(T)) - ln(\tau_0))$ are used the loss peak frequencies f_{max} that are obtained directly from data by fit of second order polynomial in a small interval of data points just around the loss peak. The relaxation times for all 53 liquids are presented in Figure 4.15 where the temperature dependence of the relaxation time is graphically presented.

The temperature index $I_{\Delta E}$ reflects the degree of deviations from Arrhenius behavior at any given temperature. In Figure 4.16 is shown by means of the loss peak frequency the how the temperature index changes with temperature or how much it deviates from Arrhenius behavior. In the investigated experimental window are the most liquids $I_{\Delta E}$ values lies between 2 and 8. The way the
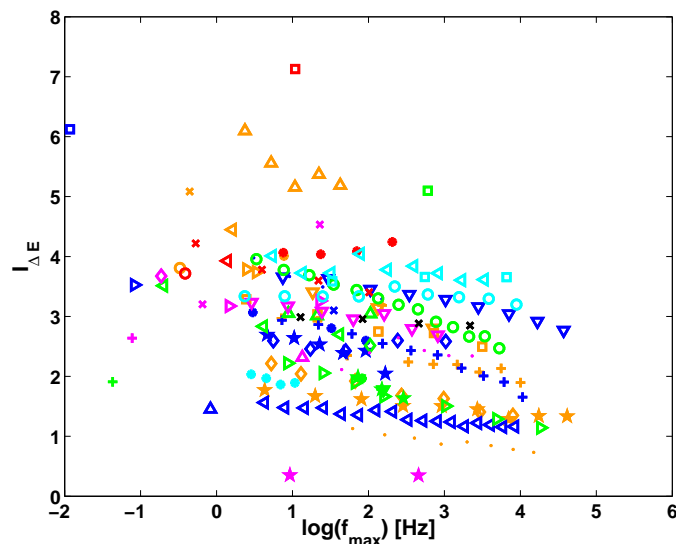
Figure 4.16: The activation energy temperature index $I_{\Delta E}$ gives the degree of non-Arrhenius behavior here shown as function of the loss peak frequency f_{max} for all data sets. Arrhenius behavior corresponds to $I_{\Delta E} = 0$. The different liquids covers a relatively broad range of non-Arrhenius behaviors is represented temperature index but no extreme strong or fragile liquids are observed.

indices for different liquids are changing (the slope of the curves) varies from almost constant to a change of 1 over 2 decades (tol-pyr Δ). With other words there is no connection between the value of $I_{\Delta E}$ and the way the loss peak frequency for the different liquids. Although the general trend is that the deviation from the Arrhenius law increases with temperature decrease.

The advantage of using the temperature index for quantifying non-Arrhenius behavior comes from the fact that the index is defined at any temperature, whereas m is evaluated at the glass transition temperature and thus formally relates to the liquid's properties only at T_g, but if we define a temperature depended fragility (steepness index) as follows: $m(T) = (d \log f_{max})/(d \ln T)$ then the two quantities are closely related at all temperatures. The plot in Figure 4.16 illustrates how the fragility of a liquid depends on choice for the relaxation time which defines the T_g and $\tau_0 = 10^{-14}$s. If the reference temperature where the steepness index m is evaluated is defined for different relaxation times, $T_{ref}(\tau_{ref} = const)$) then it is obvious that m have no universal character in this definition, since m does not changes in significantly different way with reference time. Generally other problem regarded m is that in different
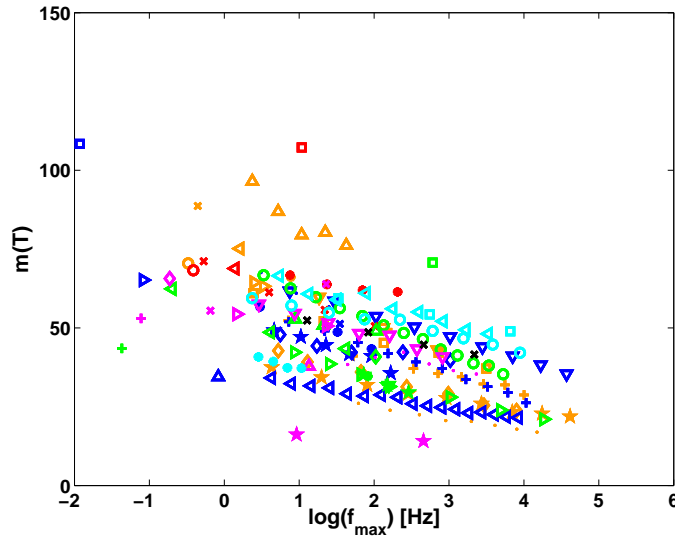
Figure 4.17: The steepness fragility index m as function of the loss peak frequency. If the one chooses different reference temperatures is m in this varies in this plot related to the temperature index. The fragility for the most liquids changes roughly with 30 from the highest to the lowest temperature (over 4-5 frequency decades).

measurement techniques the experimental $T_g = T_g(\tau = 100)$ s deviates. For example in shear relaxation is quicker that the dielectric [67]

Do minimum slopes correlate with how non-Arrhenius the liquid is?

We tested the implied correlation between α_{min} and non-Arrhenius behavior by proceeding as follows. Figure 4.18(a) plots $I_{\Delta E}$ for all data sets. For liquids exhibiting approximate $\sqrt{t}$ relaxation there is little correlation between the approximate high-frequency power law and the degree of non-Arrhenius behavior. Even the very fragile liquid benzophenone (BP, cyan $\square$) ($m = 125$ [90]) exhibits approximate $\sqrt{t}$ relaxation.

For liquids with $\alpha_{min} > -0.4$ we likewise found poor correlation between α_{min} and degree of non-Arrhenius behavior. Thus for DHIQ (red $\square$) relaxation is characterized by $\alpha_{min} \in [-0.25, -0.10]$), sorbitol (blue $\square$), by $\alpha_{min} \in [-0.3, -0.26]$, and salicylsalicylic acid (SSA, blue $\times$), by $\alpha_{min} \cong -0.23$, whereas these three liquids have quite different temperature indices (Table 1). For these

65
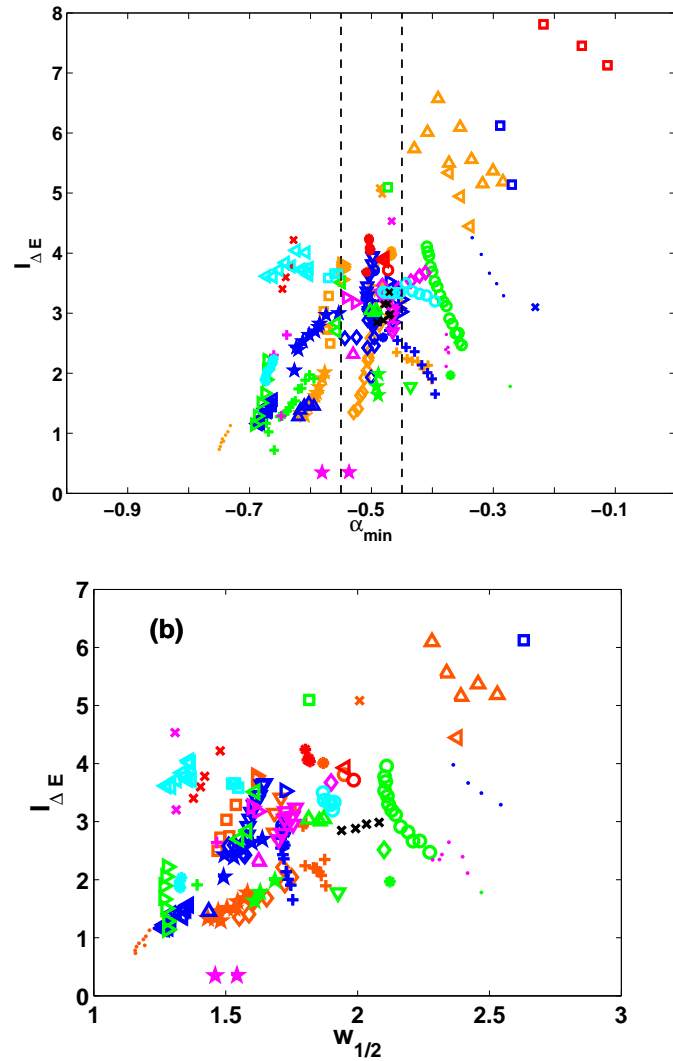
Figure 4.18: (a) The activation energy temperature index $I_{\Delta E}$ versus α_{min} for all data sets. The former quantity measures the degree of deviation from Arrhenius temperature dependence of the loss-peak frequency; Arrhenius behavior corresponds to $I_{\Delta E} = 0$. The dashed lines embrace the values between -0.55 and -0.45. A broad range of non-Arrhenius behaviors is represented among liquids exhibiting approximate $\sqrt{t}$ relaxation, thus close to $\alpha_{min} = -0.5$ the temperature index varies by a factor of 2.5. In terms of fragility this quantity takes on values from roughly 50 to 125, which is practically the entire span of fragilities of the 53 liquids included in the data analysis. (b) Temperature index $I_{\Delta E}$ versus the normalized width $w_{1/2}$ (Eq. (4.4)), not showing any clear correlation.

liquids fragilities reported in the literature are $m = 139$, $m = 100$, and $m = 31(45)$, respectively The lack of clear connection between the shape of the relaxation and the fragility is also clear in the plot $I_{\Delta E}$ versus $w_{1/2}$ in Figure 4.18 (b).

To summarize, liquids with approximate $\sqrt{t}$ relaxation exhibit a wide range of temperature indices (fragilities); there is no obvious correlation between the degree of non-Arrhenius temperature dependence of the loss peak frequency and the high-frequency decay of the loss.

4.4 The loss peak permittivity ε''_{max}

Do minimum slopes correlate with dissipation magnitudes?

As a measure of dielectric strength one would prefer the overall loss $\Delta\varepsilon$, but since this quantity may be difficult to determine accurately instead quantify the strength by the maximum loss. These two quantities are only strictly proportional for liquids with same relaxation function, of course, but this fact is not important here because the dielectric strengths span more than four decades.

As can be seen from Fig. 4.19 (a) there is little overall correlation between having $\sqrt{t}$ relaxation and the value of the maximum loss $\log(\varepsilon''_{max})$. However, liquids with large dielectric strength like PDE (cyan □), PG (blue ◁), PC (red ×), EG (magenta +), 1,3PD (orange ●), butyronitrile (green +), and DBAF (green ▷) consistently show minimum slopes that are numerically larger than $1/2$. The corresponding α_{min} values are only weakly temperature dependent, which agrees with results for other hydrogen-bonding systems [28]. Liquids with $|\alpha_{min}| > 0.65$ tend to have Kirkwood correlation factors [79] significantly larger than unity, reflecting strong correlations between the motions of different dipoles. Higher Kirkwood correlation factors mean longer-range orientational and dynamical correlations, leading to spatial averaging of what might otherwise still be $\alpha_{min} = -1/2$ behavior (for Kirkwood correlation factors going to infinity one expects an approach to Debye relaxation because of the increasingly large degree of cooperativity). Figure 4.19 (b) shows loss-peak strength versus width. There is a clear tendency that large-strength liquids are more Debye like.

To summarize, liquids with approximate $\sqrt{t}$ relaxation span a wide range of dielectric losses. There is little overall correlation between loss strength and minimum slope. Liquids with large loss strengths, though, clearly have $|\alpha_{min}| > 1/2$.
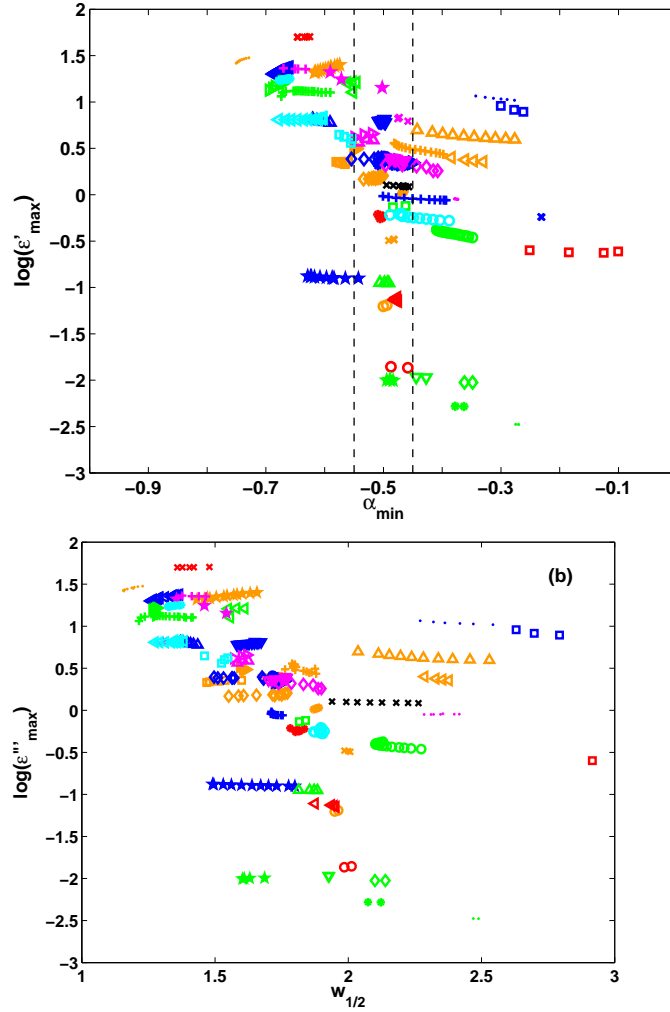
Figure 4.19: (a) Maximum dielectric loss ε''_{max} versus α_{min} for all data sets. The liquids between the two dashed lines marking the interval $-0.55 < \alpha_{min} < -0.45$ have dielectric losses varying by more than a factor of 1,000. Large-loss liquids have minimum slopes that are numerically larger than 1/2; these liquids consistently disobey approximate $\sqrt{t}$ relaxation. (b) Maximum dielectric loss plotted versus width $w_{1/2}$. Glass formers with large dielectric loss consistently tend to be more Debye like as expected from (a).

4.5 Subdivision of liquids into A and B type

Can we learn something new if we divide the liquids in A and B type? This is the question that will be illuminate in the following. First a set of characteristics and the result from the application on all 53 data is presented. Afterwards it is investigated if the different types are different in order to look after some correlations between the shape in therms of minimum slope and the temperature, T, temperature index $I_{\Delta E}$ and intensity of the dielectric loss ε''_{max}

How to distinct between A and B type liquids?

On page 19 the definitions of A an B type are introduced in a very naive way. Of course the concept develops as the phenomenology of the interaction between the α and β processes is mapped/disclosed/discovered??? experimentally.

The A type liquids are EW and in the dielectric spectra there can be some secondary processes at high as well as low frequencies. In double logarithmic plot EW is identified as a linear part in the high-frequency flank of the alpha process with a slope that is close to -0.2 ± 0.1. However no quantitative set of rules is formulated which can be use to point out the EW liquids. E. Rössler labels a substans as an EW or A type liquid if at least **one** of the following characteristics is fulfilled for the absorption spectra [130]:

1. There can be a high-frequency β process, but its magnitude is relatively small.

2. The high-frequency β process is well separated from the α process.

3. The primary process is very narrow, i.e., the stretched exponential is bigger than 0.5. Here in this work was used of course $\alpha_{min} = -0.5$.

All the liquids were evaluated according the schema and classified into the two types [130]:
The following 29 liquids are specified as A-type liquids: 2MP24D, αPoC, DC704, DC705, TCP, Glycerol, DCMMS, 13PD, PG, DPGDME, MMT, nMCL, nPB, MTHF, PPE, TPE, DC704, PC, DBAF, BN, Cumene, 3MPh, Salol, 2pic, EG, 4TBP, APED, DCMHS and BP.
The B-type liquids are TOTD, TPP, 23PPPE, PPG, DOP, TolPyr , Sor, SSA, DHIQ , SB , DHIQ, 3-FA, IB2BP and 4TBP, in all 14 liquids.
10 out of the 53 liquids do not fit into the suggested scheme because the frequency interval was too short and it could not be decided if there is an linear part in high-frequency flank with a slope of around -0.2 ± 0.1. The explanation for this can be that the slope of the primary process is too small and thus "inseparable" from eventual EW part. [130].

69

The spectral shape

B Type liquids
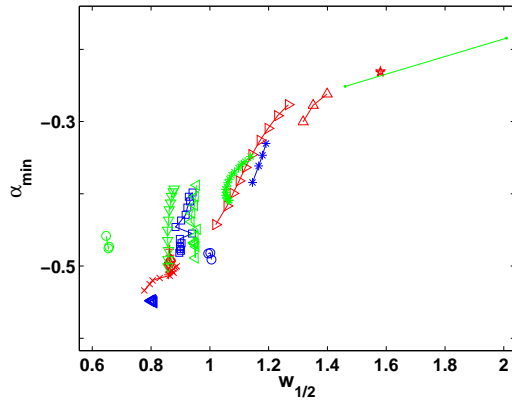
A Type liquids
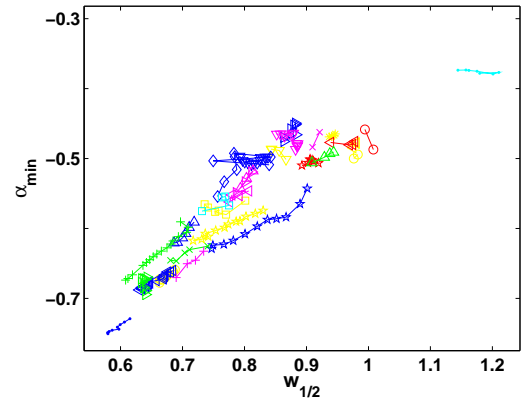
Due to number 3 of the listed characteristics there is a tendency that the A an B types look very distinctive but in both types are present liquids with minimum slope of −0.5. The biggest part of the A type are narrow but there are some exceptions as result of the other two characteristics in the rule set.

Is there something special about A and B type?

For the two type liquids are plotted the **minimum slope** versus:

The temperature dependence

B Type liquids
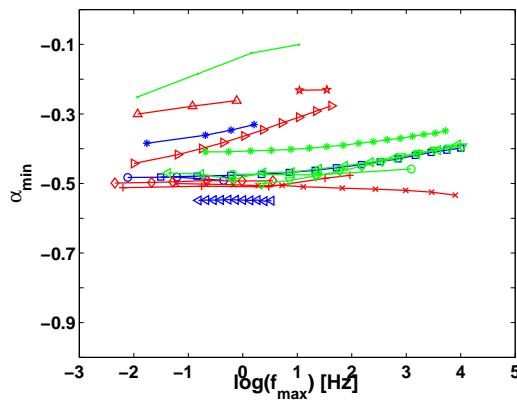
A Type liquids
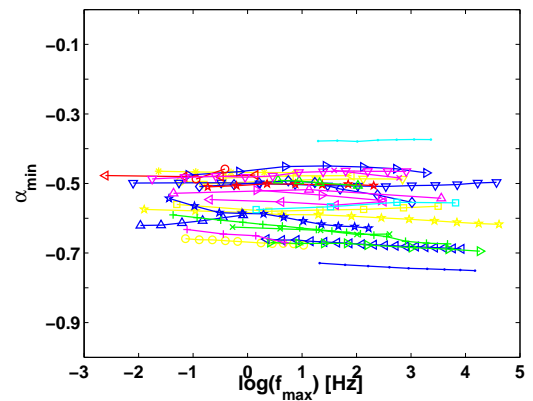
The temperature index
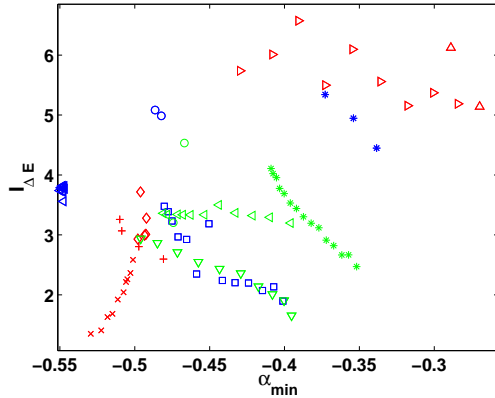
B Type liquids   A Type liquids
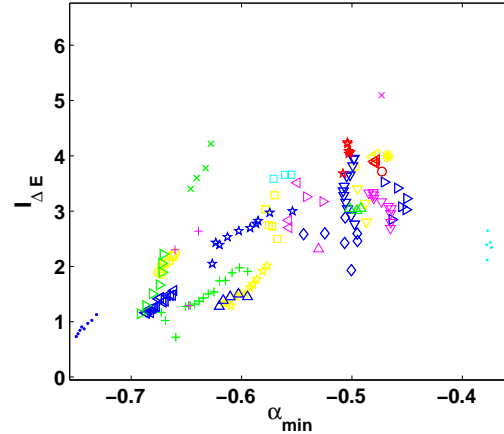
The magnitude of the dielectric loss
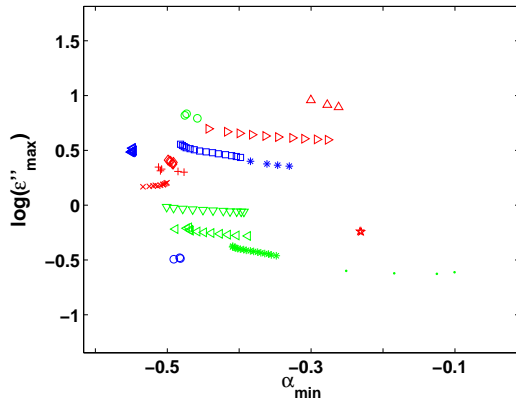
B Type liquids   A Type liquids
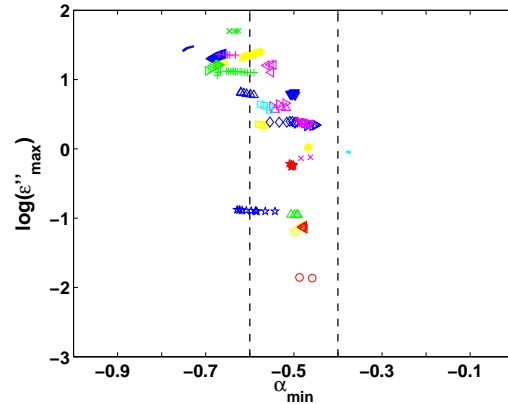
The conclusion from this investigation is the following:

A and B type are distinct what concerns the shape and temperature dependence. The shape differences are build in the set of characteristics (the third point above). There is a tendency that for A type liquids' narrow loss peaks widens and type B's broad loss narrows with temperature decrease is again found. Though the changes in type A spectral shape are as rule smaller than the temperature induced transformations in type B liquids.

Besides the shape differences, there are no other properties that the two types can be noted for. There is no correlation between the type and how non-Arrhenius the liquids are or the intensity of the loss peaks.
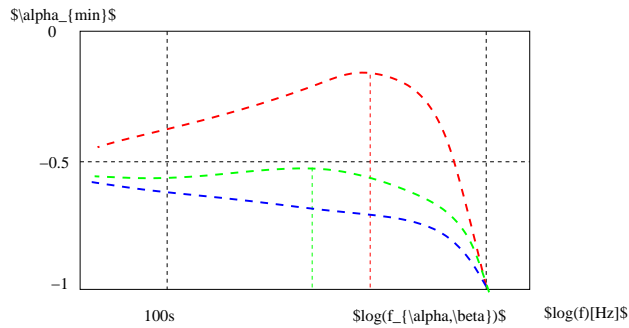
Figure 4.20: Minmum slope changes with loss peak frequency (temperature) scan - some possible scenarios. the most right part of the sketch presents the liquid relaxation at very high temperatures (10^{12} Hz) and the left is in closure of the glass transition.

The concluding remark here is: the classification of the liquids in two types has purely descriptive function, nothing about the liquids' properties – at least regarding the fragility and the loss peak magnitude – can be pointed out as special for the particular type. Both type A and type B contains different liquids from chemical point of view, i.e. the size and shape of molecules and hydrogen bonded liquids.

4.6   Summary

Minimum slope $\alpha_{min} = -0.5$ is somehow generic for the primary relaxation and and most liquids approaches the value with temperature decrease (Here expressed via the loss-peak frequency) Tangent with this slope approximates bigger part of the high frequency flank around the inflection point approaching the value of $-1/2$. Liquids that have this decay law have a invariant under temperature changes shape.

The phenomenological classification in A and B type liquids did not gave any new insight and have only descriptive character.

Fragility as steepness index is not correlated to the value of the non-exponetila decay with -0.5

Regarding the values of α_{min} one might intuitively expect that interference from β processes can only explain minimum slopes that are numerically smaller than $1/2$. but however some information can be obtained for minimum slope.

Probable scenarios for changes is shown in Figure 4.20.

Chapter 5
High pressure measurements

In the following is presented the analysis of dielectric data measured at isotherm conditions and variable pressure. As already explained the relaxation processes slow down with compression. Thus high pressure data can give information about how the compression affect the density changes and emphasize to some extent the effect of temperature. The data base is not as big as thatfor data measured at ambient pressure. Therefore there cannot be made firm conclusions as in the previous chapter but rather an investigation of whether the minimum slope concept captures relevant features/phenomena, like temperature pressure superposition for the same relaxation times (ITPS) or secondary processes, which are reported in the literature. The data used in this chapter are listed with references, color, symbol, temperature and pressure range and etc. in B.1 the spectra are also shown. Nine liquids were provided by the Paluch group (i.e., measured at SU setup) and the tenth, tetramethyltetra-phenyltrisiloxane (DC704, this work, Dow Corning 704® diffusion pump fluid), was measured on the same set-up especially for this investigation. The data selection principles – low noise, well defined loss peak, sufficiently long high frequency part, minimal influence from DC conductivity – are the same as those applied previously. The analysis is performed by use of the same MatLab routines as in the previous chapter. The structure of the text here is similar to the previous chapter as well. Since the number of data is limited the scope of the work presented in this chapter is to investigate whether the minimum slope captures some fenomena that apears under compression and cooling, e.g. changes in the spectral shape such as isochrone temperature pressure superposition and some β processes. In this part of the investigation the defined shape invariance quantity (Equation 4.5) is not used because the data are not sufficiently smooth for all the participating liquids scans. Hence the pressure temperature superposition is discussed in terms of minimum slope and the half width at half maximum
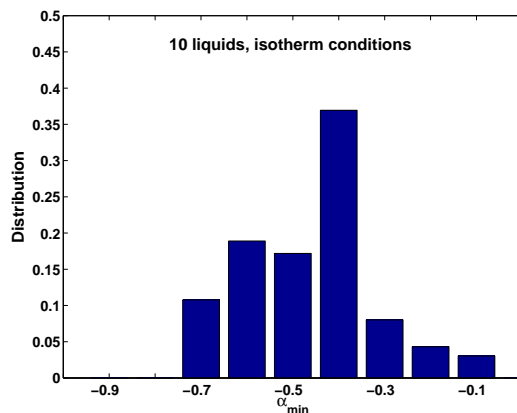
Figure 5.1: Histogram of the minimum-slope distribution for the ten organic glass-forming liquids listed in B.1. The observation intervals are of length 0.1. Since the number of pressures investigated varies from isotherm to isotherm as well the number of isotherms for each liquid, each minimum slope observation is weighted by a factor $1/(Nn)$, where N is the number of data points (pressures) in a data set for the given liquid at the given temperature, and n is the number of isotherm data sets for the given liquid. In this way all liquids contribute equally to the histogram. Note that an isotherm may contribute to more than one column in this figure since α_{min} varies with pressure.

which was defined in the previous chapter.

Since the data is so limited, no statistical analysis should be performed. Although the distribution of the minimum slopes at different pressures and isothermal conditions can show whether there are any trends, and if so then it is natural to look close into the results for every liquid to decide if the observed trend is general. The data in this analysis are a bit more complex because every liquid is measured at different number of temperatures and pressures. Thus every single minimum slope observation has to be weighted with the respect to the total number of spectra, N, at one temperature and the number of isothermal data set for the particular liquid, n. In Figure 5.1 the histogram is plotted and the most well-represented value interval for α_{min} is around -0.4. Let us investigate whether the limiting values -0.4 is a trend that is characteristic[1] for high pressure dielectric absorption spectrum.

---

[1]In shear measurements are observed much broader loss and the secondary processes with relatively higher intensity.[67]
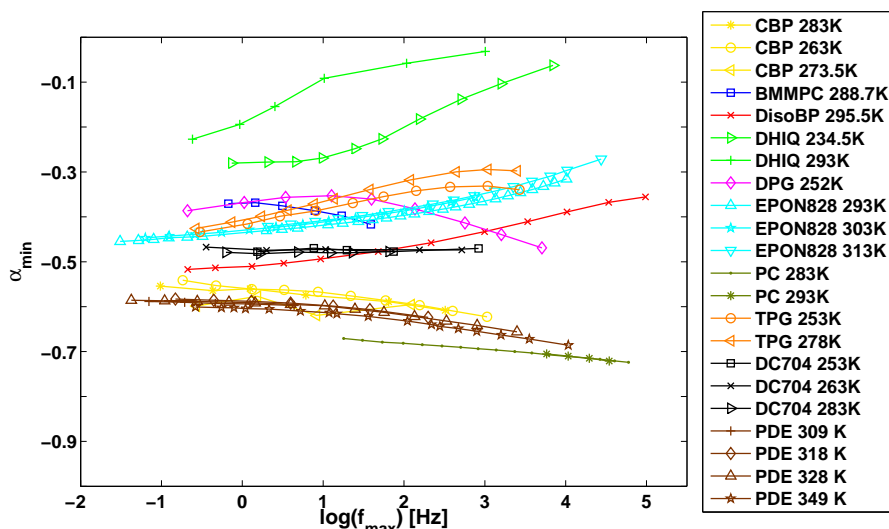
Figure 5.2: The minimum slope α_{min} plotted as a function of pressure quantified by the position of the loss peak frequency f_{max} for all 9 liquids along isotherms. Every liquid is presented with its own color and the different isotherms are marked by different symbols that can be seen the legend as well as in Table B.1, where the references are also given.

5.1   Isothermal minimum slopes

Figure 5.2 shows the minimum-slope evolution with loss peak frequency and hereby with pressure change, since for the loss peak frequency $f_{max} = f_{max}(P)$.

The observed picture in Figure 5.2 is reminiscent of the already seen figure for dielectric data at ambient pressure [110, 67, 103]. Seemingly the high frequency slope of the dielectric dissipation converge slowly toward $-1/2$ from above and below as pressure increases and α_{min} approximation is better obeyed as the α and β processes separate (see also Figure 5.3). Some exceptions from the general trend are notable – α_{min} curves that are convex.

The new information which one obtains from this figure (compared to Figure 4.7) is that some isothermal minimum slopes for the same liquid follow a master α_{min} curve while others deviate with a difference of 0.05 or more. Since changes in minimum slope can be ascribed the β relaxations, this can be expected to be observed as well as in compression data.

In Figure 5.3 is investigated how good an estimation of the high-frequency flank in the inflection point $f_{\alpha_{min}}$ the minimum slope gives. In the figure the

third-order derivative relative to the first-order derivative, $|H^{(3)}(x_0)/\alpha_{min}|$ is plotted as function of the minimum slope[2]. In this figure only three liquids show convincing the better an inverse power law describes the loss, the closer α_{min} is to $-1/2$. These glassformers are DisoBP (red +), EPON828 (cyan) and DC704 while the remaining liquids show changes that can be ascribed to β processes.

5.2 The β processes

In the previous chapter it was argued that some changes in the minimum slope are due to the bifurcation between the α and β processes, since the infection point on the double logarithmic graph marks the place where the dominance of the α process begins.

Out of the above listed liquids, DHIQ, TPG, DPG, BMMPC and DisoBP are the liquids for which secondary processes are reported or can be seen on the temperature-frequency scans in Appendix **??**.

In the plot in Figure 5.2 the three (orange and magenta) convex α_{min} curves belong to DPG and TPG.

The linearity and extrema of the minimum-slope pressure dependence can be underlined by plotting the change in slope point-by-point differentiated α_{min} vs. the loss peak frequency f_{max}. In Figure 5.3 is the slope of α_{min} is plotted in order to determine the frequencies where the β process has its maximum. This is expected to be the frequency at which the derivative of the minimum slope is zero.

For DPG the β peak is then at 10 Hz and for TPG both isotherms $d\alpha_{min}/d\log(f_{max}) = 0$ for $\log(f_{max}) \approx 3$. This is relatively close to the frequency for the β peak observed in dielectric data measured at ambient [67] where $f_{max,\beta}$ at or under 10 kHz. In Reference [121, 46] (high pressure) at frequencies around 1 kHz a low frequency shoulder is observed as well. This high frequency shoulder is ascribed to the so called *alpha'* process which is characteristic for mono-alcohols and explained as relaxation in the H-bond long range structure.

However both in the isobaric temperature-frequency scans (Appendix **??**) and in the α_{min} plot (in Figure 5.2) it can be seen that the intensity of the β process is temperature dependent: at the highest temperature the magnitude of the β is also biggest. Furthermore a secondary relaxation in the same region is observed in mechanical, shear, measurements [67]. In addition, a similar low-

---

[2]If we recall from the previous chapter $H(x) = \log \varepsilon''(x)$, $x = \log f$, and $a = f_{\alpha_{min}}$ is the log frequency at the point of minimum slope). The idea is that, since the second-order derivative is zero at the frequency of minimum slope, by Taylor's formula the smaller $|H^{(3)}(x_0)/\alpha_{min}|$, the larger the frequency range is, where the slope is almost constant.
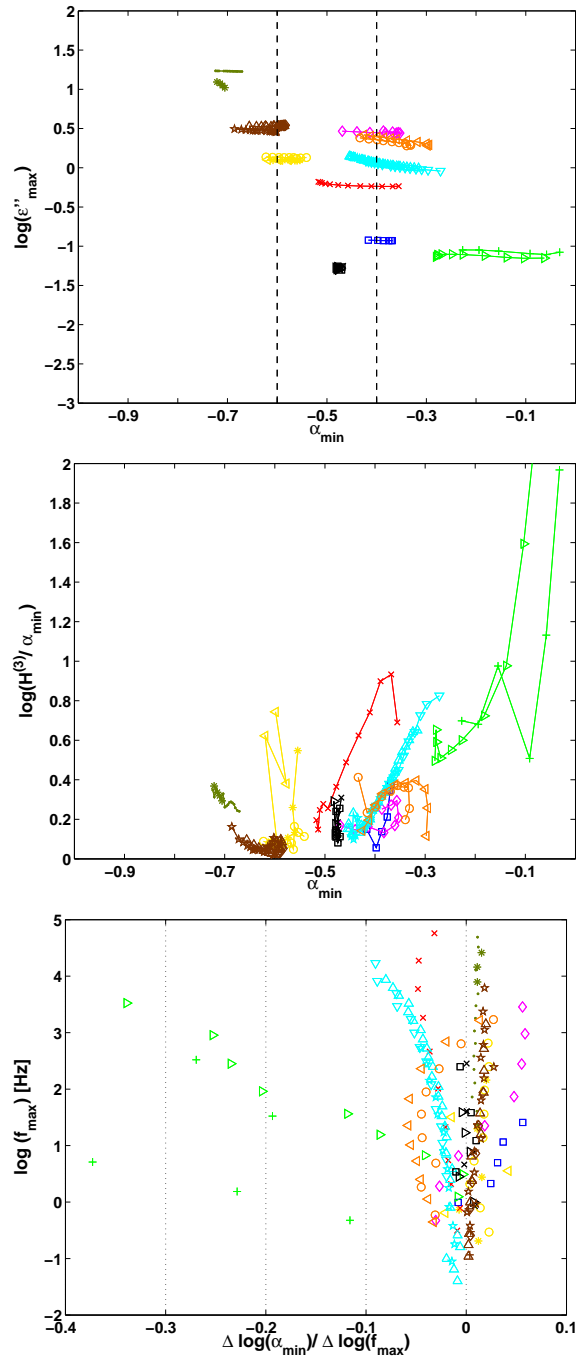
Figure 5.3: (Upper plot)Liquids with minimum slope α_{min} often have a large amplitude of the dielectric dispersion ε''_{max}. (Middle) Third-order relative to first-order derivative, $|H^{(3)}(x)/\alpha_{min})|$, at the frequency of minimum slope for all data sets where $H(x) \equiv \log \varepsilon''(x)$ ($x = \log f$). At the frequency of minimum slope the second-order derivative is zero; thus by Taylor's formula the smaller the third-order derivative is relative to the first-order derivative $\alpha_{min} = H'(x)$, the better an inverse power law description of the high-frequency loss applies. (Lowest) The slope of α_{min} gives information about how much α_{min} is pressure dependent. Both quantities contain information about the time scales of the secondary processes.

frequency shoulder has been reported for high precision dielectric relaxation for the non-polar cyclohexane at ambient pressure, which has been attributed to motions in the structure in the molecule [93]. These experimental facts indicate that this process is due to intramolecular motions and Prevosto and co-authors' conclusion might be wrong.

A detail should be noted: the two isotherm minimum slope curves seems to merge, i.e. the shape in the inflection point is same at (the given by the frequency $f = 1$ Hz). This indicates that the possible influence from β processes is not detectable or the primary and the secondary process time scales are sufficiently separated..

Following the same reasoning in the case of DPG one can then detect detect a β relaxation at 1 Hz, which is the frequency where the slope of the slope (see in Figure 5.3) intersects the line $d\alpha_{min}/d\log(f_{max}) = 0$. In Reference [48] it is found that DPG has two secondary relaxations, one at 10 kHz and an EW. The authors argue that the fastest relaxation originates from H-bond structures, while the EW is a hidden true JG process. Grzybowska and co-workers' argument is as follows: The EW in DPG and a JG process detected at a frequency of 1 Hz in the high pressure spectra of dipropylene glycol dimethyl ether (DPGDME) are equivalent, since the two liquids are oligomers. Thus in DPG spectra there should be observed a JG β process in the same frequency range. Of course one can ask: why is the secondary process at 10 kHz not detected from α_{min} as well? A possible answer is that the slowest secondary process "governs" at the inflection point. Maybe it is the EW which appears between the α and the β processes. Or the α process is not shape invariant at all. These are intriguing assertions which must be investigated further. α_{min} cannot give much information about the nature of the β process, at least at this stage.

In case of BMMPC, the high-frequency part of the spectra exhibits a shoulder that may be a β process with loss peak around $1 - 0.1$ Hz [17, 102] and again from α_{min} one can estimate the same value. For DisoBP there is a correspondence between the observed β loss peak frequency and from α_{min} approximated value of 1 MHz.

The relaxation spectra of DHIQ is characterized with a β process with high compared to α_{min}-amplitudes in 1-10 MHz region. With compression the time scales separate. The intensity of the β process decreases with temperature [114, 114, 16]. Thus the values of the isothermal minimum slope deviate from each other. However this liquid is a mixture of two isomers of the same molecule. This can give rise to more complex relaxation dynamics.

The pressure-frequency spectra for DC704 shows around 1MHz a secondary process with relatively low amplitude. The α relaxation in terms of minimum slope does not see the β relaxation, however, since the two processes are sepa-

rated, and therefore $\alpha_{min} = -0.48$ is nearly constant over 4 frequency decades.

Isochrone temperature pressure superposition

From the analysis at ambient pressure it was observed in agreement with the conventional picture that liquids with a minimum slope numerically larger than $1/2$ do not change significantly with cooling down. Other property of this glass-formers is that if a β process is present the slope is not influenced significantly by this; and last the ε''_{max} is usually one of the highest. The same is observed for these relaxations when they are subjected to compression. Thus, since whenever there are low-lying β processes the liquid is unavoidably around or above the α-β merging temperature or under the merging pressure, $|\alpha_{min}| > 1/2$ might occur as in case of PC [56] or PDE [54]. This means that in this liquids might not happen a separation of the processes and thus ITPS is obeyed. PDE's relaxation under T_g at ambient pressure shows two secondary processes [74]. For example the α_{min} curve for PDE seems to be just about to bent over but a firm confirmation needs some more points at frequencies under 100 Hz.

What about the liquids like PC and PDE? They have minimum slopes numerical bigger than $1/2$ and are reported to have a hidden JG β relaxation that is coupled to the α process; therefore the excess wing in relaxation are invariant under changes in pressure and temperature, when compared at a fixed value of the a-relaxation time [102, 56].

Let us recall the definition of the half width at half maximum in decades normalized with respect to the half Debye width $W_D/2 \approx 0.572$; $w_{1/2} = \frac{W_{1/2}}{W_D/2}$. This number is approximately 1 whenever the relaxation is Debye-like. The plot of the $w_{1/2}$ as a function of the frequency is shown in Figure 5.4 . The width follows qualitatively the behavior of α_{min} to some extent, but it seems that $w_{1/2}$ is less sensitive to temperature or pressure changes than α_{min}.

Figure 5.5 is in agreement with findings regarding the often seen correlation between the the width and if broadens or narrows with pressure increase. Here again we can see that HWHM is not as sensitive as the minimum slope to pressure changes. The width captures the main trends at high pressures, though, specifically the temperature pressure superposition at same relaxation times (ITPS) which is observed for some of the glassformers [99]. α_{min} together with $w_{1/2}$ as functions of the frequency describe the changes in the shape of high frequency dielectric loss at some relaxation time. If the minimum slope and width for two or more isotherms lie on the top of each other, this indicates that the relaxation has the same shape for $f > f_{max}$ to the inflection point. Thus, from this plot we can also estimate the frequency below which the α relaxation (high frequency part) is no longer affected by secondary processes that appears at times that are smaller than the α-relaxation time and do not couple to pres-
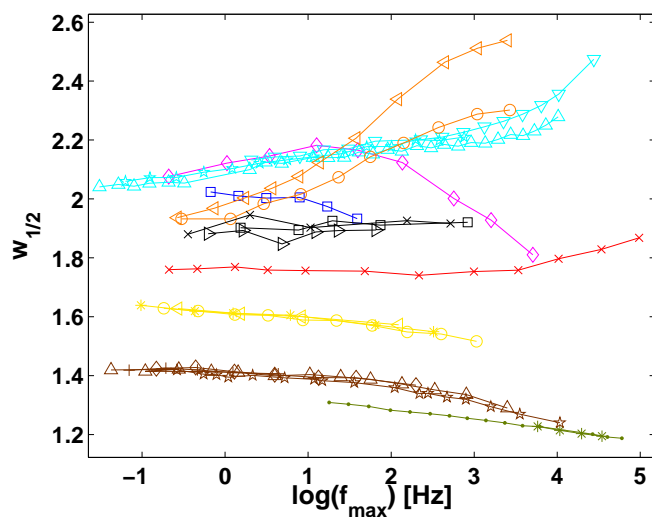
Figure 5.4: The half width vs. loss peak for data at high pressure. In this plot the data points for PHIQ are absent because at the frequency $f(\varepsilon''_{max}/2)$ is in the part of the spectra where the secondary β process is well-revealed peak, i.e. do not relates to the shape of the α peak anymore.

sure and temperature in the same way as the primary process. This happens at the frequency where the shape quantities' curves merge into one, i.e., the relaxation time determines the shape of the relaxation and that is coinvariant under temperature or pressure changes [99].

For DC704 which has a numerical minimum slope of 0.48, α_{min} is constant. While for all other liquids α_{min} changes in such a way that if α_{min} approaches -0.5, then its value is rather constant. It is interesting that materials with values of α_{min} numerically bigger that $1/2$, like for PC, have a minimum slope that changes very "slowly" and almost linearly with $\log f$ over more than 6 decades. Thus one can expect that in general α_{min} changes until it reaches 0.5 and will be constant. One apparent exception is PDE. It seems to have a constant α_{min} around -0.6 (Figure 5.2), but together with the Figure 5.3, can be a sign of a hidden β process at frequencies under 1Hz that can contribute to the primary process as in the case of DPG.
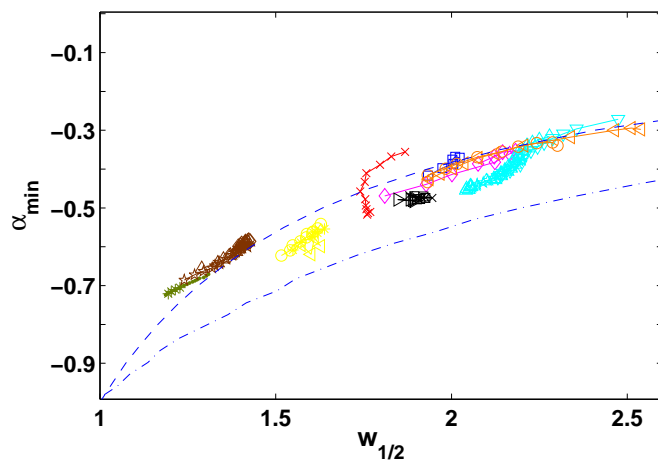
Figure 5.5: The minimum slope α_{min} plotted as a function of the normalized half width at half maximum in decades (with respect to the half Debye width $W_D/2 \approx 0.572$). The fitting function exponents $-\beta_{CD}$ and $-\beta_{KWW}$ and their respective HWHM are plotted with dashed and dashed-dot respectively lines.

5.3 Summary

In conclusion, the minimum slope and the width of the loss peak - shape parameters that describes only the high frequency part of the dispersion - capture excellently the superposition of loss with same relaxation times but at different temperatures and pressures. The considerable advantage of these two parameters is that they are model-free and thus independent of fitting procedures. With compression of the viscous liquid the minimum slope value may converge to $-1/2$ (Figure 5.2) as the α and β processes separate (Figure 5.3). The deviations from this power law are most likely due to interference from one or more secondary relaxation processes, with or without distinct maxima. If one or more secondary processes appear in the Hz range, it is practically impossible to separate α and β processes and this will be mirrored in the value of the minimum slope.

The magnitude of β process depends on the temperature its is seen for liquids which have a merging temperature within the experimental window and thus is mirrored in α_{min} changes with loss peak frequency. If the "distance" between τ_α and τ_{beta} then the signature of the temperature is not detectable in α_{min} vs. f_{max} plots.

Chapter 6
Final remarks

6.1 Coalescence of isotherm and isobaric data and computer simulations studies

In this section an attempt is made to merge data from laboratory experiments and results from computer simulations in order to provide insight into the physics of the phenomena or at least to give a tool to study vitrification.

In the following I will discuss which real liquids behave like a particular, recently defined, class of model systems termed *strongly correlating liquids* and provide some information about the underlying mechanisms. Conversely, the real liquids relaxation can suggest phenomena to look for in the simulated liquids. A feature of the strongly correlating liquids involves the concept of *density scaling* that is observed for real glassformers (TV^γ) but here the arguments are led mainly in terms of isochrone temperature pressure superposition (ITPS, cf. Section 2.3) which is one of the characteristics of the strongly correlating liquids.

Strongly correlating liquids

In Roskilde group N. P. Bailey, U. R. Pedersen , N. Gnan. S. Toxværd, T. B. Schrøder and J. C. Dyre define a class of *strongly correlating liquids* based on investigations of molecular dynamic simulations of simple models [134, 118, 119, 6, 7].

In the NVT ensemble the particle interactions of strongly correlating liquids can be approximated by an effective inverse power-law $U(r) \propto (r^{-n})$ ("soft sphere"-potential). From this it is shown that such systems exhibit a *hidden scale invariance* of the dynamics, that is: State points with the same parameter $\Gamma = T_1^{-1}\rho_1^\gamma = T_2^{-1}\rho_2^\gamma$ have (*nearly*) the same dynamics and structure (ρ is the

density and $\gamma = n/3)$[1] State points with same Γ have the same relaxation spectrum defined by the relaxation time. [118] In other words state points along isochrones are shape invariant, i.e. isochrone pressure temperature superposition is obeyed.

The simple van der Waals systems are strongly correlating liquids [134, 118, 119, 6, 7]. The natural question is whether a fulfilled ITPS is sufficient to classify a real glassformer as a strongly correlating liquid? Let us consider a hydrogen bonded liquid. Hydrogen bonded liquids are not strongly correlating liquids since the interaction potential is not spherically symmetric and cannot be approximate by a inverse power law [119]. Long range networks are formed. Simulations of Methanol show that at high temperature the H-O - - bonds break, strong particle pair interactions take over and the dynamics approximates that of strongly correlating liquids [6]. If we recall - ITPS implies that the structure and dynamics are preserved, changes in the H-network lead to a violation of the shape co-invariance with compression and heating. Although experimental loss peaks of H-bonded glass-formers which are characterized by a relatively high stretched exponent (between $0.6 - 0.75$) and with a loss peak that widens with dynamics slow down, still obeys ITPS [19, 48, 55, 131, 117, 98]. Thus the answer to the question above is no. If one uses ITPS as tool for pointing out those real strongly correlating liquids that can be expected to behave like the simple molecular models then one must exclude H-bonded liquids. In general one should be aware about dynamic complexity in real liquids.

The laboratory liquids

ITPS couples macroscopic thermodynamics with microscopic dynamics. ITPS can be understood as the particles in the liquid not "caring" about the T, P-conditions and acting always in the same way, just with different rates of action mirrored onto the observation of invariance of structural relaxation and time. In other words no matter where in the energy landscape the liquid is the molecules in the system relax in the same way, just on different time scales – the dynamics and the structure are the same when scaled. Thus if ITPS is fulfilled for the experimental relaxation times then the scaling law $\log(\tau) = f(T^{-1}\rho^\gamma)$ should be fulfilled [2, 18, 132, 99, 56]. The frequency span is almost the same for all the measurements in this work. i.e. the relaxation processes are on same timescale and a plot of the minimum slope vs. the loss peak frequency describes the changes in the spectral shape with temperature and pressure.

---

[1]Experimentally, density scaling was demonstrated though $\Gamma = TV^\gamma$ [19, 18]. The $\gamma = n/3$ relationship was also emphasized by Roland and co-workers [132]. Thus, since $\tau = \tau(T^{-1}\rho^\gamma)$, the averaged relaxation time is the same for these state points.
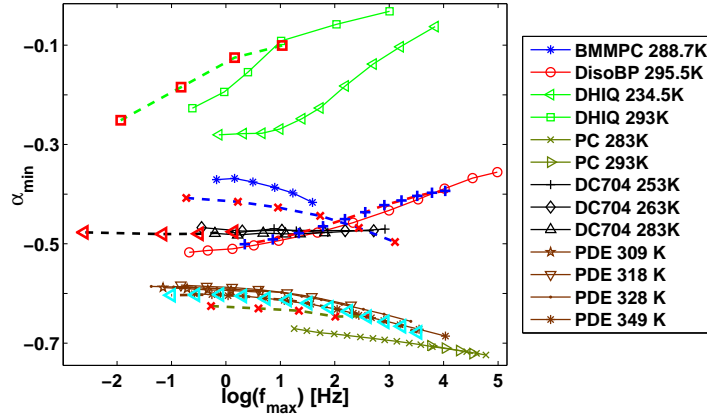
Figure 6.1: Minimum slope as function of the loss peak frequency for the liquids for which we have both ambient and high pressure data: The figure plots α_{min} from data taken at ambient pressure for different temperatures and α_{min} from measurements at isothermal condition but increasing pressure. The line colors refer to the colors associated with liquid data at high pressure (Table B.1) The liquids are BMMPC (blue), DisoBP (red), DHIQ (light green), DC704(black), PC (dark green) and PDE (brown) (see on legend or in Table B.1). The isobaric α_{min} are plotted with dashed lines and colored symbols that can be found in Table A.1. The last notation is not in the legend.

In Figure 6.1 the shape changes via α_{min} vs. f_{max} are shown for liquids used in both analyses (data at ambient pressure (isobaric) and varying temperature, and isothermal compression). These liquids are BMMPC, DisoBP, DHIQ, DC704, PC and PDE. All are van der Waals liquids. Despite all having relatively polar molecules, hydrogen bonds do not form. This make them good candidates for strongly correlating liquids. Now we can investigate whether, among these real van der Waals liquids, there are couterparts of the simple strongly correlating liquids by testing if ITPS is obeyed by means of the minimum slope, i.e. if the α_{min}-curves for the single liquid lie on the top of each other at different thermodynamic conditions. If we take away points for the glassformers for which the isotherm and isobaric α_{min} curves are not on the top of each other (within some uncertainty) then there are three liquids that obey ITPS – DisoBP, PDE and DC704 (See in Figure 6.2). The minimum slope captures intrinsically the interaction between the α and β processes given that the inflection point $f_{\alpha_{min}}$ is the boundary frequency where the α relaxation process takes over. Thus the fingerprint of the different β processes will be seen. DisoBP and PDE show
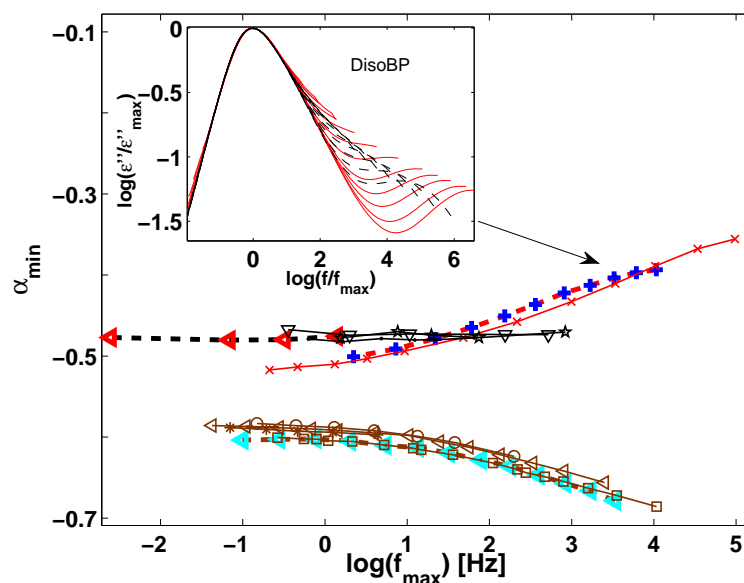
Figure 6.2: The candidates for real simple strongly correlating liquids DisoBP (red line), DC704(black line) and PDE (brown line) have isothermal and isobaric slopes that are same at given relaxation time. The spectral shape at given loss peak frequency f_{max} is same under different thermodynamic conditions. In other words in this situation the β process do not affect the spectral shape invariance

isochrone spectral shape invariance, no matter that the two liquids are different types according to the A and B type classification schema. PDE is an EW liquid[2], while DisoBP is a "classical" B-type with α and β processes that separates upon cooling at ambient pressure (black dashed line in the inset in Figure 6.2). The intensity of the same β process is much higher in the isothermal (room temperature) dissipation (red line in the inset in Figure 6.2) but a time scale separation is observed as well. However the two α_{min} curves are on the top of each other, i.e., the shape at the inflection point of the dielectric loss at given relaxation time is same no matter what the intensity of the beta relaxation limited of course to these two datasets.

---

[2]PDE deserves to be investigated further by other techniques because of the reported underlying relatively low intensity β processes [102, 56, 74] in the accessible frequency window (might explain the minor deviation of the slopes at the highest temperature (349 K) from the rest of the isotherm data).

DC705 shows even a more strong invariance $\alpha_{min}(f_{max}, T, p) = const$ for all f_{max} TTPS in the experimental window.

ITPS in terms of minimum slope is fulfilled for the glass-formers DisoBP, PDE and DC704. This means: If one chooses a particular relaxation time τ (f_{max}) then the shape of the relaxation can be described by the same value for the slope in the inflection point. The slope at inflection point is the same at a given relaxation time no matter if there is a secondary relaxation for some glassformers. α_{min} gives a measure of the intermolecular interactions. The studies in MD simulation should be the perfect tool and key to understanding the dynamics under densification. These findigs agree to some extent with Ngai's suggested correlation between the stretching exponent and the relaxation time. In fact in his argument is that ITPS used as an evidence for the stretched exponent governs the relaxation properties of the primary relaxation (This is the main assumption in the in Ngai's coupling model.) [96, 5, 100]. If the dependent and the independent variables interchange place in the CM then $\beta_{KWW} = \beta_{KWW}(\tau)$.

In this study we can see DC704, DisoBP and PDE[3] as possible candidates to be the real strongly correlating liquids: They are van der Waals liquids, obey (at least within the frequency window) ITPS (and can be expected to fulfil density scaling relation or liquid specific γ. It is hes been reported for PDE $\gamma \approx 4.5$ [34, 20]).

What from the real world can be interesting to see in computer simulations? Some simulated strongly correlating liquids have correlation functions that show a high frequency slope of $-1/2$ Figure 6.3. Bearing in mind DC704 TTPS one can state a conjecture that an ideal strongly correlating liquid that obeys a general time temperature pressure superposition decays with $\sqrt{(t)}$ and this conjecture can be tested with computer simulations.

---

[3]PC needs some more relaxation process survey before a definitive classification can be undertaken
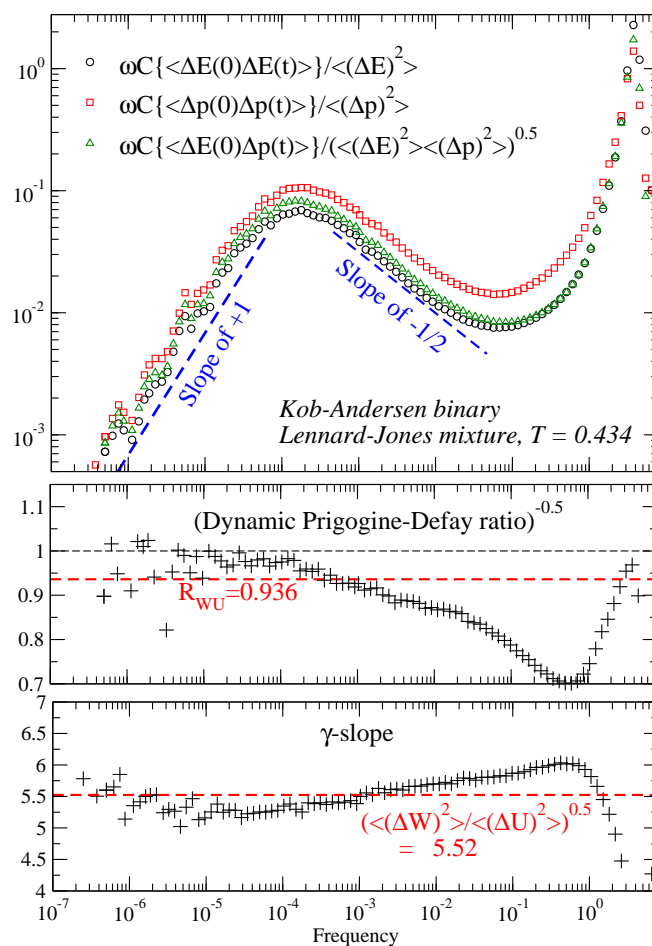
Figure 6.3: Results from computer simulations of a strongly correlating liquid. In the normalized imaginary parts of natural response functions - the frequency dependent isochoric specific heat capacity per unit volume $c''_V(\omega)$, isothermal bulk modulus $K''_T(\omega)$ and isochoric pressure coefficient $\beta''_V(\omega)$ respectively (*NVT* ensemble of the Kob-Andersen Lennard-Jones liquids at $T = 0.434$) the peak on the left is the structural relaxation peak. The left-hand side of the structural relaxation peak has slope 1 and the right-hand side has close to slope $-1/2$. In the lower panels is the plot of the inverse square root of the dynamic Prigogine-Defay ratio ($\Lambda(\omega) = c''_V(\omega)K''_T(\omega)/(T(\beta''_V(\omega))^2)$ and the corresponding slope which is related to the scaling factor *gamma*. The instantaneous $W - U$ (virial and potential energies) correlation coefficient $R_{WU} = 0.936$ and slope $\gamma_{WU} = 5.52$ are indicated with red dashed lines. This Figure is copied from Reference [118]

Chapter 7
Outlook

In the following I will try to sketch some of the questions that appeared during the work with the project. The most points regard high pressure experiments.The last years the number of high pressure dielectric scans nearly is exploded in the last two decades in spite that the technique is relatively old. Thus, the most questions concerns the influence of the high pressure on some properties,

7.1 What one can use minimum slope for?

Since there is strong indication for that α_{min} captures temperature and pressure induced changes in liquids. It should paid some more attention.

Study of the convex α_{min} curves in α_{min} vs f_{max} plot where indicated presence of a β relaxation is experimental tested.

1. Are there other liquids with well revealed β process which does not violates the temperature-pressure superposition at same relaxation times,

2. Can one use the β-process induced curves in the α_{min} to give information about relative magnitude of the secondary process?

3. What kind of β processes can be detected? Intra- or intermolecular?

4. Is beta relaxation really a broad symmetric loss peak? The stated question is as follows: Is Cole-Cole fitting function the best to describe he secondary relaxation?.

5. The origin of β-process

6. High pressure, dielectric and mechanical scans of excess wing materials - is EW always seen in the spectral shape.

7. Model investigation of description of the interaction between α and β processes - dependence on temperatue or pressure. The models should model a convolution of the two processes. fx. the electrical circuit model suggested by N.B. Olsen. Do this this model shows a linear parts in the spectra like EW?

8. Study of the correlation between the high dielectric magnitude and Kirkwood factor. - does the degree of cooperativity influences the magnitude of α relaxation and the minimum slope.

9. Observation:$T_g = \frac{2}{3}T_m$. can we find an counterpart of this phenomenological rule $T_g(p) = \frac{2}{3}T_m(p)$ if $p = const$ or
$p_g(T) = a\, p_m(T)$, $a < 1$ if $T = const$?

10. Experiment: Squeeze and then cool down $\rightarrow$ $T_g^*(p)$ Cool down and then squeeze $\rightarrow$ $T_g^{**}(p)$ We expect $T_g^*(p) \approx T_g^{**}(p)$. Question?: Is the time to equilibrate until $p_g^*(T) = p_g^{**}(T)$ symmetric, i.e., takes equal time? Experiential procedure.

11. Observation: $p(T)$ influences the network generation in glassformers Q: H-bonds spoils the "nice" slopes then a pressure induced breaks in the H bonds should give the true slope. What about monoalchohols? Does the dielectric Debye relaxation survive the the high pressure.

12. Minimal model calculated for high pressure.

13. "Wing" glassformers and the observation $p \rightarrow \tau_{beta} \approx const$

14. β process indicates some relaxation times where the translational and rotational motion decouples -problem - the motion of charge carriers is not an universal feature in the dielectric relaxation spectra. - however - does the decoupling appears at $\alpha - \beta$ merging frequency/temperature

Chapter A
Table of liquids in the analysis

Table A.1: List of all liquids studied giving relevant references and information such as glass transition temperature T_g, and intervals for quantities characterizing the data: the activation energy temperature index, $I_{\Delta E} \equiv |d \ln \Delta E / d \ln T|$; temperature interval for measurements used here T; maximum dielectric loss interval $\log \varepsilon''_{max}$; and minimum slopes of the log-log plot of the loss $|\alpha_{min}|$.

Liquid	Abbrevi-	T_g (K)	Intervals				Symbol
	ation		$I_{\Delta E}$	T (K)	$log \varepsilon''_{max}$	$|\alpha_{min}|$	and ref.
1,2-propanediol	PG	168 [87]	1.16; 1.56]	180; 205	1.3; 1.375	0.66; 0.69	◁ [103]
1,3-propane diol	13PD	167[127]	0.73; 1.13	165; 189	1.419; 1.477	0.73; 0.75	● (a)
2,3-dimethyl- pentane	2,3- DMP	87.5	1.78; 1.78	98; 99	$-1.971; -1.967$	0.43; 0.44	▽ [136]
2,3-epoxy- propyl- phenylether	23EPPPE	193	3.74; 3.79	196; 200	0.483; 0.522	0.55; 0.55	▷ [103]
2,4,6-trimethyl- heptane	246TMH	122.7	2.51; 2.51	134; 135	$-2.025; -2.024$	0.35; 0.36	◇ [136]
2-methyl- pentane- 2:4-diol	2MP24D	187	3.2; 3.5	210; 232	$-0.28; -0.202$	0.39; 0.49	○ [103]
2-methyl- tetrahydrofuran	MTHF	90.7	2.77; 3.66	91; 103	0.776; 0.815	0.5; 0.51	▽ [103]
2-phenyl- 5-acetomethyl- 5-ethyl- 1,3-	APED	222[44]	2.69; 3.23	220; 240	0.357; 0.397	0.46; 0.49	▽

Table A.1 – continued from previous page

Liquid	Abbreviation	T_g (K)	Intervals				Symbol and ref.
			$I_{\Delta E}$	T (K)	$log\varepsilon''_{max}$	$|\alpha_{min}|$	
dioxocyclo-hexane							[103]
2-picoline	2pic	130	3.17; 3.26	135; 141	0.618; 0.658	0.52; 0.55	▷[43]
3-fluoro-aniline	3FA	172[147]	5.1; 5.1	235; 239	−0.135; −0.121	0.46; 0.48	□ [151]
3,3,4,4-benzophenone-tetracarboxylic dianhydride	BPC	212	3.67; 3.67	338; 362	0.258; 0.321	0.41; 0.5	◇ [102]
3-methyl-heptane [136]	3MH	97	1.78; 1.78	109; 110	−2.477; −2.477	0.27; 0.27	●
3-methyl-pentane	3MP	79	1.97; 1.97	88; 89	−2.283; −2.281	0.36; 0.38	✳ [136]
3-methyl phosphate	3MPh	136	2.7; 3.51	141; 150	1.104; 1.214	0.55; 0.56	◁ [8]
4-methyl-heptane	4MH	99	1.63; 1.98	111; 114	−2.004; −1.995	0.48; 0.49	★ [136]
4-tertbuthyl-pyridine	4TBP	166	2.32; 13.79	164; 177	0.566; 0.602	0.52; 0.54	△ [8]
4,7,10-trioxatridecane-1,13- diamine	TOTDD	108	4.45; 4.45	177; 181	0.356; 0.401	0.33; 0.38	◁ [103]
5-polyphenyl-ether	PPE	248	4.04; 4.24	252; 264	−0.258; −0.214	0.5; 0.51	✳ [67]
α-phenyl-o-cresol	PoC	219	4.01; 4.01	220; 228	0.011; 0.032	0.46; 0.47	✳ [103]
benzophenone	BP	212	3.59; 3.66	215; 230	0.56; 0.647	0.55; 0.58	□[90]
biphenyl-2yl-isobutylate	BP2BF	210 [44]	1.86; 2.03	190; 200	1.232; 1.253	0.66; 0.68	✳ [103]
butyronitrile	But	95	1.91; 1.91	98; 116	1.061; 1.121	0.59; 0.67	+[64]
decahydro-isoquinoline	DHIQ	180[129]	7.13; 7.13	180; 185	−0.626; −0.599	0.1; 0.25	□ [129, 67]
dibutyl-ammonium-formide	DBAF	153	1.14; 2.22	162; 185	1.127; 1.218	0.67; 0.69	▷ [65]
dibutyl phthalate	DBP	177	2.6; 3.07	178; 192	0.301; 0.348	0.48; 0.51	✳ [103]
di-*iso*-butyl phthalate	DisoBP	191 [147]	1.65; 2.94	201; 221	−0.06; −0.016	0.39; 0.5	+ [103]
dicyclohexyl-methyl-2-methyl-succinate	DCMMS	220	2.8; 3.41	224; 240	0.381; 0.411	0.49; 0.5	▽ [30]
dicyclohexyl	DCHMS	222[44]	2.11; 2.64	218; 230	−0.05; −0.041	0.37; 0.38	●

Liquid	Abbrevi-ation	T_g (K)	Intervals				Symbol and ref.
			$I_{\Delta E}$	T (K)	$log\varepsilon''_{max}$	$|\alpha_{min}|$	
-2-methyl-succinate							[103]
diethyl phthalate	DEP	187[147]	2.93; 2.93	183; 192	0.375; 0.412	0.49; 0.5	○ [103]
diglycidyl-ether of bisphenol A (epoxy-resin)	ER		[3.67; 3.67]	[338; 362]	[0.258; 0.321]	[0.41; 0.5]	◇ [95]
dioctyl phthalate	DOP	189 [75]	1.35; 2.21	190; 220	0.168; 0.205	0.5; 0.53	◇ [103]
dipropylene-dimethyl-glycol-dimethylether	DPGDME	137[48]	3.52; 3.52	139; 151	0.327; 0.373	0.45; 0.48	▷ [103]
ethylene glycol	EG	152	2.64; 2.64	158; 165	1.354; 1.364	0.63; 0.67	+ [9]
glycerol	Gly	193[127]	1.29; 1.77	192; 236	1.317; 1.401	0.57; 0.62	★ [110]
isoeugenol		220	2.85; 2.99	225; 248	0.085; 0.104	0.46; 0.49	× [103]
isopropyl-benzene (cumene)	Cumene	126	3.01; 3.05	135; 139	$-0.951; -0.948$	0.49; 0.51	△ [103]
methyl-m-toluate	MMT	165	2.42; 2.6	173; 189	0.371; 0.397	0.49; 0.55	◇ [103]
n-ε-methyl-caprolactam	nMC	172 [50]	1.45; 1.45	186; 196	0.778; 0.816	0.59; 0.62	△ [103]
n-propyl-benzene	nPB	122 [147]	2.05; 2.7	127; 137	$-0.902; -0.878$	0.54; 0.63	★ [103]
phenol-phthalein-dimethylether	PDE	295 [123]	3.61; 4.04	301; 325	0.808; 0.833	0.6; 0.68	◁ [54]
phenylsalicate (salol)	Salol	215[51]	3.2; 4.53	177; 187	0.793; 0.834	0.46; 0.48	× [43]
polypropylene-glycol 400	PPG	73.23	1.9; 3.19	200; 226	0.436; 0.556	0.4; 0.48	+ [110]
propylene carbonate	PC	160	3.4; 4.22	162; 170	1.699; 1.703	0.63; 0.65	× [145]
salicyl-salicylic acid	SSA	279[31]	3.1; 3.1	305; 308	$-0.243; -0.238$	0.23; 0.23	× [103]
sorbitol	Sor	268 [147]	6.12; 6.12	268; 273	0.895; 0.959	0.26; 0.3	□ [103]
sucrose-benzoate	SB	337	2.47; 3.96	343; 373	$-0.461; -0.373$	0.35; 0.41	○ [124]
tetraphenyl-tetramethyl-trisiloxane	DC704	211	3.93; 3.93	211; 219	$-1.148; -1.109$	0.48; 0.48	◁ [67]
tricresyl-	TCP	211	2.5; 3.29	214; 236	0.33; 0.356	0.56; 0.58	□

Table A.1 – continued from previous page

Liquid	Abbrevi-ation	T_g (K)	Intervals				Symbol and ref.
			$I_{\Delta E}$	T (K)	$log\varepsilon''_{max}$	$|\alpha_{min}|$	
phosphate isomer mixure							[52]
trimethyl-pentaphenyl trisiloxane	DC705	230	$3.81; 3.81$	$233; 235$	$-1.203; -1.191$	$0.49; 0.5$	○ [103]
triphenyl phosphite	TPP	204	$5.08; 5.08$	$204; 208$	$-0.493; -0.479$	$0.48; 0.49$	× [110]
triphenyl-ethylene	TPE	249[108]	$3.72; 3.72$	$256; 258$	$-1.866; -1.856$	$0.46; 0.49$	○ [67]
toluene-pyridine mixture	TolPyr	123[109]	$5.16; 6.1$	$126; 131$	$0.597; 0.698$	$0.28; 0.44$	△ [112]
xylitol	Xylitol	248[147]	$3.29; 3.98$	$254; 266$	$1.019; 1.065$	$0.28; 0.34$	● [103]

Chapter B
Table of liquids measured at high temperature

List of all liquids studied at high pressure - giving relevant references and information such as pressure interval of the data taken in the anaysis p, and intervals for quantities characterizing the data: T; maximum dielectric loss interval $\log \varepsilon''_{max}$; and minimum slopes of the log-log plot of the loss $|\alpha_{min}|$.

Table B.1:

Liquid	Abbre-viation	Ref.	T (K)	Intervals			Symb.
				P (Pa)	$log\varepsilon''_{max}$	$|\alpha_{min}|$	
chlorinated biphenyl	CBP, Aroclor	[102]	283	174988275;277326525	0.091;0.097	0.55 ; 0.61	∗
			263	81870600;172860450	0.117;0.137	0.54 ; 0.62	○
			274	1414;2112	0.101;0.105	0.58 ; 0.62	◁
1,1-bis-(p-methoxyphenyl)-cyclohexane	BMMPC	[53]	289	2026500;29485575	$-0.929;-0.923$	0.37 ; 0.42	□
Di-*iso*-butyl ph-thalate	D*iso*BP	[113]	296	7295400;14590800	$-0.238;-0.179$	0.36 ; 0.52	×
decahydro-isoquinoline	PHIQ	[104]	235	1070245313;1570537500	$-1.154;-1.102$	0.06 ; 0.28	▷
			293	645946875;899259375	$-1.106;-1.047$	0.03 ; 0.23	+
di-propylene-glycol	DPG	[47]	252	5978175;14590800	0.442;0.468	0.35 ; 0.47	◇
diglycidyl-ether of bisphenol-A	EPON828	[95]	293	88051425;246523725	$-0.006;0.147$	0.32 ; 0.45	△
			303	204777825;335284425	0.027;0.142	0.36 ; 0.45	⋆
			313	213694425;375105150	$-0.042;0.088$	0.27 ; 0.42	▽
propylene-carbonate	PC	[56]	283	20771625;28877625	1.227;1.235	0.67 ; 0.72	●

Table B.1 – continued from previous page

Liquid	Abbre-viation	Ref.	T (K)	Intervals			Symb.
				P(Pa)	$log\varepsilon''_{max}$	$|\alpha_{min}|$	
			293	25939200;28371000	1.021;1.093	0.71 ; 0.72	∗
tri-propylene-glycol	TPG	[121]	253	7295400;14590800	0.279;0.381	0.33 ; 0.43	○
			278	12868275;20366325	0.282;0.42	0.29 ; 0.43	◁
tetra-methyltetra-phenyl-trisiloxane	DC704	[104]	253	95752125;146414625	−1.303;−1.255	0.47 ; 0.48	□
			263	135066225;208932150	−1.306;−1.25	0.47 ; 0.47	×
			283	259290675;308129325	−1.3;−1.265	0.48 ; 0.48	▷
phenolphthalein-dimethylether	PDE	[54]	309	-79;227	0.554;0.561	0.59 ; 0.6	+
			318	-79;512	0.533;0.542	0.58 ; 0.62	◇
			328	29;1045	0.523;0.537	0.59 ; 0.66	△
			349	571;1649	0.456;0.494	0.6 ; 0.69	⋆

Bibliography

[1]   G. Adam and J. H. Gibbs. On temperature dependence of cooperative relaxation properties in glass-forming liquids. *J. Chem. Phys.*, 43:139, 1965.

[2]   C. Alba-Simionesco, A. Cailliaux, A. Alegria, , and G. Tarjus. Scaling out the density dependence of the a relaxation in glass-forming polymers. *EUROPHYSICS Letters*, 68:58, 2004.

[3]   C. A. Angell. *Journal of Non-Crystalline Solids*, 13:133, 1991.

[4]   C. A. Angell, A. Dworkin, P. Figuiere, A. Fuchs, , and H. Szwarc. Strong and fragile plastic crystals. *Journal of Chemical Physics*, 62:773, 1985.

[5]   C. A. Angell, K. L. Ngai, G. B. McKenna, P. F. McMillan, and . Martin S. W. Relaxation in glassforming liquids and amorphous solids. *Journal of Applied Physics*, 88:3113, 2000.

[6]   Nicholas P. Bailey, Ulf R. Pedersen, Nicoletta Gnan, Thomas B. Schrøder, and Jeppe C. Dyre. Pressure-energy correlations in liquids. I. results from computer simulations. *J. Chem. Phys.*, 129:184507, 2008.

[7]   Nicholas P. Bailey, Ulf R. Pedersen, Nicoletta Gnan, Thomas B. Schrøder, and Jeppe C. Dyre. Pressure-energy correlations in liquids. II. analysis and consequences. *J. Chem. Phys*, 129:184508, 2008.

[8]   T. Blochowicz, C. Gainaru, P. Medick, C. Tschirwitz, and E. A. Rössler. The dynamic susceptibility in glass forming molecular liquids: The search for universal relaxation patterns ii. *Journal of Chemical Physics*, 124(13):134503, 2006.

[9]   T. Blochowicz, C. Tschirwitz, S. Benkhof, and E. A. Rössler. *J. Chem. Phys.*, 118:7544, 2003.

[10]   R. B′ohmer, R. V. Chamberlin, G. Diezemann, B. Geil, A. Heuerand G. Hinze, S. C. Kuebler, R. Richert, B. Schiener, H. Sillescu, H.W. Spiess,

U. Tracht, and M. Wilhelm. Nature of the non-exponential primary relaxation in structural glass-formers probed by dynamically selective experiments. *JOURNAL OF NON-CRYSTALLINE SOLIDS*, 235:1, AUG 1998.

[11] R. Böhmer, K. L. Ngai, C. A. Angell, and D. J. Plazek. Non-exponential relaxations in strong and fragile glass formers. *J. Chem. Phys.*, 99:4201, 1993.

[12] C. J. F. Böttcher. *Theory of electric polarization*, volume I. Elsevier scientific publishing company, 1973.

[13] C. J. F. Böttcher and P. Bordewijk. *Theory of electric polarization*, volume 1. Elsevier Scientific Publishing Company, 2 edition, 1978.

[14] A. Brodin, C. Gainaru, V. Porokhonskyy, and E. A..Roessler. Evolution of dynamic susceptibility in molecular glass formers - a critical assessment. *JOURNAL OF PHYSICS-CONDENSED MATTER*, 19(20), MAY 23 2007.

[15] H. B. Callen and T. A. Welton. Irreversibility and generalized noise. *Phys.Rev.*, 83:34, 1951.

[16] R. Casalini., K. J. McGrath, and C. M. Roland. Isobaric and isochoric properties of decahydroisoquinoline, an extremely fragile glass-former. *JOURNAL OF NON-CRYSTALLINE SOLIDS*, 352(42-49, Sp. Iss. SI):4905–4909, NOV 15 2006.

[17] R. Casalini, M. Paluch, and C. M. Roland. Influence of molecular structure on the dynamics of supercooled van der waals liquids. *PHYSICAL REVIEW E*, 65:031505, 2003.

[18] R. Casalini and C. M. Roland. Thermodynamical scaling of the glass transition dynamics. *Physical Review E: Statistical, Nonlinear, and Soft Matter Physics*, 69:062501, 2004.

[19] R. Casalini and C. M. Roland. *Phys. Rev. E*, 72:031503, 2005.

[20] R. Casalini and C. M. Roland. Scaling of the supercooled dynamics and its relation to the pressure dependences of the dynamic crossover and the fragility of glass formers. *Physical Review B*, 71(1), JAN 2005.

[21] R. V. Chamberlin. Experiments and theory of the nonexponential relaxation in liquids, glasses, polymers and crystals. *PHASE TRANSITIONS*, 65(1-4, Part B):169–209, 1999.

[22] M. H. Cohen and G. S. Grest. Liquid-glass transition, a free-volume approach. *Physical Review B*, 20:1077, 1979.

[23] M. H. Cohen and D. Turnbull. *J. Chem. Phys.*, 31:1164, 1959.

[24] K. S. Cole and R. H. Cole. *J. Chem. Phys.*, 9:341, 1941.

[25] Lucia Comez, Daniele Fioretto, Hartmut Kriegs, and Werner Steffen. Temperature and pressure dependence of the a relaxation and configurational entropy of a prototype glass former. *Physical Review E*, 66:032501, 2002.

[26] D. W. Davidson and R. H. Cole. Dielectric relaxation in glycerine. *J. Chem. Phys.*, 18:141, 1950.

[27] D. W. Davidson and R. H. Cole. Dielectric relaxation in glycerol, propylene glycol and n-propanol. *J. Chem. Phys.*, 19:1484, 1951.

[28] L. De Francesco, M. Cutroni, and A. Mandanici. *Philos. Mag. B*, 82:625, 2002.

[29] P. Debye. *Polar Molecules*. The Chemical Catalog Company, Inc., 1929.

[30] R. Diaz-Calleja, A. Garcia-Bernabe, M.J. Sanchis, and L.F. del Castillo. Interconversion of mechanical and dielectrical relaxation measurements for dicyclohexylmethyl-2-methyl succinate. *Physcial Review E*, 72(5):051505, 2005.

[31] H. P. Diogo, S. S. Pinto, , and J. J. Moura Ramos. *J. Therm. Anal. Cal.*, 77:893, 2004.

[32] P.K. Dixon, L. Wu, S.R. Nagel, B.D. Williams, and J.P. Carini. *Phys. Rev. Lett*, 65:1108, 1990.

[33] Ernst-Joachim Donth. *The glass transition: relaxation dynamics in liquids and disordered materials*. Springer series in materials science Physics and astronomy online library, Heidelberg : Springer, 2001.

[34] C. Dreyfus, A. Le Grand, J. Gapinski, W. Steffen, and A. Patkowski. *Eur. J. Phys.*, 42:309, 2004.

[35] J. C. Dyre. Colloquium: The glass transition and elastic models of glass-forming liquids. *Reviews of Modern Physics*, 78:953–972, 2006.

[36] J.C. Dyre and N.B. Olsen. Landscape equivalent of the shoving model. *Physical Review B*, 69:042501, 2004.

[37] Jeppe C. Dyre. *Phys. Rev. B*, 51:276, 1995.

[38] M. D. Ediger, C. A. Angell, and Sidney R. Nagel. Supercooled liquids and glasses. *Journal of Physical Chemistry*, 100:13200, 1996.

[39] John D. Ferry. *Viscoelastic properties of polymers*. John Wiley & Sons, INC., second edition, 1961.

[40] G.S. Fulcher. Analysis of recent measurements of the viscosity of glasses. *Journal of American Ceramic Society*, 8:339–355, 1925.

[41] G.S. Fulcher. Analysis of recent measurements of the viscosity of glasses. ii. *Journal of American Ceramic Society*, 8:789, 1925.

[42] Gainaru, C., Lips, O., Troshagina, A., Kahlau, R., Brodin, A., Fujara, F., Roessler, and E. A. On the nature of the high-frequency relaxation in a molecular glass former: A joint study of glycerol by field cycling NMR, dielectric spectroscopy, and light scattering. *JOURNAL OF CHEMICAL PHYSICS*, 128(17), MAY 7 2008.

[43] C. Gainaru, A. Rivera, S. Putselyk, G. Eska, and E. A. Rössler. Low-temperature dielectric relaxation of molecular glasses: Crossover from the nearly constant loss to the tunneling regime. *Physical Review B*, 72(17):174203, 2005.

[44] A. Garcia-Bernabé. private communication.

[45] J.H. Gibbs and E.A. DiMarzio. Nature of the glass transition and the glassy state. *Journal of Chemical Physics*, 28(3):373–383, 1958.

[46] K. Grzybowska, A. Grzybowski., J. Ziolo., S.J. Rzoska., and M. Paluch. Anomalous behavior of secondary dielectric relaxation in polypropylene glycols. *Journal of Physics-Condensed Matter*, 19(37), SEP 19 2007.

[47] K. Grzybowska, S. Pawlus, M. Mierzwa., M.Paluch, and K. L. Ngai. *J. Chem. Phys.*, 125:144507, 2004.

[48] K. Grzybowska, S. Pawlus, M. Mierzwa., M.Paluch, and K. L. Ngai. Changes of relaxation dynamics of a hydrogen-bonded glass former after removal of the hydrogen bonds. *Journal of Chemical Physics*, 125(14), OCT 14 2006.

[49] I. Gutzow and J. Schmelzer. *The Vitreous State: Thermodynamics, Structure, Rheology, and Crystallization*. Springer, Berlin, 1995.

[50] C. Hansen and R. Richert. Dipolar dynamics of low-molecular-weight organic materials in the glassy state. *Journal of Physics-Condensed Matter*, 9(44):9661–9671, 1997.

[51] M. Hatasea, M. Hanayab, , and M. Oguni. *J. Non-Cryst. Solids*, 333:129, 2004.

[52] T. Hecksher, A. I. Nielsen, N. B. Olsen, , and J. C. Dyre. Little evidence for dynamic divergences in ultraviscous molecular liquids. *Nature Physics*, 4:737, 2008.

[53] S. Hensel-Bielowka, J. Zioło, M. Paluch, and C. M. Roland. The effect of pressure on the structural and secondary relaxations in 1,1 -bis (p-methoxyphenyl) cyclohexane. *J. Chem.Phys*, 117:2317, 2002.

[54] S. Hensel-Bielowka and M. Paluch. Origin of the high-frequency contributions to the dielectric loss in supercooled liquids. *Phys. Rev. Lett*, 89:025704, 2002.

[55] S. Hensel-Bielowka, M. Paluch, and K. L. Ngai. Emergence of the genuine johari-goldstein secondary relaxation in m-fluoroaniline after suppression of hydrogen-bond-induced clusters by elevating temperature and pressure. *Journal of Chemical Physics*, 123(1), JUL 1 2005.

[56] S. Hensel-Bielowka, S. Pawlus, C. M. Roland, J. Zioło, and M. Paluch. Effect of large hydrostatic pressure on the dielectric loss spectrum of type-a glass formes. *Physical Review E*, 69:050501, 2004.

[57] R. Hilfer. H-function representations for stretched exponential relaxation and non-debye susceptibilities in glassy systems. *Physical Review E*, 65(6, Part 1):061510, JUN 2002.

[58] Ian M. Hodge. Strong and fragile liquids - a brief critique. *Journal of Non-Crystalline Solids*, 202:164, 1996.

[59] A. Hofmann, F. Kremer, E.W. Fischer, and A. Schonhals. *Disorder Effects on Relaxational Processes*, page 308. Springer, Berlin, 1994.

[60] W. Huang, S. Shahriari, and R. Richert. Dynamics of glass-forming liquids. x. dielectric relaxation of3-bromopentane as molecular probes in 3-methylpentane. *Journal of Chemical Physics*, 123(16):164504, 2005.

[61] H. Huth, L.-M. Wang, C. Schick, and R. Richert. Comparing calorimetric and dielectric polarization modes in viscous 2-ethyl-1-hexanol. *Journal of Chemical Physics*, 126(10), MAR 14 2007.

[62] B. Igarashi, T. Christensen, E. H. Larsen, N. B. Olsen, I. H. Pedersen, T. Rasmussen, , and J. C. Dyre. An impedance-measurement setup optimized for measuring relaxations of glass-forming liquids. *Review of Scientific Instruments*, 79:045106, 2008.

[63] Brian Igarashi, Tage Christensen, Ebbe H.Larsen, Niels Boye Olsen, Ib H.Pedersen, Torben Rasmussen, , and Jeppe C.Dyre. A cryostat and temperature control system optimized for measuring relaxations of glass-forming liquids. *Review of Scientific Instruments*, 79:045105, 2008.

[64] N. Ito, , K. Duvvuri, D. V. Matyushov, and R. Richert. Solvent response and dielectric relaxation in supercooled butyronitrile. *Journal of Chemical Physics*, 125(2):024504, 2006.

[65] N. Ito, W. Huang, and R. Richert. Dynamics of a supercooled ionic liquid studied by optical and dielectric spectroscopy. *Journal of Physical Chemistry B*, 110(9):4371–4377, 2006.

[66] J. Jäckle. Models of the glass transition. *Rep. Prog. Phys.*, 49:171, 1986.

[67] B. Jakobsen, K. Niss, , and N. B. Olsen. Dielectric and shear mechanical alpha and beta relaxations in seven glass-forming liquids. *Journal of Chemical Physics*, 123(23):234511, 2005.

[68] G. P. Johari. Intrinsic mobility of molecular glasses. *Journal of Chemical Physics*, 58:1766, 1973.

[69] G. P. Johari. *Ann. N.Y. Acad. Sci.*, 279:117, 1976.

[70] G. P. Johari. Localized molecular motions of beta-relaxation and its energy landscape. *Journal of Non-Crystalline Solids*, 307:317, 2002.

[71] G. P. Johari and M. Goldstein. Viscous liquids and glass transition. II. secondary relaxations in glasses of rigid molecules. *Journal of Chemical Physics*, 53:2372, 1970.

[72] G. P. Johari and M. Goldstein. Viscous liquids and glass transition III secondary relaxations in aliphatic alcohols and other nonrigid molecules. *Journal of Chemical Physics*, 55:4245, 1971.

[73] G. P. Johari, G. Power, J. Vij, and K. Ngai. *Journal of Chemical Physics*, 116:5908, 2002.

[74] S. Kahle, J. Gapinski, G. Hinze, A. Patkowski, and G. Meier. *J. Chem. Phys.*, 122:074506, 2005.

[75] E. Kaminska, K. Kaminski, M. Paluch, J. Ziolo, and K. L. Ngai. *J. Chem. Phys.*, 126:174501, 2007.

[76] Kessairi, Khadra, Capaccioli, Simone, Prevosto, Daniele, Sharifi, Soheil, Rolla, and Pierangelo. Effect of temperature and pressure on the structural (alpha-) and the true johari-goldstein (beta-) relaxation in binary mixtures. *JOURNAL OF NON-CRYSTALLINE SOLIDS*, 353(47-51):4273–4277, DEC 1 2007.

[77] K. Kessairi, S. Capaccioli, D. Prevosto, M. Lucchesi, S. Sharifi, and P. A. Rolla. Interdependence of primary and johari-goldstein secondary relaxations in glass-forming systems. *J. Phys. Chem. B*, 112:643, 2008.

[78] S. Capaccioliand K. Kessairi, D.Prevosto, M. Lucchesi, and K. L. Ngai. Genuine johari-goldstein beta-relaxations in glass-forming binary mixtures. *JOURNAL OF NON-CRYSTALLINE SOLIDS*, 352(42-49, Sp. Iss. SI):4643–4648, NOV 15 2006.

[79] J. G. Kirkwood. *J. Chem. Phys*, 4:592, 1936.

[80] D. Kivelson, G. Tarjus, X. Zhao, and S.A. Kivelson. Fitting of viscosity: Distinguishing the temperature dependences predicted by various models of supercooled liquids. *Physical Review E*, 53(1):751–758, 1996.

[81] M. Köhler, P. Lunkenheimer, and A. Loidl. Dielectric and conductivity relaxation in mixtures of glycerol with LiCl. *Eur. Phys. J. E*, 27:115, 2008.

[82] R. Kohlrausch. Theorie des elektrischen rückstandes in der leidener flasche. *Annalen der Physik,*, 91:49, 1854.

[83] F. Kremer and A. Schönhals, editors. *Broadband Dielectric Spectroscopy*. Springer-Verlag, Berlin, Heidelberg, New York, 2003.

[84] R. Kubo. Statistical-mechanical theory of irreversible processes. *J. Phys. Soc. Japan*, 12:570, 1957.

[85] A. Kudlik, S. Benkhof, T. Blochowicz, C. Tschirwitz, , and E. Rössler. The dielectric response of simple organic glass formers. *JOURNAL OF MOLECULAR STRUCTURE*, 479(2-3):201–218, APR 27 1999.

[86] R.L. Leheny and S.R. Nagel. *Europhys. Lett.*, 39:447, 1997.

[87] C. Leon, K. L. Ngai, , and M. Roland. *Journal of Chemical Physics*, 110:11585, 1999.

[88] C. Leon and K.L. Ngai. *J. Phys. Chem. B*, 103:4045, 1999.

[89] P. Lunkenheimer and A. Loidl. Dielectric spectroscopy of glass-forming materials: alpha-relaxation and excess wing. *Journal of Chemical Physics*, 284:205, 2002.

[90] P. Lunkenheimer, L. C. Pardo, M. Koehler, and A. Loidl. Broadband dielectric spectroscopy on benzophenone: alpha relaxation, beta relaxation, and mode coupling theory (ewintoblunk08********). *Physical Review E*, 77:031506, 2008.

[91] P. Lunkenheimer, A. Pimenov, B. Schiener, R. B′ohmer, and A. Loidl. *Europhys. Lett.*, 33:611, 1996.

[92] P. Lunkenheimer, U. Schneider, R. Brand, and A. Loidl. Glassy dynamics. *Contemporary Physics*, 41:15, 2000.

[93] Andrea Mandanici, Wei Huang, Maria Cutroni, and Ranko Richert. Dynamics of glass-forming liquids. xii. dielectric study of primary and secondary relaxations in ethylcyclohexane. *J. Chem. Phys.*, 128:124505, 2008.

[94] G. B. McKenna. Glass dynamics: Diverging views on glass transition. *Nature Physics*, 4:673, 2008.

[95] Mierzwa, M., S. Pawlus, M.Paluch, E. Kaminska., and K. L. Ngai. Correlation between primary and secondary johari-goldstein relaxationsin supercooled liquids: Invariance to changes in thermodynamic conditions. *Journal of Chemical Physics*, 128(4):044512, JAN 28 2008.

[96] K. L. Ngai. *J. Non-Cryst. Solids*, 257:7, 2000.

[97] K. L. Ngai. *Journal of Physics: Condensed Matter*, 15:1107, 2003.

[98] K. L. Ngai and S. Capaccioli. Impact of the application of pressure on the fundamental understanding of glass transition. *JOURNAL OF PHYSICS: CONDENSED MATTER*, 20:244101, 2008.

[99] K. L. Ngai, R. Casalini, S. Capaccioli, M. Paluch, and C. M. Roland. Do theories of the glass transition, in which the structural relaxation time does not define the dispersion of the structural relaxation, need revision? *Journal of Physical Chemistry B*, 109(37):17356–17360, SEP 22 2005.

[100] K. L. Ngai, R. Casalini, and C. M. Roland. *Macromolecules*, 38:1779, 2005.

[101] K. L. Ngai, P .Lunkenheimer, C. Leon, U. Schneider, R. Brand, and A. Loidl. Nature and properties of the johari-goldstein beta-relaxation in the equilibrium liquid state of a class of glass-formers. *JOURNAL OF CHEMICAL PHYSICS*, 115(3):1405–1413, JUL 15 2001.

[102] K. L. Ngai and M. Paluch. Classification of secondary relaxation in glass-formers based on dynamic properties. *Journal of Chemical Physics*, 120(2):857, JAN 8 2004.

[103] Albena I. Nielsen, Tage Christensen, Bo Jakobsen, Kristine Niss, Niels Boye Olsen, Ranko Richert, and Jeppe C. Dyre. *Journal of Chemical Physics*, Accepted, 2009.

[104] Albena I. Nielsen, Sebatian Pawlus, Marian Paluch, and Jeppe C. Dyre. Pressure deppendence of the dielectric loss minimum slope for ten molekular liquids. *Philosphical Magazine*, 88:4101, 2008.

[105] K. Niss. *Fast and slow dynamics of glass-forming liquids - What can we learn from high pressure experiments?* PhD thesis, Université Paris-Sud, 2007.

[106] Kristine Niss and Christiane Alba-Simionesco. Effects of density and temperature on correlations between fragility and glassy properties. *Physical Review B*, 74:024205, 2006.

[107] Kristine Niss, Cecile Dalle-Ferrier, Gilles Tarjus, and Christiane Alba-Simionesco. On the correlation between fragility and stretching in glass-forming liquids. *JOURNAL OF PHYSICS: CONDENSED MATTER*, 19:076102, 2007.

[108] Kristine Niss and Bo Jakobsen. Dielectric and shear mechanical relaxation in glass forming liquids. In *Tekster fra IMFUFA*, volume 424. 2003.

[109] N. B. Olsen, T. Christensen, and J. C. Dyre. Beta relaxation of nonpolymeric liquids close to the glass transition. *Physical Review E*, 62:4435, 2000.

[110] N.B. Olsen, T. Christensen, and J.C. Dyre. Time-temperature superposition in viscous liquids. *Physical Review Letters*, 86(7):1271–1274, 2001.

[111] Niels Boye Olsen. Personal communication.

[112] Niels Boye Olsen. Scaling of β-relaxation in the equilibrium liquid state of sorbitol. *Journal of Non-Crystalline Solids*, 235-237:399, 1998.

[113] M. Paluch, J. Zioło, S. J. Rzoska, and P. Habdas. Effect of glass structure on the dynamics of the secondary relaxation in diisobutyl and diisoctyl phthalates. *Phys. Rev. E*, 54:4008, 1996.

[114] M. Paluch, S. Pawlus, S. Hensel-Bielowka, E. Kaminska, D. Prevosto, S. Capaccioli, P. A. Rolla, and K. L. Ngai. Two secondary modes in decahydroisoquinoline: Which one is the true johari goldstein process? *Journal of Chemical Physics*, 122(23), JUN 15 2005.

[115] M. Paluch, C. M. Roland, J. Gapinski, and A. Patkowski. Pressure and temperature dependence of structural relaxation in diglycidylether of bisphenol a. *Journal of Chemical Physics*, 118, 2003.

[116] M. Paluch, M. Sekula, S. Pawlus, S. L. Rzoska, J. Ziolo, and C. M. Roland. Test of the einstein-debye relation in supercooled dibutylphthalate at pressures up to 1.4 gpa. *Physical Review Letters*, 90(17), MAY 2 2003.

[117] S. Pawlus, S. Hensel-Bielowka, M. Paluch, R. Casalini, and C. M. Roland. Hydrogen bonding and secondary relaxations in propylene glycol trimer. *Physical Review B*, 72(6), AUG 2005.

[118] Ulf R. Pedersen. *Long-time simulations of viscous liquids - From strongly correlated liquid to crystals*. PhD thesis, Roskilde University, 2009.

[119] Ulf R. Pedersen, Nicholas P. Bailey, Thomas B. Schrøder, , and Jeppe C. Dyre. Strong pressure-energy correlations in van der Waals liquids. *Physical Review Letters*, 100:015701, 2008.

[120] D. J. Plazek, C. A. Bero, and I. C. Chay. *J. Non-Cryst. Solids*, 172-174:181, 1994.

[121] D. Prevosto, S. Capaccioli, M. Lucchesi, P. A. Rolla, M. Paluch, S. Pawlus, and J. Zioło. Emergence of a new feature in the high pressure – high temperature relaxation spectrum of tri-propylene glycol. *J. Chem. Phys*, 122:061102, 2005.

[122] D. Prevosto, K. Kessairi, S. Capaccioli, M. Lucchesi, and P. A. Rolla. Excess wing and johari-goldstein relaxation in binary mixtures of glass formers. *PHILOSOPHICAL MAGAZINE*, 87(3-5, Sp. Iss. SI):643–650, JAN-FEB 2007.

[123] D. Prevosto, S. Sharifi, S. Capaccioli, P. A. Rollaand S. Hensel-Bielowka, and M. Paluch. New experimental evidence about secondary processes in phenylphthalein-dimethylether and 1,1 '-bis(p-

methoxyphenyl)cyclohexane. *Journal of Chemical Physics*, 127(11), SEP 21 2007.

[124] J. R. Rajesh, W. Huang, R. Richert, and E. L. Quitevisa. *J. Chem. Phys.*, 124:014510, 2006.

[125] R. Richert. A simple current-to-voltage interface for dielectric relaxation measurements in the range 10^{-3} to 10^7 hz. *Review of Scientific Instruments*, 67:3217, 1996.

[126] R. Richert. Heterogeneous dynamics in liquids: Fuctuations in space and time,. *J. Phys-condens Mat*, 14:R703, 2002.

[127] R. Richert and C.A. Angell. Dynamics of glass-forming liquids. v. On the link between moleculardynamics and configurational entropy. *Journal of Chemical Physics*, 108(21):9016–9026, 1998.

[128] R. Richert and A. Blumen, editors. *Disorder Effects on Relaxational Processes*. Springer, Berlin, 1994.

[129] R. Richert, K. Duvvuri, and L. T. Duong. Dynamics of glass-forming liquids. VII. Dielectric relaxation of supercooled tris-naphthylbenzene, squalane, and decahydroisoquinoline. *Journal of Chemical Physics*, 118:1828, 2003.

[130] E. Roessler.

[131] C. M. Roland, R. Casalini., R. Bergman, and J. Mattsson. Role of hydrogen bonds in the supercooled dynamics of glass-forming liquids at high pressures. *Physical Review B*, 77(1), JAN 2008.

[132] C. M. Roland, S. Hensel-Bielowka, M. Paluch, and R. Casalini. Supercooled dynamics of glass-forming liquids and polymers under hydrostatic pressure. *Reports on Progress in Physics*, 68(6):1405–1478, JUN 2005.

[133] U. Schneider, R. Brand, P. Lunkenheimer, and A. Loidl. Excess wing in the dielectric loss of glass formers: A johari-goldstein β-relaxation? *Phys. Rev. Lett.*, 84:5560, 2000.

[134] Thomas B. Schrøder, Ulf R. Pedersen, Nicholas Bailey, Søren Toxværd, and Jeppe C. Dyre. Hidden scale invariance in molecular van der waals liquids: A simulation study. *arXiv:0812.4960v1 [cond-mat.soft]*, 2008.

[135] K. U. Schug, H. E. King, and R. Böhmer. *J. Chem. Phys.*, 109:1472, 1998.

[136] S. Shahriari, A. Mandanici, L.-M. Wang, , and R. Richert. *Journal of Chemical Physics*, 8960:121, 2004.

[137] S. Shervin, A. Mandanici, L.M. Wang, and R. Richert. Dynamics of glass-forming liquids. viii. dielectric signature of probe rotation and bulk dynamics in branched alkanes. *Journal of Chemical Physics*, 121(18):8960, 2004.

[138] G. Tammann and W. Hesse. *Zeitschrift für anorganische und allgemeine Chemie.*, 156:245, 1925.

[139] H. Vogel. Das temperaturabxhängigkeitsgesetz der viskosität von flüssigkeiten. *Physikalische Zeitschrift*, 22:645–646, 1921.

[140] M. Vogel and E. Rössler. Slow β-process in simple organic glass formers studied by one- and twodimensional 2h nuclear magnetic resonance I. *J. Phys. Chem. B*, 104:4285, 2001.

[141] M. Vogel and E. Rössler. Slow β-process in simple organic glass formers studied by one and twodimensional 2H nuclear magnetic resonance. II. discussion of motional models. *J. Chem. Phys.,*, 115:10883, 2001.

[142] H. Wagner and R. Richert. Spatial uniformity of the β-relaxation in D-sorbitol,. *J. Non-Cryst. Solids*, 241:19, 1998.

[143] H. Wagner and R. Richert. *J. Chem. Phys.*, 110:11660, 1999.

[144] L.-M. Wang, Y. Tian, R. Liu, and R. Richert. Calorimetric versus kinetic glass transitions in viscous monohydroxy alcohols. *Journal of Chemical Physics*, 128(8), FEB 28 2008.

[145] L.-M. Wang, V. Velikov, , and C. A. Angell. *J. Chem. Phys.*, 117:10184, 2002.

[146] Li-Min Wang and Ranko Richert. Debye type dielectric relaxation and the glass transition of alcohols. *J. Phys. Chem. B*, 109:11091, 2005.

[147] Li-Min Wang and Ranko Richert. Primary and secondary relaxation time dispersions in fragile supercooled liquids. *Physical Review B*, 76, 2007.

[148] R. Wehn, P. Lunkenheimer, and A. Loidl. Broadband dielectric spectroscopy and aging of glass formers. *Journal of Non-Crystalline Solids*, 353:3862, 2007.

[149] S. Weinstein, , and R. Richert and. Probing heterogeneous thermal relaxation by nonlinear dielectric spectroscopy. *Journal of Physics-Condensed Matter*, 19(20), MAY 23 2007.

[150] S. White. Ionic diffusion in quartz. *Nature*, 225:375, 1970.

[151] J. Wiedersich, T. Blochowicz, S. Benkhof, A. Kudlik, N.V. Surovtsev, C. Tschirwitz, V.N. Novikov, and E. Rössler. Fast and slow relaxation processes in glasses. *Journal of Physics: Condensed Matter*, 11:A147–A156, 1999.

[152] G. Williams and D. C.Watts. Non-symmetrical dielectric relaxation behaviour arising from a simple empirical decay function. *Trans. Farad. Soc.*, 66:80, 1970.

[153] M. L. Williams, R. F. Landel, and J. D. Ferry. The temperature dependence of relaxation mechanisms in amorphous polymers and other glass-forming liquids. *J. Am. Ceram. Soc.*, 77:3701, 1953.

[154] Zhao, Z. F., Wen, P., Shek, C. H., Wang, and W. H. Measurements of slow beta-relaxations in metallic glasses and supercooled liquids. *Physical Review B*, 75(17), MAY 2007.

Pressure dependence of the dielectric loss minimum slope for ten molecular liquids

A.I. Nielsen[a]*, S. Pawlus[b], M. Paluch[b] and J.C. Dyre[a]

[a]*DNRF Centre 'Glass and Time', IMFUFA, Department of Sciences, Roskilde, Denmark;*
[b]*Institute of Physics, Silesian University, Katowice, Poland*

We present a comprehensive study of data for the dielectric relaxation of ten glass-forming organic liquids at high-pressure along isotherms, showing that the primary (α) high-frequency relaxation is well-characterized by the minimum slope and the width of the loss peak. The advantage of these two parameters is that they are model independent. For some materials with β processes in the mHz and kHz range, the high-frequency slope tends to be $-\frac{1}{2}$ with pressure increase. In addition, the two parameters capture the relaxation shape invariance at a given relaxation time but different combinations of pressure and time.

Keywords: compression; time pressure temperature super position; minimum slope; width; dielectric

Glass may be regarded as the fourth state of conventional matter: isotropic as the liquid state, but solid as the crystalline state. With the notable exception of helium, any liquid may be turned into glass by cooling it fast enough to avoid crystallization [1–5].

Physical systems usually relax following perturbations forced upon them. The relaxation of the systems consists of processes going on at different time-scales. The dominant and slowest relaxation process of a glass-forming liquid is the so-called α process. The α process defines the liquid relaxation time, an important quantity because the glass transition takes place when the relaxation time significantly exceeds the inverse relative cooling rate. Compression of supercooled liquid slows down the α relaxation (increases the characteristic relaxation time, τ). On the other hand, this effect can be compensated by heating up the liquid. Different combinations of p and T can result in the same relaxation dynamics at the same τ, or materials obey the temperature–pressure superposition at the same relaxation times (TTPS) [6–11]. There are different kinds of secondary (β) relaxation, including Johari-Goldstein (JG) and those of intramolecular motions [11–16] or any excess wings.

In a paper from 2001, it was shown that the high-frequency slope of the dielectric loss for a group of materials tends to be $-\frac{1}{2}$ as the temperature approaches the glass transition temperature, $T \to T_{\mathrm{g}}$, and this was linked to time–temperature superposition (TTS) [17].

*Corresponding author. Email: albenan@ruc.dk

But a general prevalence of −0.5 for the slope has been found in highly viscous liquids, no matter whether TTS is obeyed [18]. In those papers, the dielectric scans were taken at ambient pressure. In the following, we investigate whether this result holds for dielectric frequency scans for ten liquids along isotherms with increasing pressure ($p \rightarrow p_g$), and if the model-independent shape quantities, *minimum slope* and *half loss peak width*, capture TTPS. The minimum slope, of course, may well be affected by secondary processes, well expressed in the experimental frequency window as well as the underlying low-frequency β relaxation (or an excess wing), but no attempt is made to compensate for these effects. The point is that the minimum slope is an objective shape parameter.

We have measured the dielectric loss, ε'', as a function of frequency for a number of organic glass formers slightly below the glass transition pressure. In order to avoid bias, data were selected prior to their analysis. A model-independent data analysis was performed; i.e. without fitting data to any of the standard functions (stretched exponential, Havriliak-Negami, Cole-Cole, Cole-Davidson, etc.). Thus, there is no need to distinguish between liquids with and without clearly resolved secondary (β) processes. Very accurate data are required in order to obtain reliable slopes by numerical differentiation. The selection criteria were low noise, well-defined loss peak, and sufficient length of the high-frequency part of the dissipation in order to find the minimum slope. In order to avoid bias, data were selected prior to analysis. The data analysis was automated as far as possible via Matlab programs [18].

Moreover, following the philosophy of making as direct and unbiased data analysis as possible, no attempt was made to subtract possible contributions from DC conductivity. Of course, if the conductivity overruled the primary relaxation, then the particular scan was excluded from the analysis. In order to avoid the influence of the conductivity, a frequency scan was discarded if one of the following points was not fulfilled: the low-frequency slope is 1 (within the measure noise); or TTS around the loss peak is obeyed (of course, in a range where β relaxation does not interfere).[1]

The chemicals are chlorinated biphenyl (CBP, Aroclor [16]), 1,1'-bis(p-methoxyphenyl) cyclohexane (BMMPC, [19]), Di-*iso*-butyl phthalate (D*iso*BP, [20]), di-propylene glycol (DPG, [21]), tri-propylene glycol (TPG, [10]), diglycidyl ether of bisphenol-A (EPON828, [21]), propylene carbonate (PC, [8]), phenolphthalein-dimethylether (PDE [23]), tetramethyltetra-phenyltrisiloxane (DC704, this work, Dow Corning 704® diffusion pump fluid), perhydroisoquinoline (decahydroisoquinoline, PHIQ, this work, 99%, Aldrich, Figure 1b). DC704 is represented in Figure 1a with three isotherms $T = 253\,\text{K}$, $p \in [6;\ 2460]$ bar, $T = 263\,\text{K}$, $p \in [1333;\ 2404]$ bar and $T = 283\,\text{K}$, $p \in [2559;\ 2404]$ bar, and PHIQ with two isotherms in Figure 1b, $T = 232\,\text{K}$, $p \in [0;\ 1000]$ bar and $T = 293\,\text{K}$, $p \in [3375;\ 17500]$ bar. The measurements were carried out on the set-up described in [24,25]. The pressure-transmitting liquid was a silicon oil. The measure cell consisted of a capacitor – two parallel parts of the steel cylinder, separated by Teflon stripes and kept together by two Teflon rings – placed into a tightly closed Teflon container filled up with the sample liquid.[2]

The low-frequency (long-time) properties of the α process are fairly trivial; the vast majority of glass-forming liquids here exhibit what corresponds to a cut-off in the relaxation time distribution function at long-times [25–27]. Focusing on the short-time (high-frequency) relaxation properties, at each temperature and pressure we identified the minimum slope in the standard log–log plot, $\alpha_{\min} \equiv \min\,(d \log \varepsilon'' / d \log f) < 0$, where f is the frequency and log is the base-10 logarithm (see Figure 2a). This identifies the inflection
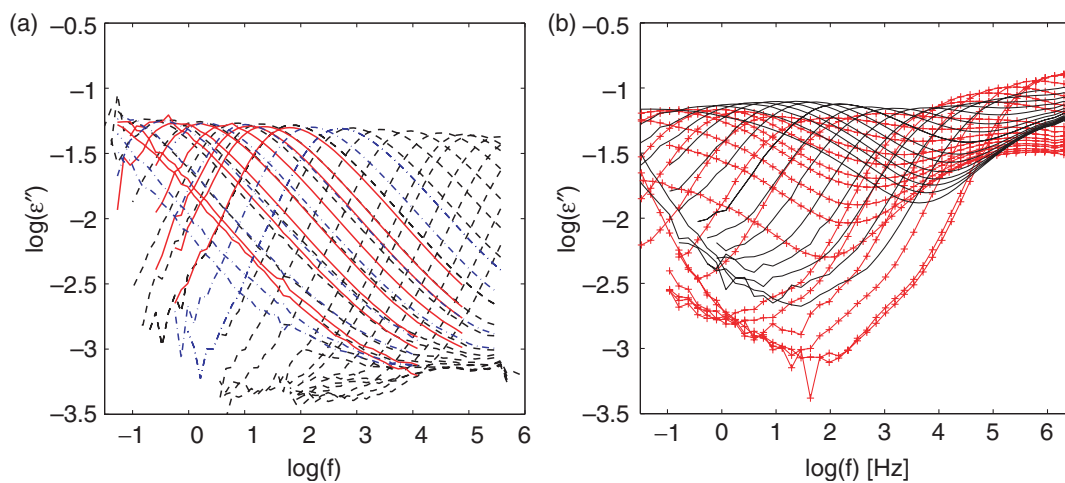
Figure 1. (Color online). Full dataset log–log plot of the dielectric loss ε'' as a function of frequency for (a): DC 704 at $T = 253$ K, $p \in [6; 2460]$ bar (black $--$), $T = 263$ K, $p \in [1333; 2404]$ bar (red $-$), and $T = 283$ K, $p \in [2559; 2404]$ bar (blue $- \cdot -$). There is a secondary process at 0.1–1 MHz that is relatively pressure insensitive. (b): PHIQ at $T = 232$ K, $p \in [0; 1000]$ bar (black $-. -$) and $T = 293$ K, $p \in [3375; 17500]$ bar (red $+$). The scan is characterized by a well-resolved pressure-independent β process with relatively high amplitude at 1 MHz. Only a few of the presented are used in the analysis.
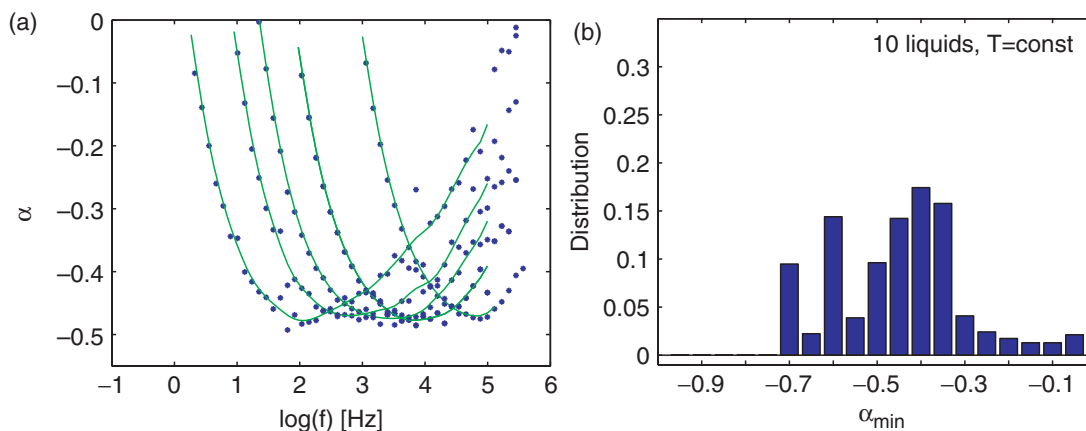
Figure 2. (Color online). (a): The slope of the double logarithmic dielectric dissipation (with stars) at some chosen pressures from the data in Figure 1a: DC704 at 253K. The green line indicates the averaged values that are used to find the minimum slope, $\alpha_{\min}$. (b): Histogram of the minimum-slope distribution for the ten organic glass-forming liquids (one column for $-0.85 < \alpha_{\min} < -0.75$, one for $-0.75 < \alpha_{\min} < -0.65$, etc.). Since the number of pressures investigated varies from isotherm to isotherm and the number of isotherms for each liquid, each minimum slope observation is weighted by a factor $1/(Nn)$. N is the number of data points (pressures) in a dataset for the given liquid at the given temperature, and n is the number of isotherm datasets for the given liquid. In this way, all liquids contribute equally to the histogram. Note that an isotherm may contribute to more than one column in this figure, since $\alpha_{\min}$ vary with pressure.

point above the loss-peak frequency. The number $\alpha_{\min}$ gives the best approximate inverse power-law description of the loss decay above the peak: $\varepsilon''(f) \propto f^{-|\alpha_{\min}|}$ applies to a good approximation over a significant frequency range. Only data with a well-defined minimum slope or a clear slope plateau in the point-by-point numerical differentiation were used.

If relatively low noise appears in the derivative, a smoothing is obtained by averaging the values (Figure 2a) and the minimum value found. The averaging was done to maximize the number of datasets. The distribution of the minimum slopes for the ten different liquids for all temperatures and frequency–pressure scans is presented in Figure 2b. The above-mentioned limitations, as well as the different pressure and frequency ranges and intervals, imply that the number of datasets (isotherms) per liquid varies from one to three, and the number of data points (pressures) for each dataset at constant temperature for a liquid varies from four up to 26. To compensate for this, we give equal weight to each liquid in Figure 1b. If N is the number of data points included in the analysis for a given liquid at one temperature and n is the number of isotherms for this particular liquid, each minimum-slope observation was weighted by a factor $1/(Nn)$ for this isotherm.

We find a slightly different result as we had previously observed for liquid dynamics controlled by temperature changes [18]. The histogram in Figure 2a shows that the high-frequency relaxation of viscous liquids squeezed at constant temperature is most often characterized with $-0.45 < \alpha_{min} < -0.35$. In the previous study of the dielectric response of 52 liquids at ambient pressure, the most represented value interval for the minimum slope is around -0.5, or more precisely, approximately 45% of the observed values of the minimum slope are $-0.55 < \alpha_{min} < -0.45$ [18]. The number of different chemicals is too small to conclude anything about the generality of this observation. Therefore, we have to look in more detail at how α_{min} changes with compression, in order to find the trends.

Figure 3a shows the minimum slope evolution with loss peak frequency. It can be seen that it is similar to the temperature data at ambient pressure [17,18,31]; the high-frequency slope of the dielectric dissipation may converge slowly to $-\frac{1}{2}$ as pressure increases.
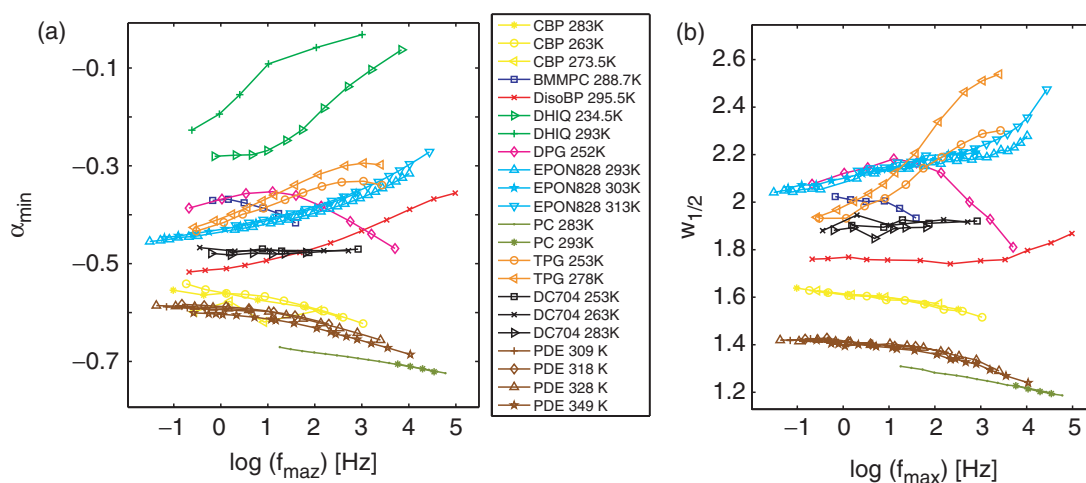
Figure 3. (Color online). (a): The minimum slope α_{min} plotted as a function of pressure quantified by the position of the loss-peak frequency f_{max} for all nine liquids along isotherms. Every liquid has its own color. (b): The evolution of the half-width at half-maximum in decades write for the loss peak and normalized with the same quantity for a Debye process defined as $w_{\frac{1}{2}} = W_{\frac{1}{2}}/W_D/2$, where $W_{\frac{1}{2}}$ is the number of decades of frequency on the right of the loss peak normalized with respect to the half Debye width $W_D/2 \approx 0.572$ ($w_{\frac{1}{2}} \to 1$ indicates Debye-like relaxation). In this plot the data points for PHIQ are absent because the corresponding loss at the frequency at half-maximum loss coincides with the β relaxation loss.

In an attempt to describe the shape of the α relaxation fully, we need a second shape parameter. We use the width, W, at half the dissipation maximum in decades. In an attempt to use as many datasets as possible and to avoid the effect of the DC-contribution to the left of the loss peak we use only the number of decades of the frequency on the right of the loss peak, $W_{\frac{1}{2}}$. From observations of different master curves, the following can be stated more or less generally: if there are changes in the shape of the loss, these are mainly due to changes of the slope of the high-frequency part. Thus, we can expect the same information about the shape from the full width and also from the width between the frequency at the loss peak and the highest frequency corresponding to half the loss. Here, we normalized the width $w_{\frac{1}{2}}$ with respect to the half Debye width $W_D/2 \approx 0.572$. If $w_{\frac{1}{2}} = W_{\frac{1}{2}}/W_D/2 \rightarrow 1$, then the relaxation is Debye-like. A plot of $w_{\frac{1}{2}}$ as a function of the frequency is shown in Figure 3b. The width follows qualitatively the behavior of $\alpha_{\min}$ to some extent, but it seems that it is less sensitive to temperature or pressure changes than the minimum slope.

Figure 3 is in agreement with findings regarding temperature–pressure superposition at same relaxation times, that the dielectric relaxation for some liquids depends only on the relaxation times and not on the temperature or pressure [6]. $\alpha_{\min}$, together with $w_{\frac{1}{2}}$, as functions of the frequency, describes the changes in the shape of the high-frequency dielectric loss at some relaxation time. If the minimum slope and width for two or more isotherms lie on top of each other, this means that the relaxation has the same shape for $f > f_{\max}$ to the inflection point. Thus, from this plot we can also estimate the frequency, below which the α relaxation (high-frequency part) is no longer affected by secondary processes that appear at times, and that are smaller than the α-relaxation time and do not couple to the pressure and temperature in the same way as the primary process. This happens at a frequency where the curves of the shape quantities join into one; i.e. the relaxation time determines the shape of the relaxation and that is co-invariant of temperature or pressure changes [6].

The pressure–temperature superposition at the same relaxation time is relatively well obeyed in the case of the Van der Waals liquids PC (dark green), PDE (brown), and DC704 (black) if we look at both shape parameters $\alpha_{\min}$ and $w_{\frac{1}{2}}$. In contrast to the plot of TPG data (orange), it can be seen that the primary process shape is dominated by the secondary relaxation at pressures less than this; i.e. corresponding to loss peaks above 10 Hz. In the case of PHIQ (light green), one can even see in Figure 3a that a TTPS is not observed in the measured frequency window. The same phenomenon is observed for PHIQ at ambient pressure [30] as well as under pressure [29] where even two types of secondary relaxations are identified. The dielectric relaxation for this liquid is characterized by a β process with relatively high amplitude. For the other liquids with secondary processes above 1 kHz we can see that deviations into $\alpha_{\min}$ isotherms are relatively small, and the β process is characterized by low amplitude compared to the loss peak. It is clear that the temperature governs the β process amplitude as well as the influence on the $\alpha_{\min}$ value: the higher the temperature, the larger $\alpha_{\min}$ at the same relaxation time. From this we can state that TTPS (and TTS) can only be observed if the influence of the β process is relatively small. The spectrum for DC704 shows a secondary process with relatively low amplitude around 1 MHz. Thus, the α relaxation observed near p_g is well separated from β, and, therefore, $\alpha_{\min} = 0.048$ is nearly constant over four frequency decades.

What about the liquids like PC and PDE? They have minimum slopes numerically bigger than $\frac{1}{2}$ and they are reported to include a hidden JG β relaxation that is coupled to

the α process and, therefore, the excess wings in the relaxation are invariant to pressure and temperature, when compared at a fixed value of the α-relaxation time [8,16].

Regarding the values of α_{min}, one might intuitively expect that interference from β processes can only explain minimum slopes that are numerically smaller than $\frac{1}{2}$. Although for many years it was believed that secondary processes were found only in the kHz–MHz frequency range, it is now generally recognized that these processes in some cases take place at much lower frequencies [28,32]. From measurements on liquids with a well-defined β process in the kHz range, however, we and others (see, e.g. [33]) consistently find that when the liquid is cooled down to a temperature *above* the temperature where the α and β processes merge, the high-frequency decay of the 'collapsed' α-β process has a minimum slope that is usually numerically larger than $\frac{1}{2}$. The same should be expected for the pressure-sensitive time-scale of the β process. Thus, since whenever there are low-lying β processes, the liquid is unavoidably around or above the α-β merging temperature, or under the merging pressure, $|\alpha_{min}| > 1/2$ might occur as in the case of PC [8] or PDE [23]. This means that, in these liquids, a separation of the processes might not happen and thus TTPS is obeyed. PDE relaxation under T_g at ambient pressure shows two secondary processes [34]. If the dissipation is characterized with a well-defined β process then $\alpha_{min} \to -\frac{1}{2}$. In other words, 'genuine' $\alpha_{min} = -\frac{1}{2}$ behavior only appears when the system is significantly below the merging temperature or above the merging pressure, as in the case of DC704.

An obvious question is whether the observed prevalence of minimum slopes around -0.4 is general or whether we should expect a value of -0.5. If $\alpha_{min} = -\frac{1}{2}$ was significant, one would expect that the closer the minimum slope is to $-\frac{1}{2}$, the better an inverse power-law description applies. This is investigated in Figure 4a, which plots the third-order derivative relative to the first-order derivative, $|H^{(3)}(x_0)/\alpha_{min}|$, where $H(x) = \log \varepsilon''(x)$, $x = \log f$, and x_0 is the log frequency at the point of the minimum slope. The idea is that, since the second-order derivative is zero at the frequency of the minimum slope, by
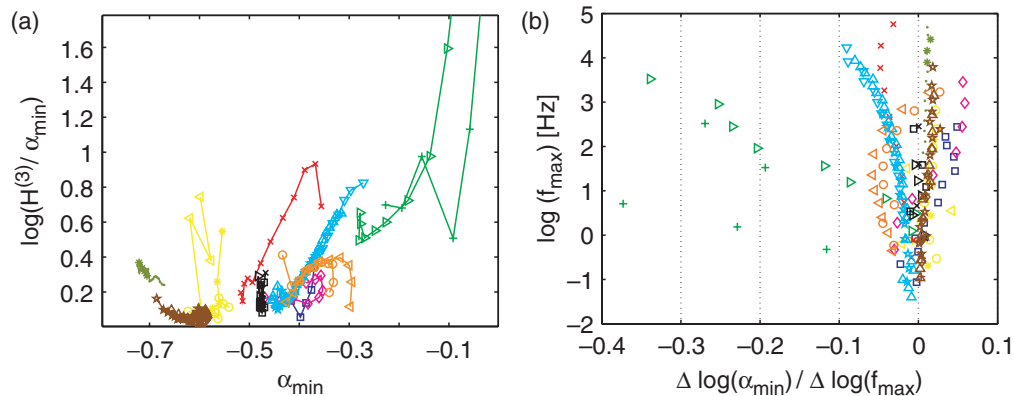
Figure 4. (Color online). (a): Third-order relative to first-order derivative, $|H^{(3)}(x)/\alpha_{min}|$, at the frequency of the minimum slope for all datasets, where $H(x) \equiv \log \varepsilon''(x)$ ($x = \log f$). At the frequency of minimum slope the second-order derivative is zero; thus by Taylor's formula the smaller the third-order derivative is relative to the first-order derivative $\alpha_{min} = H'(x)$, the better an inverse power law description of the high-frequency loss applies. (b): The slope of α_{min} gives information about how much α_{min} is pressure-dependent. Both quantities contain information about the time-scales of the secondary processes.

Taylor's formula the smaller $|H^{(3)}(x_0)/\alpha_{\min}|$, the frequency range is larger where the slope is almost constant. Figure 4a shows that the better an inverse power-law describes the loss, the closer $\alpha_{\min}$ is to $-\frac{1}{2}$ for DisBP (red +) and EPON828 (cyan). For DC704 $|H^{(3)}(x_0)/\alpha_{\min}|$ lowers with pressure, while $\alpha_{\min}$ values are nearly constant, which means that $f^{|\alpha_{\min}|}$ applies to a bigger frequency range. The increase, and afterwards, decrease in $|H^{(3)}(x_0)/\alpha_{\min}|$ values (within the noise) captures the α-β merging process in the relaxation of BMMPC (blue) around 1 Hz and DPG (magenta) at 100 Hz (but DPG has more complex relaxation due to two β processes [35,36]).

Let us again look at the information that we can extract from Figure 4a about the excess wing relaxations. For PDE the value of $|H^{(3)}(x_0)/\alpha_{\min}|$ decreases with pressure increase, but it begins to increase slowly again. So, from a certain relaxation time (pressure) the frequency range of the $-\alpha_{\min}$ slope approximation begins to be smaller. This is an indication of a α-β merging process between 1 and 0.1 Hz. This might be the case for CBP (yellow) as well. We cannot say anything consistent about the PC relaxation pattern. The experiental window is rather narrow. Confirmation of this observation for these liquids should be done on dielectric measurements at higher pressures.

The linearity of the minimum-slope pressure dependence can be seen in Figure 4b, which plots the change in slope point-by-point of the $\alpha_{\min}$ curves with the slowing of the relaxation. For DC704, which has a numerically minimum slope of 0.48, $\alpha_{\min}$ is constant, while for all other liquids $\alpha_{\min}$ is changing in such a way that if $\alpha_{\min}$ approaches -0.5, then its value is rather constant. It is interesting that materials with values of $\alpha_{\min}$ numerically bigger than $\frac{1}{2}$, like for PC, have a minimum slope that changes very 'slowly' and almost linearly with $\log f$ over more than six decades. Thus, one can expect that, generally, $\alpha_{\min}$ will change until it reaches 0.5 and will be constant. One apparent exception is PDE; it seems to have a constant $\alpha_{\min}$ around -0.6 (Figures 4b and 3a), but together with Figure 4a, this may be a sign of a hidden β process at frequencies under 1 Hz that can contribute to the primary process as in the case of DPG.

In conclusion, the minimum slope and the width of the loss peak – shape parameters that describe only the high-frequency part of the dispersion – capture excellently the superposition of loss with the same relaxation times but at different temperatures and pressures. The considerable advantage of these two parameters is that they are model-free and thus independent of fitting procedures. With compression of the viscous liquid, the minimum slope value may converge to $-\frac{1}{2}$ (Figure 2a) as the α and β processes separate (Figure 4a). The deviations from this power law are most likely due to interference from one or more secondary relaxation processes, with or without distinct maxima. If one or more secondary processes appear in the Hz range, it is practically impossible to separate the α and β processes and this will be mirrored in the value of the minimum slope.

Notes

1. If one believes in a simple additive relation between the primary relaxation and DC conductivity, then it is easy to show mathematically that $\varepsilon'' \rightarrow \propto \omega^{-\beta}$) for large ω. The cases

where α process and DC decouple, but if all temperature curves are superimposed TTS is obeyed around the loss peak like in the situation for DisoBP. This means that the α process has no significant contribution from DC.

2. In our case, the construction of the capacitor for pressure investigations ensures an excellent separation of the sample from the pressure transmitting liquid – silicon oil. The observed DC conductivity results from some ions existing in every measured liquid irrespective of the purification procedure. The noise below 1 Hz is due to relatively small (below 0.1) values of ε'' of the presented samples and limitation experimental time.

References

[1] I. Gutzow and J. Schmelzer, *The Vitreous State: Thermodynamics, Structure, Rheology, and Crystallization*, Springer, Berlin, 1995.
[2] M.D. Ediger, C.A. Angell and S.R. Nagel, J. Phys. Chem. 100 (1996) p.13200.
[3] C.A. Angell, K.L. Ngai, G.B. McKenna et al., J. Appl. Phys. 88 (2000) p.3113.
[4] E. Donth, *The Glass Transition*, Springer, Berlin, 2001.
[5] J.C. Dyre, Rev. Mod. Phys. 78 (2006) p.953.
[6] K.L. Ngai, R. Casalini, S. Capaccioli et al., J. Phys. Chem. B 109 (2005) p.17356.
[7] K. Niss, C. Dalle-Ferrier, G. Tarjus et al., On the correlation between fragility and stretching in glassforming liquids, Available at arXiv:cond-mat/0611253 v1 (2006).
[8] S. Hensel-Bielowka, S. Pawlus, C.M. Roland et al., Phys. Rev. E 69 (2004) p.050501(R).
[9] M. Paluch, C.M. Roland, J. Gapinski et al., J. Chem. Phys. 118 (2003).
[10] D. Prevosto, S. Capaccioli, M. Lucchesi et al., J. Chem. Phys. 122 (2005) p.061102.
[11] K. Kessairi, S. Capaccioli, D. Prevosto et al., J. Phys. Chem. B 112 (2008) p.643.
[12] G.P. Johari and M. Goldstein, J. Chem. Phys. 53 (1970) p.2372.
[13] G.P. Johari, Ann. N.Y. Acad. Sci. 279 (1976) p.117.
[14] K.L. Ngai, J. Phys. Condens. Matter 15 (2003) p.S1107.
[15] G.P. Johari, G. Power and J.K. Vij, J. Chem. Phys. 116 (2002) p.5908.
[16] K.L. Ngai and M. Paluch, J. Chem. Phys. 120 (2004) p.857.
[17] N.B. Olsen, T. Christensen and J.C. Dyre, Phys. Rev. Lett. 86 (2001) p.1271.
[18] A. I. Nielsen et al. Submitted.
[19] S. Hensel-Bielowka, J. Zioło, M. Paluch et al., J. Chem. Phys. 117 (2002) p.2317.
[20] M. Paluch, J. Zioło, S.J. Rzoska et al., Phys. Rev. E 54 (1996) p.4008.
[21] K. Grzybowska, S. Pawlus, M. Mierzwa et al., J. Chem. Phys. 125 (2006) p.144507.
[22] M. Mierzwa, S. Pawlus, M. Paluch et al., J. Chem. Phys. 128 (2008) p.044512.
[23] S. Hensel-Bielowka and M. Paluch, Phys. Rev. Lett. 89 (2002) p.025704.
[24] M. Paluch, M. Sekula, S. Maslanka et al., J. Chem. Phys. 120 (2004) p.2020.
[25] C.M. Roland, S. Hensel-Bielowka, M. Paluch et al., Rep. Prog. Phys. 68 (2005) p.1405.
[26] F. Kremer and A. Schönhals, eds., *Broadband Dielectric Spectroscopy*, Springer, Berlin, 2002.
[27] A. Kudlik, S. Benkhof, T. Blochowicz et al., J. Mol. Struct. 479 (1999) p.201.
[28] N.B. Olsen, J. Non-Cryst. Solids 235 (1998) p.399.
[29] M. Paluch, S. Pawlus, S. Hensel-Bielowka et al., J. Phys. Rev. B 72 (2005) p.224205.
[30] R. Richert, K. Duvvuri and L.-T. Duong, J. Chem. Phys. 118 (2003) p.1828.
[31] B. Jakobsen, K. Niss and N.B. Olsen, J. Chem. Phys. 123 (2005) p.234511.
[32] U. Schneider, R. Brand, P. Lunkenheimer et al., Phys. Rev. Lett. 84 (2000) p.5560.
[33] L.-M. Wang and R. Richert, Phys. Rev. B 76 (2007) p.064201.
[34] S. Kahle, J. Gapinski, G. Hinze et al., J. Chem. Phys. 122 (2005) p.074506.
[35] R. Casalini and C.M. Roland, Phys. Rev. Lett. 91 (2003) p.015702.
[36] R. Casalini and C.M. Roland, Phys. Rev. B 69 (2004) p.094202.

Prevalence of approximate $\sqrt{t}$ relaxation for the dielectric α process in viscous organic liquids

Albena I. Nielsen[a], Tage Christensen[a], Bo Jakobsen[a], Kristine Niss[a],
Niels Boye Olsen[a], Ranko Richert[b], and Jeppe C. Dyre[a]

[a]*DNRF Centre "Glass and Time", IMFUFA, Department of Sciences,*
Roskilde University, Postbox 260, DK-4000 Roskilde, Denmark
[b]*Department of Chemistry and Biochemistry, Arizona State University, Tempe, Arizona 85387-1604, USA*

This paper presents dielectric relaxation data for organic glass-forming liquids compiled from different groups and supplemented by new measurements. The main quantity of interest is the "minimum slope" of the α dielectric loss plotted as a function of frequency in a log-log plot, i.e., the numerically largest slope above the loss peak frequency. The data consisting of 347 spectra for 53 liquids show prevalence of minimum slopes close to $-1/2$, corresponding to approximate squareroot(time) dependence of the dielectric relaxation function at short times. The paper studies possible correlations between minimum slopes and: 1) Temperature (quantified via the loss-peak frequency); 2) How well an inverse power law fits data above the loss peak; 3) Degree of time-temperature superposition; 4) Loss-peak half width; 5) Deviation from non-Arrhenius behavior; 6) Loss strength. For the first three points we find correlations that show a special status of liquids with minimum slopes close to $-1/2$. For the last three points only fairly insignificant correlations are found, with the exception of large-loss liquids that have minimum slopes that are numerically significantly larger than $1/2$ and half loss peak widths that are significantly smaller than those of most other liquids. We conclude that – excluding large-loss liquids – approximate $\sqrt{t}$ relaxation appears to be a generic property of the α relaxation of organic glass formers.

INTRODUCTION

The glass transition takes place when a liquid is cooled so fast that it does not have sufficient time to equilibrate [1–6]. Below the glass transition temperature T_g the sample is in a solid but structurally disordered state, where the molecular positions are akin to those of the higher-temperature supercooled liquid state. Above T_g the liquid is in metastable equilibrium, but generally has much longer relaxation time than less-viscous liquids like ambient water. This makes the study of relaxation processes in highly viscous liquids possible and useful for obtaining information about these liquids' dynamical properties.

Physical systems usually relax with time following perturbations forced upon them. The simplest form of relaxation is an exponential decay towards equilibrium. This is, however, rarely observed. Another simple case is the so-called $\sqrt{t}$ relaxation where the relaxation function $h(t)$ at short times decays as $h(0) - h(t) \propto \sqrt{t}$. This is observed in systems as diverse as Rouse dynamics of polymer chains [7], metallic glasses [8], molecular nanomagnets [9, 10], and turbulent transport, e.g., in astrophysics [11]. For random walks, the equivalent of $\sqrt{t}$ relaxation is referred to as single-file diffusion which is observed, e.g., in ion channels through biological membranes, diffusion in zeolites, and charge-carrier migration in one-dimensional polymers [12].

Below we present data showing prevalence of $\sqrt{t}$ relaxation in glass-forming organic liquids. The data were taken on organic liquids studied in the extremely viscous state just above the glass transition where the relaxation time is in some cases larger than 1 second. In a paper from 2001 the equivalent of $\sqrt{t}$ relaxation – high-frequency dielectric losses decaying as $\propto f^{-1/2}$ where f is frequency – was linked to time-temperature superposition (TTS) via the conjecture that the better a liquid obeys TTS, the more accurate is $\sqrt{t}$ relaxation obeyed [13]. The present paper takes a slightly different approach by not focusing specifically on possible correlation to TTS, but on the overall behavior of viscous liquids. From a compilation of dielectric relaxation data from leading groups in the field supplemented by own measurements for altogether 53 organic liquids we find a clear prevalence of $\sqrt{t}$ relaxation. Every effort has been made to avoid possible bias in the data selection. It is important to note, however, that no objective criteria have been applied for choosing the liquids – they were included whenever data of sufficient quality happened to be available to us.

Relaxation processes in supercooled liquids occur over a wide range of time scales. The typical processes observed in viscous liquids (e.g., by dielectric relaxation spectroscopy) are the slow, primary, so-called α process that is associated with the calorimetric glass temperature, and the faster secondary [14] β process(es) [15–17]. These processes almost

always deviate from what corresponds to a simple exponential relaxation function [6, 18], a Debye frequency dependence. The relation between α and β processes manifests itself differently for different liquids. In many cases they are observed as two separate processes with well-defined and clearly distinguishable relaxation times. In other cases the β process is partly hidden by the primary process and manifests itself only as a high-frequency wing [19–21].

The time scales of the α and β processes may be separated by lowering temperature or increasing pressure. The β process does not slow down significantly on lowering temperature as long as one works in the equilibrium liquid phase [19, 22]; in some cases it even becomes faster as temperature is lowered [19, 23]. If the β process is in the high-frequency end of the experimental window, a clear separation between α and β relaxations appears upon cooling. A similar increased separation is observed when pressure is increased at constant temperature because the α process slows down considerably with compression while the β relaxation time is almost pressure insensitive [24, 25]. Furthermore, as pressure increases at constant temperature one generally finds that the β process' intensity decreases, which reduces its influence on the α process [19, 24, 26].

The α process has a characteristic asymmetry. This is reflected in the popular fitting function, the stretched exponential (Kohlrausch-Williams-Watts, KWW) function $h(t) = h_0 \exp\left[-(t/\tau)^{\beta_{KWW}}\right]$ [27–30]. The parameter $0 < \beta_{KWW} < 1$ is termed the stretching exponent. An alternative fitting function is the Cole-Davidson (CD) function which relates directly to the frequency domain by predicting for the dielectric constant $\varepsilon(\omega) - \varepsilon_\infty = \Delta\varepsilon(1 + i\omega\tau)^{-\beta_{CD}}$ [31, 32]. For both functions, in a log-log plot the slope on the high-frequency side of the dielectric loss (the negative imaginary part of the dielectric constant) converges to $-\beta_{KWW}$ and $-\beta_{CD}$, respectively [33]. Typical values of these quantities reported in the literature range between 0.3 and 0.7 [22, 34]. Thus the typical high-frequency decay of the α dielectric loss is somewhere between $\propto f^{-0.3}$ and $\propto f^{-0.7}$ (although there are also several exceptions to this). This is the "conventional wisdom" of the field, where no exponent is supposed to be more typical than any other but with a strong correlation with fragility. In contrast to this, we find below a prevalence of what corresponds to $\beta_{KWW} = 1/2$ or $\beta_{CD} = 1/2$ at high frequencies for liquids covering a wide range of fragilities. We do not fit the data to these two fitting functions, though, but analyze data directly without fitting to particular functions; in fact we find a range of widths at half loss, showing that none of these two functions fit data accurately.

There are reports in the literature of a number of liquids that have power-law exponent close to $-1/2$ [13, 22, 35]. As already mentioned, Olsen et al. in 2001 [13] conjectured that if the α-process obeys time-temperature superposition accurately, the frequency dependence of the high-frequency α loss is close to having the universal exponent $-1/2$, i.e.,

$$\varepsilon''(f) \propto f^{-1/2}, \ f >> f_{\max}.$$

Is this particular exponent predicted by any models? The answer is yes; in fact there are quite a few models predicting a high-frequency exponent of $-1/2$ (see, e.g., Refs. [36, 37] and their references). In the 1960's and 1970's, in particular, several theories were proposed predicting this exponent, famous among which are: Glarum's defect diffusion model [38–40]; the "inhomogeneous media" model of Isakovich and Chaban [41]; the Barlow-Erginsav-Lamb (BEL) model postulating a mechanical equivalent of a simple electrical circuit [36, 42]; the Montrose-Litovitz model invoking diffusion and relaxation of some unspecified order [43]. The idea of a universal exponent equal to $-1/2$ gradually fell out of favor, however, to be replaced by the presently popular view that relaxation functions are basically determined by the fragility [34].

In this work we present an empirical investigation of the best dielectric data we could acquire, resulting in a collection of data for 53 organic glass formers. The data were collected in order to investigate whether or not the exponent $-1/2$ has a particular significance. As mentioned, this exponent for the high-frequency decay of the relaxation function corresponds to $\sqrt{t}$ relaxation in the time domain. The possible prevalence of exponent $-1/2$ is investigated by analyzing dielectric relaxation, and not other, data. This is because the complex dielectric permittivity is by far the most accurately measured of all relaxing quantities and, furthermore, this quantity is available for many liquids measured over broad frequency ranges [44]. Numerous dielectric measurements have been published on different liquids, and dielectric spectroscopy setups continuously improve [45, 46]. In order to make the procedure as objective as possible the data analysis used is model independent and, as far as possible, automated. "Model independent" means that data are analyzed in terms of quantities obtained directly from the raw data.

Simple monoalchohols were excluded from the analysis because of their well-known dominant low-frequency Debye-like relaxation that is not related to the calorimetric glass [47]. Similarly, plastic crystals and polymers were

excluded because their glass transitions are not a liquid-glass transition. Besides this no selection criteria were applied except that too noisy data were discarded.

In Sec. II experimental details are provided and new data are presented. Section III discusses data selection criteria and details of the data analysis. Section IV presents the results for the minimum slopes in the form of a histogram. Section V analyzes various possible correlations by investigating whether minimum slopes correlate with: 1) how well an inverse power-law describes the high-frequency loss, 2) temperature, 3) how well time-temperature superposition applies, 4) loss peak width, 5) deviations from Arrhenius behavior, and 6) dissipation magnitude. Section VI summarizes our findings.

<div align="center">EXPERIMENTAL</div>

The 53 liquids studied in this paper are listed in Table I that for each liquid gives temperature and frequency ranges, etc. Part of the data analyzed were kindly provided by the Rössler group (Bayreuth, Germany), the Loidl-Lunkenheimer group (Augsburg, Germany), and the Paluch group (Katowice, Poland), part were detailed in previous publications involving some of the authors of this paper, part were measured for this paper at three different experimental setups in our labs at Roskilde and Tempe. The three setups used are briefly described below, where the new measurements are also presented. If nothing else is noted, chemicals were purchased from Sigma-Aldrich Chemical Company and used as acquired – most of them are moderate-viscosity liquids at room temperature.

Roskilde University Setup, (RU setup). The dielectric cell is a multilayered gold-plated capacitor with empty capacitance 71 pF. The capacitance was measured with an HP 3458A multimeter in the range of $10^{-3} - 10^2$ Hz in conjunction with an HP 4284A LCR meter used in the frequency range $10^2 - 10^6$ Hz. The multimeter measurements were performed on a homebuilt setup that consists of a voltage divider involving the multimeter in combination with a homebuilt arbitrary wavefunction generator [49]. The latter produces low-frequency ($10^{-3} - 10^2$ Hz) sinusoidal signals with voltages that are reproducible within 10 ppm [49].

The sample was placed into a homebuilt nitrogen-cooled cryostat which has absolute temperature accuracy better than 0.2 K and temperature stability during measurement better than 20 mK. The two measuring devices are connected to the measuring cell through a mechanical switch between the two frequency ranges (applied at 100 Hz). To ensure that the liquids were in thermal equilibrium after a temperature step, we waited 20 minutes before each measurement. Two frequency scans were taken at each temperature; data were only accepted if no differences were observed between the two spectra (beyond noise).
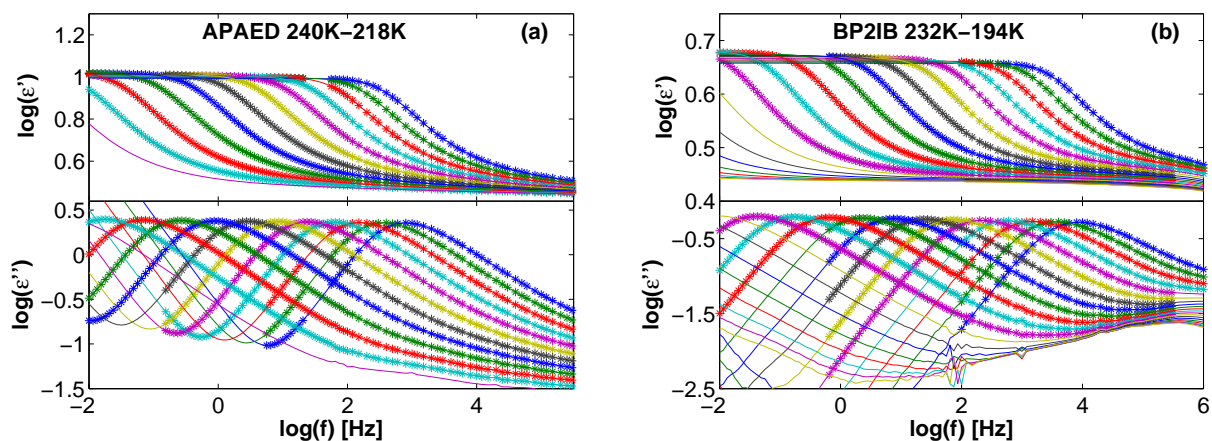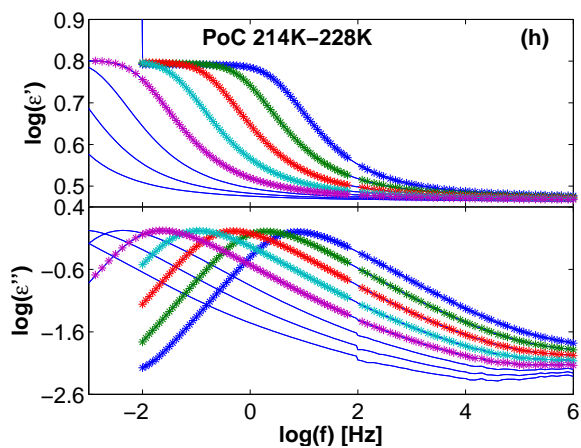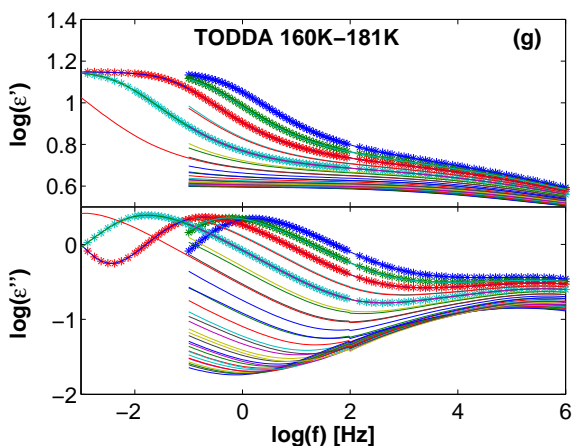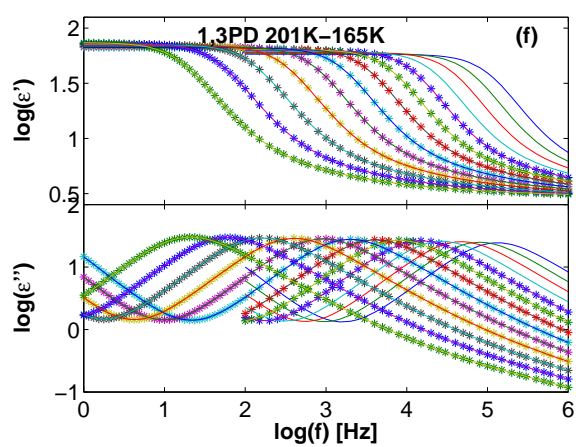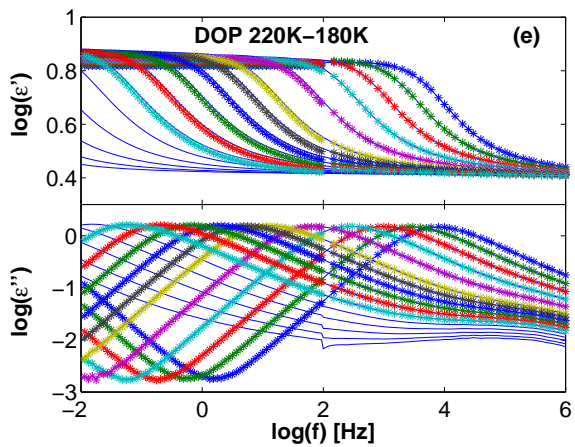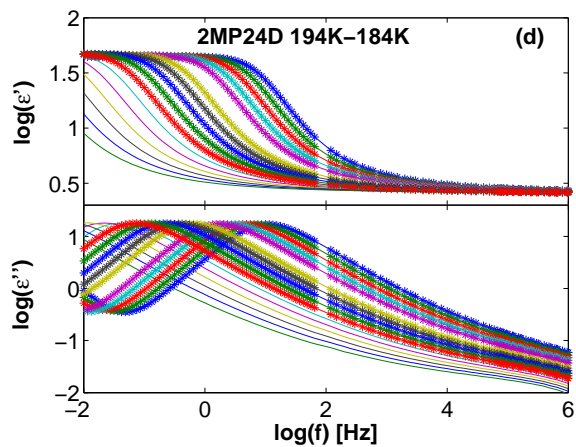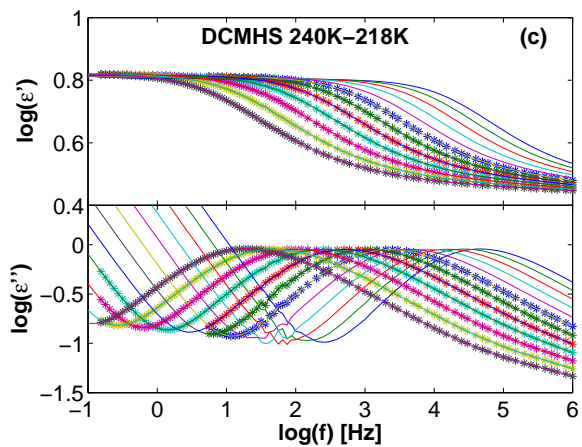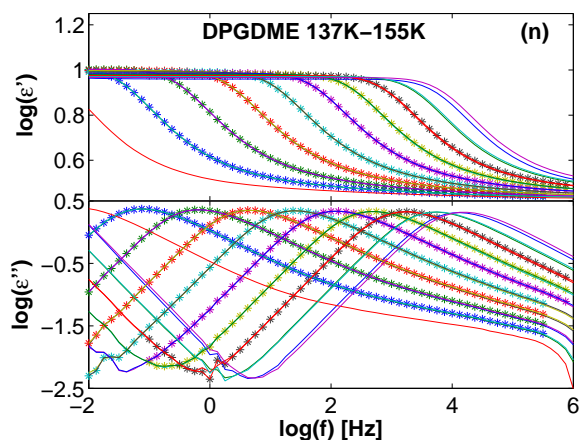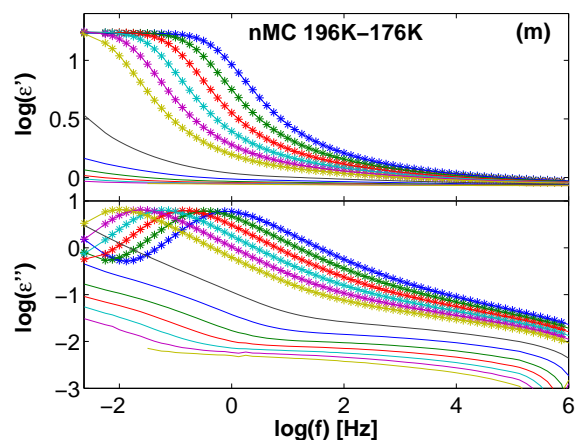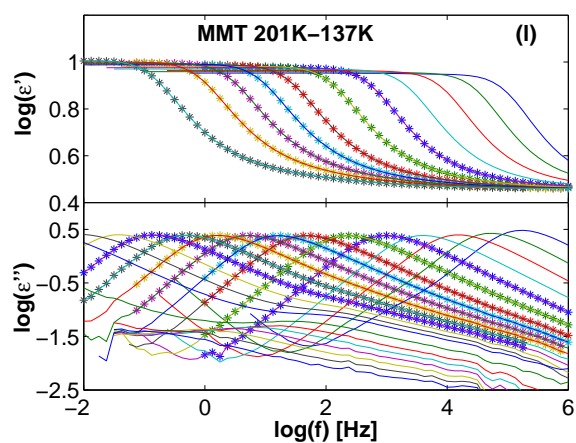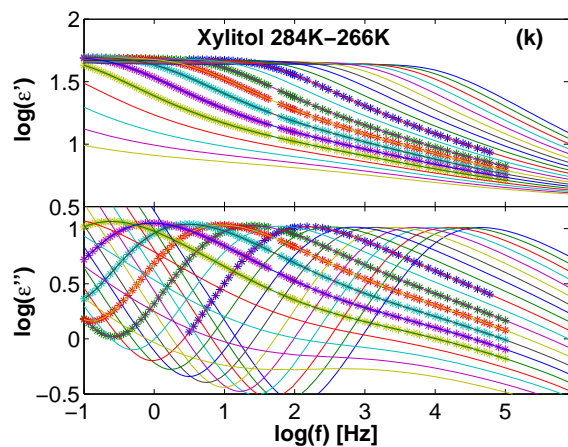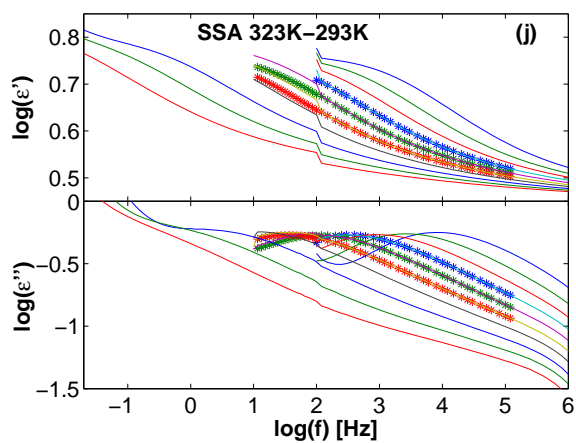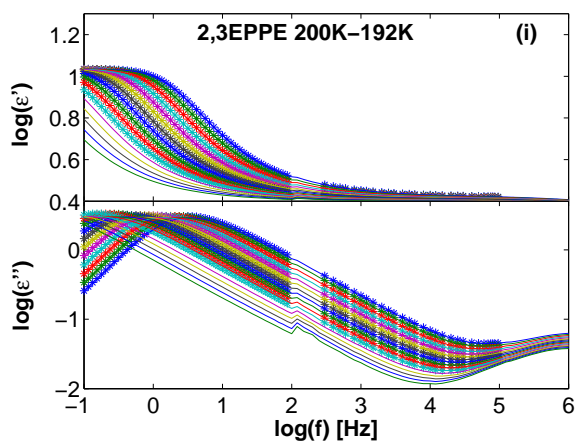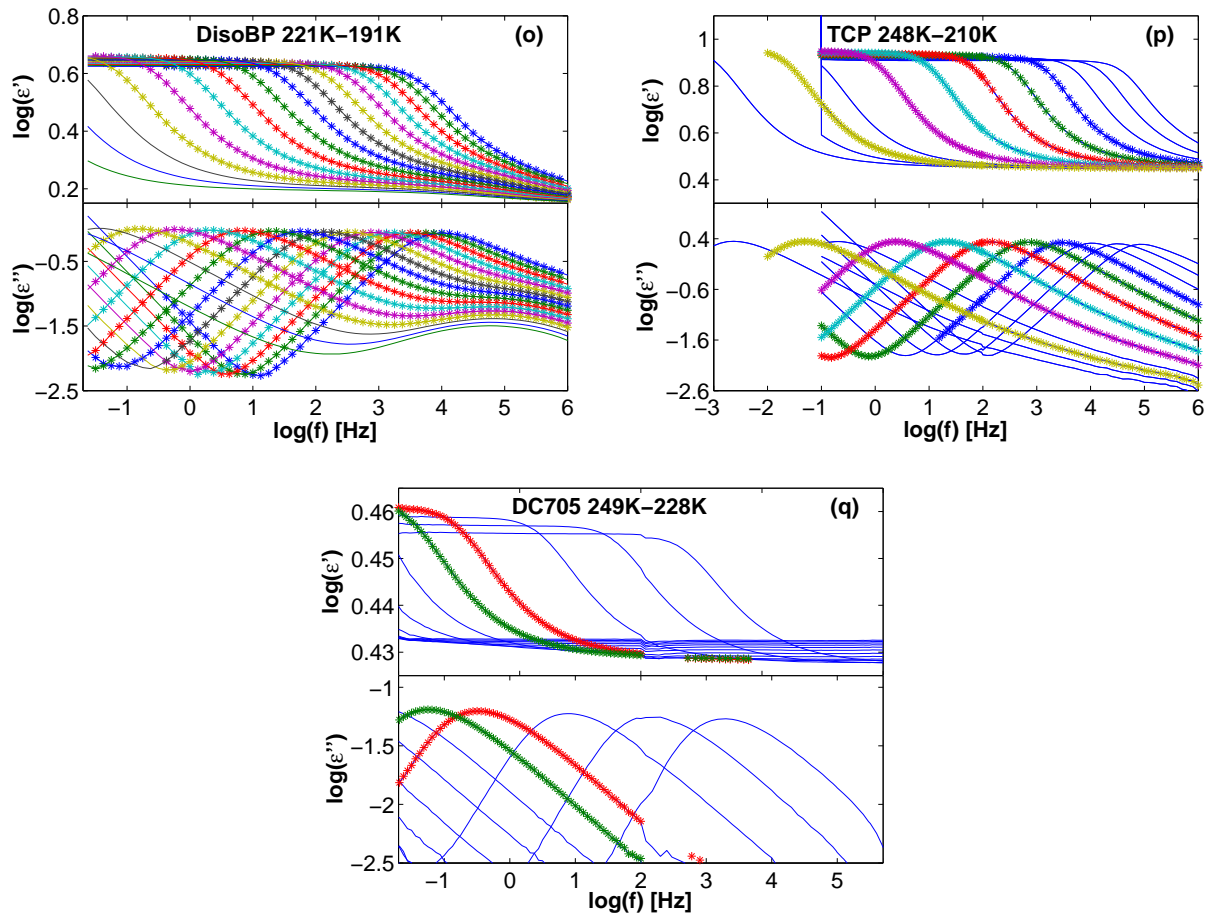
FIG. 1: Frequency-temperature scans for (a) 2-phenyl-5-(acetomethyl)-5-ethyl-1,3-dioxa-cyclohexane (APAED), (b) biphenyl-2-yl isobutylate (BP2IB) (c) dicyclo-hexyl-2-methyl succinate (DCHMS), (d) 2-methyl-pentane-2,4-diol (2MP24D), (e) dioctyl phthalate (DOP), (f) 1,3 propandiol (13PD), (g) trioxatridecane diamine (TODDA), (h) α phenyl-o-cresol (PoC), (i) 2,3-epoxypropyl phenylether (2,3EPPE), (j) salicylsalicylic acid (SSA) and (k) xylitol. (l) methyl-m-toluate (MMT). (m) N-ϵ-methyl-caprolactam (nMC) (n) dipropylene glycol dimethyl ether (DPGDME) (o) di-iso-butyl phthalate (DisoBP) (p) tricresyl phosphate (TCP) and (q) trimethyl-pentaphenyl trisiloxane (DC705). The full curves give the temperature-frequency scans, stars mark the data and corresponding data range selected for the analysis. On the plots (a)-(k) there is a systematic error around 100 Hz due to the supply net frequency and the fact that we at 100 Hz switch between two measuring techniques.

The following liquids (with noted purity, abbreviation, and figure) were measured on this setup: 2-phenyl-5-(acetomethyl)-5-ethyl-1,3-dioxacyclohexane (APAED, Fig. 1(a)), biphenyl-2-yl isobutylate (BP2IB, Fig. 1((b)), dicyclo-hexyl-2-methyl succinate (DCHMS, Fig. 1(c)), (the three liquids (a), (b), and (c) were synthesized at Díaz-Calleja's laboratory at Universidad Politécnica de Valencia; 2-methyl-pentane-2,4-diol (98%, British Drug Houses Ltd., 2MP24D, Fig. 1(d)), dioctyl phthalate (99%, DOP, Fig. 1(e), 1,3 propandiol (98%, 13PD, Fig. 1(f)), trioxatridecane diamine (TODDA, Fig. 1(g)), α phenyl-o-cresol (98%, PoC, Fig. 1(h)), 2,3-epoxypropyl phenylether (99%, 2,3EPPE, Fig. 1(i)), tricresyl phosphate (98%, Alfa Aesar, TCP, Fig. 1(p), data for structural relaxation times published in [57]), trimethyl-pentaphenyl trisiloxane (Dow Corning 705 silicon diffusion pump oil, Dow Corning Corp., DC705, Fig. 1(q)), 1,2 propandiol (99%, Merk, PG), dibutyl phthalate (98%, DBP), and diethyl phthalate (97%, DEP). – Spectra for these liquids are shown in Fig. 1 except for the last three liquids that have often been reported in the literature. Salicylsalicylic acid (99%, SSA, Fig. 1(j)), xylitol ($\geq$ 99%, Fig. 1(k)) and D(-)sorbitol (99%, AppliChem, Sor) are crystals at room temperature. They were melted in an oven, placed in the warmed-up (melting temperature) capacitor and subsequently cooled to room temperature. Xylitol was kept at 370 K for one hour; D(-)sorbitol at 390 K for four hours; SSA kept at 419 K for one hour. All other liquids were cooled starting from room temperature.

Arizona State University Setup 1, (ASU Setup1). This setup is basically described in Refs. [50–52], but used here with some recent improvements. The measuring cell has empty capacitance 17 pF. The sample cell was placed on a temperature-controlled plate in an evacuated He-refrigerator cryostat (Leybold RDK 6-320) driven by a Cool Pak 6200 compressor. The temperature of the base plate and the cell was controlled by a Lakeshore 340 temperature controller equipped with calibrated DT-470-CU diodes as sensors. The capacitance cell was connected to a Solartron SI-1260 gain/phase analyzer equipped with a Mestec DM-1360 trans-impedance amplifier [50]. The liquids were supercooled in the cryostat chamber. Due to the relatively low cooling rate, around 1.5 K/min, the waiting time between a temperature step and the start of measurements was 10 minutes after 5 minutes temperature stabilization.

The following liquids (characterized by particularly low glass transition temperatures) were measured on this setup: 2-methyltetrahydrofuran (99.1%, *distilled*, MTHF), methyl-*m*-toluate (98%, Avocado Research Chemicals Ltd., MMT, Fig. 1 (l)) and n-propyl-benzene (99%, nPB).

Arizona State University Setup 2, (ASU Setup2). The measuring cell, which has empty-cell capacitance 27 pF, consists of two steel discs electrodes of diameter 20 mm separated by six 50μm thick Teflon stripes. The cell was placed inside a nitrogen-gas cooled cryostat where temperature was stabilized and measured by a Novocontrol Quatro controller. The impedance measurements were performed in the range 0.1 Hz - 10 MHz using a Solartron SI-1260 gain-phase analyzer. A Mestec DM-1360 trans-impedance amplifier was used (as for ASU Setup 1). The empty sample capacitor was used as reference to calibrate the frequency-dependent trans-impedance of the amplifier.

The following liquids were measured on this setup: *N-ε*-methyl-caprolactam (99%, nMC, Fig. 1 (m)), dipropylene glycol dimethyl ether ($\geq$ 98%, DPGDME, Fig.1 (n)) and di-*iso*-butyl phthalate (99%, DisoBP, Fig. 1 (o)).

The data to our disposition were thus obtained on several different setups working in different frequency intervals with varying number of measurement frequencies per decade. From the spectra measured at the RU setup we removed the points around 100 Hz because of the systematic error due to the switch; all other data sets were used as measured, or received from the different groups. If two data series for the same liquid were available from different groups/setups, the series with most frequencies measured per decade was used.

Decahydroisoquiline (DHIQ) is represented by two datasets, one measured by Jakobsen et al [35] (RU Setup) and one by Richert et al [53] (ASU Setup2). These measurements compliment each other nicely, except for a minor deviation ($\sim$ 0.5 K) in the absolute temperature calibration.

Following a basic philosophy of analyzing the raw data directly, no attempts were made to subtract contributions from the DC conductivity and no attempts were made to subtract contributions from β relaxation(s). This procedure is fundamental to this paper's approach. Thus while one may argue what is the correct way of compensating for these and possibly other interfering effects in order to isolate the "true" α process, it should be much easier to reach consensus regarding the raw data themselves and their properties.

DATA ANALYSIS METHODS

The minimum slope of the dielectric loss plotted in a log-log plot is identified directly from raw data; thus no assumptions concerning the nature of the relaxation process are made, for instance of how α and β processes interact, whether or not the excess wing is a hidden β process, etc. [21]. The slope in the log-log plot is given by

$$\alpha = \frac{d \log \varepsilon''}{d \log(f)}, \tag{1}$$

where f is the frequency. Figure 2 illustrates the minimum slope concept by showing the high-frequency imaginary part of the complex dielectric constant (upper panel) at a given temperature for one liquid (DPGDME, $T = 139$ K) and, in (b), the corresponding slope where, of course, $\alpha = 0$ at the loss peak frequency $f_{\max}$. The minimum of the derivative above the loss peak frequency defines the minimum slope, $\alpha_{\min}$, which is always a negative number.

Since the second-order derivative is by definition zero where the slope is minimal, at the inflection point, the linear tangent approximation works particularly well here. This means that the approximate power-law description $\varepsilon'' \propto f^{\alpha_{\min}}$ gives a good representation of the high-frequency loss over a sizable frequency range. Thus if, for instance, the minimum slope $\alpha_{\min}$ is close to $-1/2$, then to a good approximation $\varepsilon'' \propto 1/\sqrt{f}$ for $f >> f_{\max}$ over a significant
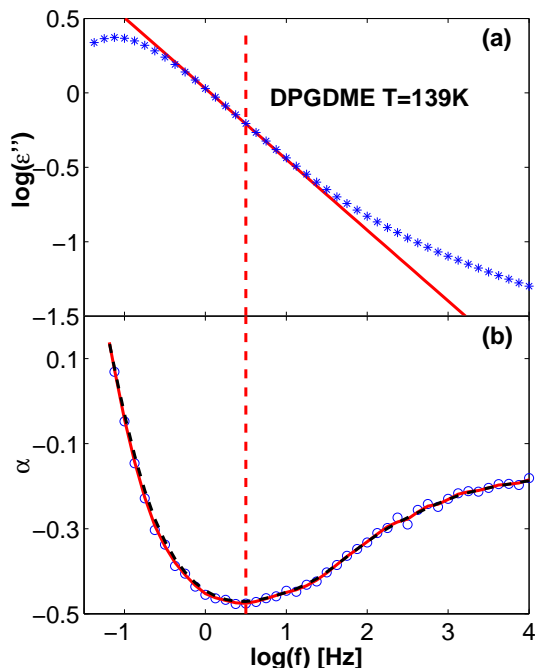
FIG. 2: Illustration of the procedure used to calculate the minimum slope. (a) Data for the dielectric loss, ε'', of dipropylene glycol dimethyl ether (DPGDME) at $T = 139$ K in double-logarithmic plot ($*$). The red line marks the inflection point tangent that has slope equal to the minimum slope α_{min}. (b) The calculated values of the slope by numerical differentiation from these data ($\circ$). The red curve marks the slope data after averaging twice (over two neighboring points), the dashed line is after ten applications of the averaging routine. The vertical dashed line through both plots marks the position of the minimum slope frequency.

frequency range. In the time domain this corresponds to $\sqrt{t}$ relaxation being a good approximation of the relaxation function.

To determine the minimum slope for a given data set, the set was first numerically point-by-point differentiated. Only data sets with a well-defined minimum slope – or a clear plateau of constant slope – were included in the analysis. Moreover, data sets were only included if there was so little noise in the resulting slopes that determination of α_{min} with two significant digits was possible. These selection criteria imply that several frequency scans at high temperatures, as well numerous noisy data sets, were eventually omitted from the data analysis.

As a means to increase the reliability of the α_{min} estimate we applied averaging. Thus the noise in the numerical derivative was reduced by repeatedly applying a routine that averages over two neighboring points. The number of times this averaging procedure was applied varied with the data set, but kept below ten. As an example, for the data in Fig. 2(b) a double iteration of the averaging routine was used; the black dashed line shows the result if averaging was instead applied ten times. If averraging ten times changed α_{min} more than 0.01, the data set was discarded. Subsequent applications of the smoothing procedure result in numerically slightly larger values of the minimum slope, but this was never a serious problem. If the resulting curve after ten averagings was still too noisy, the frequency scan was discarded. Thus some subjectivity enters the analysis, but we took care to keep the element of subjectivity as small as possible; whenever questions arouse making the applied procedure dubious, the data set was discarded. This procedure left a total of 53 liquids in the data collection out of an initial collection of 84 liquids; for each liquid the number of identified minimum slope values varies between 2 and 17 with values ranging from -0.75 up to -0.10. Altogether 347 minimum slopes were identified for the 53 liquids at various temperatures.

The above-described approach for the characterization of the high-frequency relaxation was adopted in order to be as objective as possible by avoiding the need to make a choice of fitting intervals. In latter case it is necessary if one fits data to, e.g., a stretched exponential (KWW) or CD function to decide below which frequency the α process is
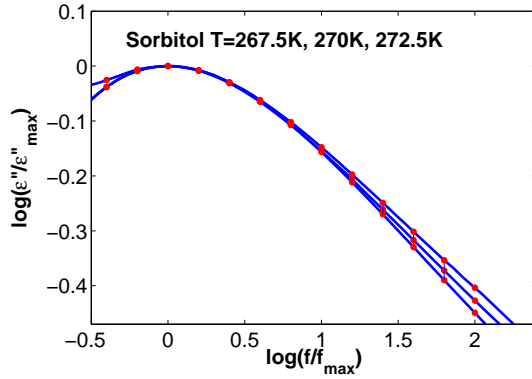
FIG. 3: Master plot of sorbitol data taken at 267.5, 270 and 272.5 K, i.e., log-log plot of the data normalized to have maximum equal to unity at unity normalized frequency. The TTS measure Δ is defined as the area difference between two neighboring temperature curves in this plot (where the area is calculated by including 0.4 decade of lower and two decades of higher frequencies than the loss peak frequency) divided by the difference of the logarithms of the actual loss peak frequencies (Eq. (4)). The points on the graphs mark the ε'' values used for the calculation of Δ

no more likely to be affected by secondary (β) processes. The subjectivity in the choice of fitting intervals results in numbers β_{KWW} and β_{CD} that are in many cases not uniquely determined with two-decimal accuracy – giving the same data set to different people will generally result in slightly differing fitting parameters.

We need one further parameter to characterize the shape of the loss peak. For this we choose the width at half loss measured in decades. In order to be able to make optimal use of the data sets (that are often significantly affected by the existence of the DC contribution to the left of loss peak) we used only the number of decades of frequency to the right of the loss peak frequency until the loss is halved. The obtained widths are conveniently normalized with respect to the half Debye width on the log scale, $W_{D/2} = 0.571$. Thus if the observed half width on the log scale is $W_{1/2}$, we define

$$w_{1/2} \equiv \frac{W_{1/2}}{W_{D/2}}. \tag{2}$$

This quantity is always above unity; if it is close to one, the relaxation is Debye like.

Turning to the quantification of how well time-temperature superposition (TTS) applies, we note that to decide whether TTS applies one usually uses a visual evaluation of attempted master plots of losses measured at different temperatures. One way to evaluate TTS is to investigate whether shape parameters are temperature invariant; however as mentioned we wish to avoid the use of fits to analytical functions. In order to obtain a numerical measure of how well TTS applies, the width variation with temperature is first quantified as follows. Consider loss spectra at two neighboring temperatures, $T_j < T_{j+1}$, both normalized with respect to their respective loss peak frequencies $f_{\max}$ and amplitude ε''_{max} (identified by fitting a second-order polynomial to an interval of data points in double logarithmic plot, using from 5 up to 9 points around the maximum depending on the symmetry of the loss peak). The difference between the two normalized curves is reflected in the areas between the curves (Fig. 3). Let $\tilde{\varepsilon} = \varepsilon''/\varepsilon''_{max}$ and $\tilde{f} = f/f_{max}$ be normalized loss and frequency, respectively at a given temperature. We define dS_j as the area between two frequency scans at T_j and T_{j+1}: dS_j is sum of the difference in the values of $\log(\tilde{\varepsilon}_j)$ and $\log(\tilde{\varepsilon}_{j+1})$ at m frequencies in the normalized graphs. More precisely, we found ε''_j by interpolation at $m = 13$ frequencies equally spaced on the logarithmic axis ranging from $\log(\tilde{f}_1) = -0.4$ to $\log(\tilde{f}_{13}) = 2.0$. The calculation of dS_j and it was made with those 13 $\tilde{\varepsilon}$ values,

$$dS_j = \sum_{i=1}^{13} \left|\log(\tilde{\varepsilon}_{j+1}(\log(\tilde{f}_i))) - \log(\tilde{\varepsilon}_j(\log(\tilde{f}_i)))\right|. \tag{3}$$

To make reasonable sense the frequency interval $[\tilde{f}_1; \tilde{f}_{13}]$ should contain the main part of the α loss peak. We define this as including almost a half decade on the low-frequency side and two decades on the high-frequency side of the loss peak. The frequency-range asymmetry is justified by: 1) A wish to include as many dielectric spectra as possible at relatively low temperatures (i.e., in the low-frequency part of the experimental window) because many dissipation curves ends around 10mHz; the low temperature relaxation response is particularly interesting due to the separation of α and high-frequency β processes; 2) An asymmetric interval reduces the effect of the DC contribution. – Note that we need at least two frequency scans to calculate one value of the area difference and thus Δ; thus the TTS analysis does not result in 347, but in $347 - 53 = 294$ data points.

The required measure of TTS deviations should not depend on the difference between neighboring temperatures in the particular data series under scrutiny. Thus, we define the TTS deviation measure Δ_j as follows (where $d\log(f_{max,j})$ is the numerical change in log(loss peak frequency))

$$\Delta_j \;=\; \frac{dS_j}{d\log(f_{max,j})} \, . \tag{4}$$

In this way one compensates for the fact that measurements at close temperatures trivially result in curves of closely similar shapes.

TTS is better obeyed, the smaller Δ is. This TTS measure introduces a further constraint on the data selection, namely that only data sets with a well-defined maximum and at least half a decade of measurements on the low-frequency side of loss were included in the analysis. Furthermore, data must be quite accurate since the $\tilde{\varepsilon}$ values are found from data by linear extrapolation.

MINIMUM SLOPE DISTRIBUTION

Figure 4 shows the minimum slope distribution for the 53 liquids in two histograms of different resolutions. This is the main figure of the paper. The above-discussed limitations, as well as the differing temperature ranges and frequency intervals for the data sets, imply that the number of $\alpha_{\min}$ values per liquid varies widely (from 2 to 26). To compensate for this and give equal weight to each liquid, each minimum-slope observation was given the weight $1/N$ where N is the number of spectra for that particular liquid (surviving the data selection criteria).
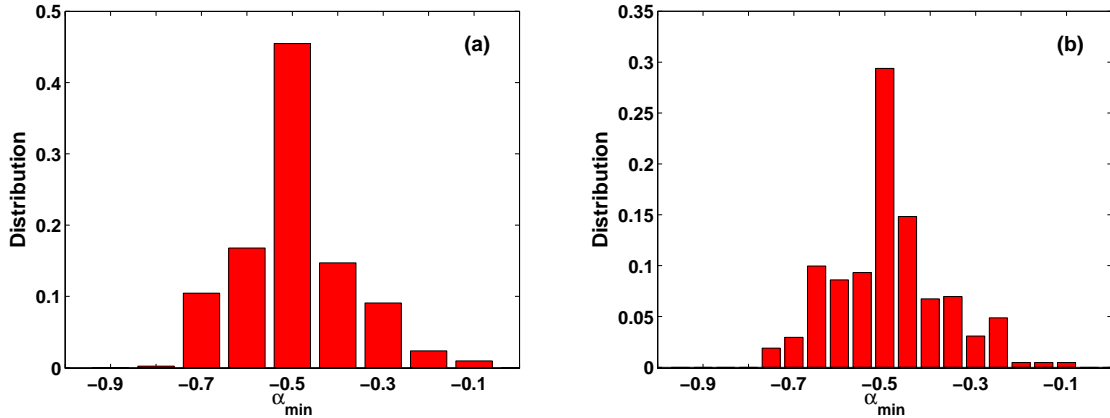
FIG. 4: (a) Histogram of the minimum slope distribution for all dielectric spectra for the 53 liquids, using subintervals of length of 0.1 . The number of loss spectra varies widely from liquid to liquid (from 2 to 26), so in order to give all liquids equal weight, each minimum slope value was given the weight $1/N$ if the liquid in question has N spectra included in the analysis. The most frequently observed values of $\alpha_{\min}$ are between -0.45 and -0.55. This implies prevalence of approximate $\sqrt{t}$ relaxation. (b) Histogram of the same data with subintervals of length 0.05. Almost a third of the minimum slopes are between -0.525 and -0.475
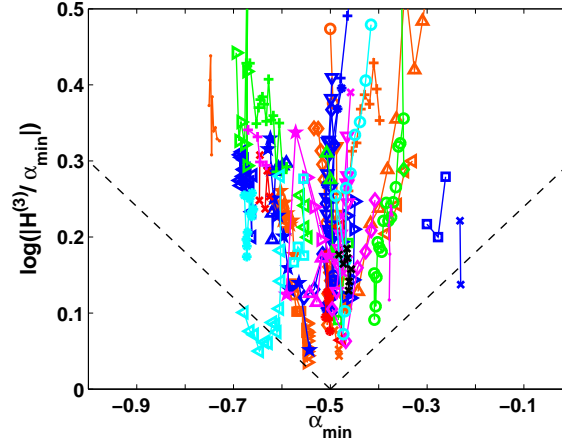
FIG. 5: A measure of how well the inflection point inverse power-law approximation applies plotted versus minimum slope. The dashed lines are guides for the eye. Every liquid data set is presented with the color and symbol listed in table I. There is a tendency that liquids where the inverse power-law approximation applies particularly well have minimum slopes close to $-1/2$; thus only two liquids have points below the dashed line.

A priori one would perhaps expect a more or less flat distribution of minimum slopes; nothing in the conventional wisdom indicates that one particular minimum slope should be more likely than another. Our data set, however, show significant prevalence of minimum slopes close to $-1/2$. This corresponds to a prevalence of approximate $\sqrt{t}$ relaxation of the dielectric relaxation function.

POSSIBLE MINIMUM SLOPE CORRELATIONS

Assuming that the liquids in the collection are representative of organic glass formers in general, there is something significant with minimum slopes close to $-1/2$. The obvious question that comes to mind is: How do minimum slopes correlate with other physical quantities? Below we consider six potential correlations.

Do minimum slopes correlate with how accurate an inverse power-law fit applies at the inflection point?

If $\sqrt{t}$ relaxation were somehow generic for the α process, one would expect that whenever the inflection point tangent gives a particularly good fit, the minimum slope is close to $-1/2$. To look into this we numerically calculated the third-order derivative relative to the first-order derivative of the losses at the inflection point in the usual log-log plot. Defining $H(\log(f)) = \log(\varepsilon''(\log(f)))$, the first-order derivative of H with respect to $\log(f)$ at the inflection point frequencyis given by $H^{(1)} = \alpha_{\min}$. The second-order derivative $H^{(2)}$ is zero here. Therefore, according to Taylor's theorem a measure of how well the inflection-point tangent approximates the loss, i.e., how well the power-law approximation $\varepsilon'' \propto f^{\alpha_{min}}$ applies, is provided by the ratio between third and first order derivates, $\left|H^{(3)}/\alpha_{\min}\right|$. The smaller this number is, the better is an inverse power-law fit.

To avoid noise problems we calculated $H^{(3)}$ as the curvature at the minimum of the (previously obtained) graph of the slope as function of frequency. The curvature was calculated by fitting to a second-order polynomial. The number of points in the fitting interval depended on the measured point density and on the symmetry of the neighborhood of this frequency; we used between five and seven points in the fitting intervals.

Figure 5 shows $\log\left(\left|H^{(3)}/\alpha_{\min}\right|\right)$ versus $\alpha_{\min}$ for all spectra. There is no tendency that the power-law approximation works particularly well for liquids with minimum slopes close to $-1/2$. There is, however, the converse tendency
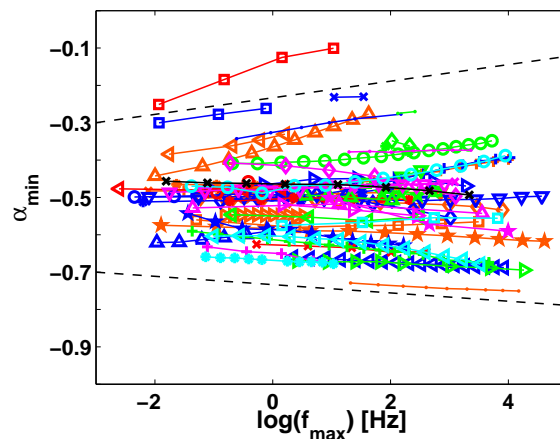
FIG. 6: Minimum slope versus loss peak frequency, the latter being a convenient measure of temperature. There is a tendency that minimum slopes approach $-1/2$ as temperature is lowered. The dashed lines are drawn as guides to the eye.

indicated by dashed lines that if one requires the power-law approximation to work very well, minimum slopes tend to be close to $-1/2$. To summarize, Fig. 5 confirms a special status associated with liquids with $\alpha_{min} \cong -1/2$.

Do minimum slopes and loss-peak frequencies correlate?

Next we investigate how minimum slopes depend on temperature. If $\alpha_{min} = -1/2$ were generic for the "pure" α process, one would expect minimum slopes to converge to this value at low temperatures (still in the metastable equilibrium phase). A convenient way to study α_{min}'s temperature dependence is to represent temperature by the loss peak frequency; in this way all liquids are regarded from the same perspective.

Figure 6 shows the results. Minimum slopes are only weakly temperature dependent, but there is a tendency with a few exceptions that liquids with minimum slopes numerically larger than $1/2$ have $|\alpha_{min}|$ decreasing numerically as temperature is lowered, whereas for liquids with minimum slopes numerically smaller than $1/2$, $|\alpha_{min}|$ tends to increase. The dashed lines are drawn to indicate this overall tendency.

Some further notes relating to this figure: Liquids like 2-methyltetrahydrofuran (MTHF, blue $\triangledown$), DBP (blue $*$), DEP (blue $\circ$), DOP (orange $\diamond$), 5-polyphenyl-ether (PPE, red $*$), tetraphenyl-tetramethyl-trisiloxane (DC704 red $\triangleleft$) and 4-methyl-heptane (4MH, green $\star$) with nearly constant minimum slope close to of $-1/2$ all have β relaxation loss peaks above 10^5 Hz. For some glass formers like MMT (blue $\diamond$) $|\alpha_{min}|$ increases above $1/2$, but eventually approaches $1/2$ as temperature is further decreased. This presumably reflects the merging of α and low-intensity β processes that one observes for scans at temperatures below T_g in Fig. 1(l). The same change in α_{min} values is observed for materials with $|\alpha_{min}| > 1/2$ like phenolphthalein dimethylether (PDE, cyan $\triangleleft$), PG (blue $\triangleleft$), propylene carbonate (PC, red $\times$), and nMC (blue $\triangle$). The dielectric scan of the last liquid nMC in Fig.1 (m) shows two secondary processes with times corresponding to frequencies around 100 Hz and in the interval $0.1 - 0.01$ Hz, respectively. The loss peak frequencies for the six chosen curves are just above the secondary process (0.01 Hz) and α_{min} is decreasing.

In summary, there is a tendency that minimum slopes slowly approach $-1/2$ as temperature is lowered. It would obviously be interesting to have lower temperature observations, but it is not realistic to extend observations to significantly lower temperatures and frequencies while still probing the metastable liquid phase.
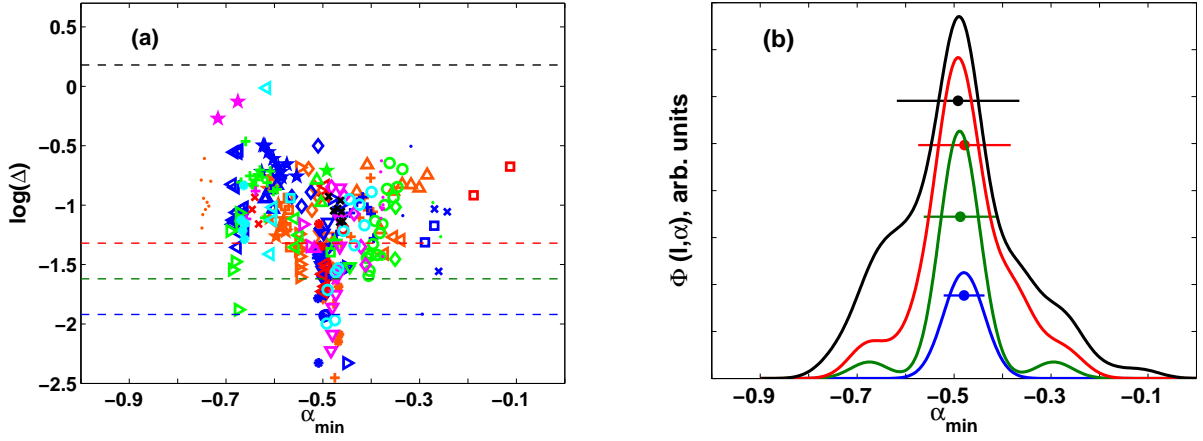
FIG. 7: (a) Time-temperature superposition (TTS) analysis. (a) shows the measure of how well TTS applies, $\log(\Delta)$, plotted versus α_{min}. With a few outliers it is seen that the smaller $\log(\Delta)$ is (i.e., the better TTS applies) the more α_{min} tends to $-1/2$. (b) The smoothed distribution $\Phi(\alpha, l)$ of the number of measuring points (normalized to the total number of points representing a given liquid) for all liquids with $\log(\Delta) < l$. The levels $l = -1.92; -1.62; -1.32; +0.18$ correspond to the colors blue, green, red and black, and are marked with dashed lines in (a). The four dots and vertical lines mark the mean values and variances of α_{min} for the four distributions.

Do minimum slopes correlate with how well time-temperature superposition applies?

Figure 7(a) shows the TTS measure $\log(\Delta)$ (Eq. (4)) plotted versus minimum slopes – in this case the latter were averaged over the two neighboring temperatures involved in defining Δ. The liquids again have varying number of points, so the population of all points on the graph does not give a clear picture of a possible correlation. To compensate for this as was previously done for the minimum slope histogram, in Fig. 7(b) we present the distribution function ϕ that gives all liquids equal weight. The distribution function, which is smoothed in this figure, gives information about how many liquids have TTS deviations below a certain level, l, for a given value of the α_{min}. If $\theta(x)$ is the theta function (unity for positive x, zero for negative), $\Lambda = 0.003$ is a smoothing parameter, α_{ij} is the minimum slope of i-th liquid at the j-th temperature in its data series and Δ_{ij} the corresponding TTS deviation measure, $n = 53$ is the total number of liquids, and N_i is the number of spectra of the i'th liquid (thus there are $N_i - 1$ TTS deviation measures for the liquid), the distribution function is defined as follows:

$$\Phi(\alpha_{min}, l) = \frac{1}{n} \sum_{i=1}^{n} \frac{1}{N_i - 1} \sum_{j=1}^{N_i - 1} \exp\left(-\frac{(\alpha_{min} - \alpha_{ij})^2}{\Lambda}\right) \theta(l - \log(\Delta_{ij})). \tag{5}$$

Figure 7(b) gives the function $\phi(\alpha_{min}, l)$ for increasing values of l plotted with blue, green, red, and black, respectively. The corresponding levels l are marked with dashed lines in Fig. 7(a). To the lowest level curve (blue) only the following liquids contribute: α-phenyl-o-cresol (PoC, orange $*$), polypropylene-glycol 400 (PPG, orange $+$), dibutyl phthalate (DBP, blue $*$), APAED (Fig. 1(a), magenta $\triangledown$), 2MP24D (Fig. 1(a) cyan $\circ$) and DPGDME (Fig.1 (n) , blue $\triangleright$). Thus these liquids obey TTS to a very good approximation; they are all characterized by almost temperature independent $\alpha_{min} \cong -1/2$.

In summary, the above confirms the conjecture of Ref. [13] that liquids accurately obeying TTS have minimum slopes close to $-1/2$. A new observation of the present paper is the general prevalence of $\sqrt{t}$ relaxation, whether or not TTS applies to a good approximation.
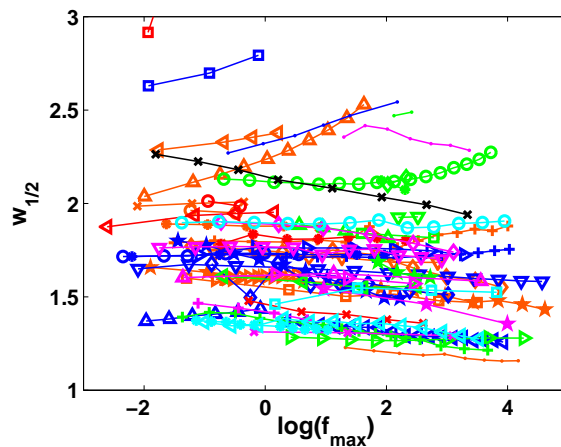
FIG. 8: Normalized width $w_{1/2}$ plotted versus loss peak frequency, the latter quantity providing a convenient measure of temperature. The width generally changes with temperature and only in some cases becomes almost constant as the temperature is lowered.

Do minimum slopes correlate with loss peak widths?

The normalized half widths $w_{1/2}$ are presented in Fig. 8 versus loss peak frequency. The widths vary between 1.2 and 3.0 with the exception of DHIQ (red $\square$) that has one spectrum with $w_{1/2} = 4.0$.

Liquids with almost Debye dissipation have almost same normalized widths ($1 < w_{1/2} < 1.5$ in Fig. 8); these liquids are: propylene carbonate (PC, red $\times$), ethylene glycol (EG, magenta $+$), 1,3PD (orange $\bullet$), butyronitrile (But, green $+$) and dibutylammonium formide (DBAF, green $\triangleright$) – all liquids with strong hydrogen(nitrogen) bonding. To the same group of small-width liquids also belong salol (magenta $\times$) that have minimum slopes close to $-1/2$ and nMC (blue $\triangle$) with data points that show that the width narrows as $T \rightarrow T_g$.

Figure 9 shows $\alpha_{\min}$ versus $w_{1/2}$. There must be some correlation between $\alpha_{\min}$ and $w_{1/2}$: If the minimum slope is numerically small, the width must be large and vice versa. In Fig. 9(a) one indeed finds such a correlation between $\alpha_{\min}$ and $w_{1/2}$. This is especially apparent for liquids with $\alpha_{\min}$ at the boundaries of the $\alpha_{\min}$ interval. Thus significant variations of $w_{1/2}$ with minimum slope appears for materials with very broad relaxation like sorbitol (blue $\square$) and DHIQ (red $\square$) – liquids with high-intensity secondary process, as well as Xylitol ($\bullet$), 3-methylheptane (3-MH, green $\bullet$), TODDA (Fig. 1(g), $\triangleleft$). Sucrose benzoate's (SB, green $\circ$) width narrows in the same way, but below some temperature it again begins to grow while the minimum slope gets smaller. This may indicate interference from underlying low-intensity β relaxation process (there is an additional well-resolved β-process above 1 MHz).

If we focus on minimum-slopes between -0.4 and -0.6 (Fig. 9(b)), however, there is a significant spread in the values of normalized widths and no strong correlation between $w_{1/2}$ and $\alpha_{\min}$. For the glass former MMT (blue $\lozenge$) the two quantities are, from some temperature on, almost constant with $\alpha_{\min} \in [0.493; 0.503]$ and $w_{1/2} \in [1.495; 1.684]$. Isoeugenol (black $\times$) has the same behavior as nMC, the loss peak broadens, but minimum slope is close to $-1/2$. Other examples of this are DOP (orange $\lozenge$), DEP (blue $\circ$), and PPE (red $\ast$). For some cases like for DisoBP (blue $+$) and DC705 (orange $\circ$) $\alpha_{\min}$ changes significantly while $w_{1/2}$ stays almost constant. The reason for this is that $w_{1/2}$ does not capture deviations beyond one decade, thus it does not necessarily change when α and β processes separate as temperature decrease. In fact, the quantity $w_{1/2}$ rarely includes the contributions from around the inflection point that determine the minimum slope.

A plot of $w_{1/2}$ versus the TTS measure $\log(\Delta)$ is shown in Fig 10. We see that $\log(\Delta)$ may be large (and varying) for a given liquid with a fairly constant $w_{1/2}$; thus as expected $\log(\Delta)$ is more sensitive than $w_{1/2}$ to capturing small changes in the shape of the α process with temperature. Both quantities are affected by noise, of course, and a drawback of $\log(\Delta)$ is that its noise sensitivity has an accumulative character. The "local" data noise from the dielectric measuring equipment can be readily seen and noisy data are readily removed from the analysis. Inaccuracies deriving from the sample not being properly thermally equilibrated or from unstable thermal experimental conditions,
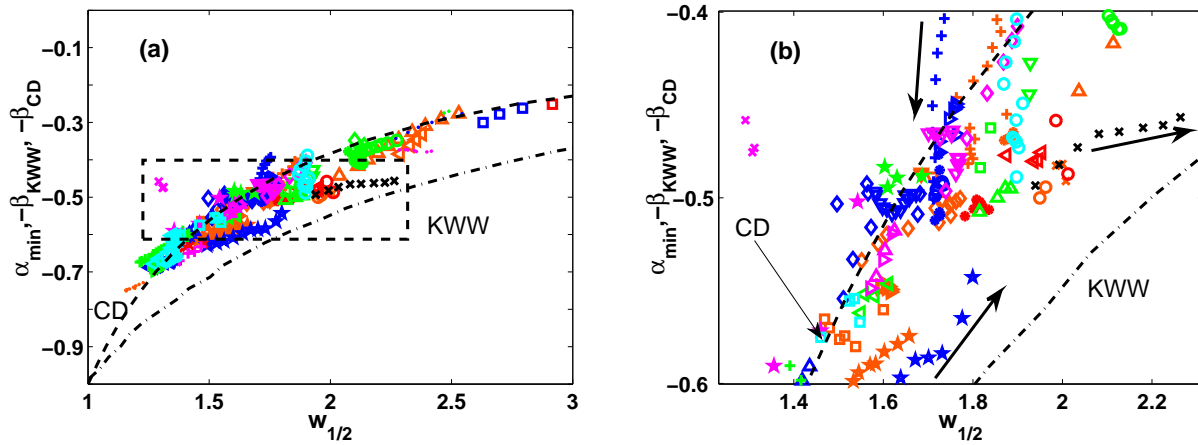
FIG. 9: (a) Normalized half width at half maximum, $w_{1/2}$ versus minimum slope $\alpha_{\min}$. There is an overall correlation between the two measures, reflecting the fact that a numerically low value of the minimum slope forces the width to be large and vice versa. The dashed-line rectangle frames the zoom-in shown on the plot (b), $-0.6 < \alpha_{\min} < -0.4$. Here we more clearly see that often minimum slopes vary whereas $w_{1/2}$ is nearly constant. In both figures the two black dashed and dash-doted curves give $-\beta_{CD}$, respectively $-\beta_{KWW}$, vs. the corresponding $w_{1/2}$. The black arrows indicate the direction of changes as temperature decreases. The values for β_{KWW} and $w_{1/2}$ for the KWW process are from [54].
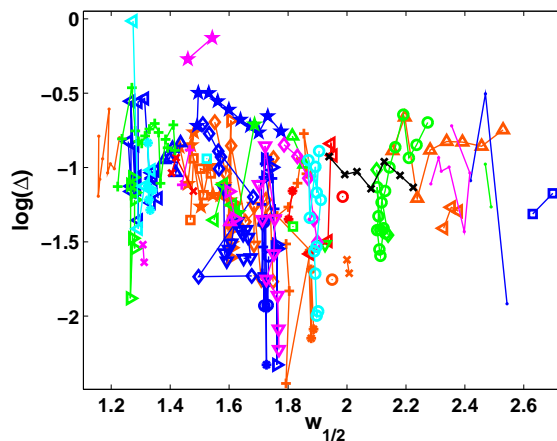
FIG. 10: Normalized width $w_{1/2}$ versus the TTS measure $\log(\Delta)$. The figure shows that $\log(\Delta)$ is more noisy than $w_{1/2}$, but also more sensitive to shape changes due to temperature decrease, while $w_{1/2}$ is in some cases almost constant.

however, are not so apparent and more difficult to avoid; these are reflected in both measures, but particularly in $\log(\Delta)$.

In summary, there is a mathematically compelling trivial correlation between minimum slopes and loss peak widths, but when one focuses on data sets with $\alpha_{\min} \cong -1/2$, a rather broad range of widths is observed, showing that there is little correlation between width and minimum slope for these liquids. Note, incidentally, that this finding emphasizes that single-parameter fits like the stretched exponential or Cole-Davidson are too simple to fit data accurately – in such fits the width determines the minimum slope and vice versa.
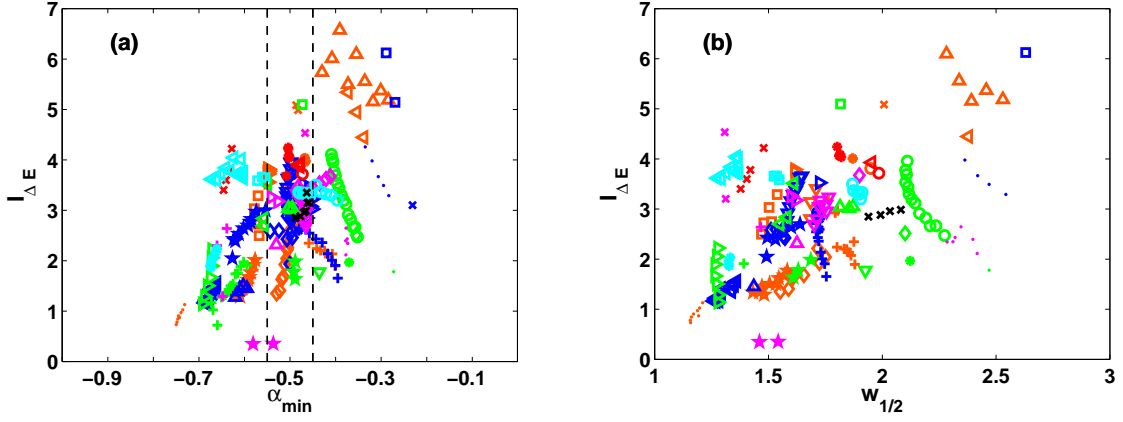
FIG. 11: (a) The activation energy temperature index $I_{\Delta E}$ versus $\alpha_{\min}$ for all data sets. The former quantity measures the degree of deviation from Arrhenius temperature dependence of the loss-peak frequency; Arrhenius behavior corresponds to $I_{\Delta E} = 0$. The dashed lines embrace the values between -0.55 and -0.45. A broad range of non-Arrhenius behaviors is represented among liquids exhibiting approximate $\sqrt{t}$ relaxation, thus close to $\alpha_{\min} = -0.5$ the temperature index varies by a factor of 2.5. In terms of fragility this quantity takes on values from roughly 50 to 125, which is practically the entire span of fragilities of the 53 liquids included in the data analysis. (b) Temperature index $I_{\Delta E}$ versus the normalized width $w_{1/2}$ (Eq. (2)), not showing any clear correlation.

Do minimum slopes correlate with how non-Arrhenius the liquid is?

The two parameters traditionally used to characterize a glass former are its stretching exponent β_{KWW} and fragility m. The latter measures how much the temperature dependence of the liquid's relaxation time (e.g., inverse loss-peak frequency) deviates from the Arrhenius equation at the glass transition. It generally accepted that the larger the fragility is, the lower is β_{KWW} [22, 34]; in fact based on experiment a quantitative relation between m and β_{KWW} has been suggested [55]. According to this picture all values between 0 and 1 for the stretching exponent can occur, depending on the fragility. Since a stretched exponential implies a high-frequency power-law loss varying with frequency as $f^{-\beta_{KWW}}$, from the traditional picture one expects liquids with $\alpha_{\min} \cong -1/2$ to have fragilities within a narrow interval.

We tested the implied correlation between $\alpha_{\min}$ and non-Arrhenius behavior by proceeding as follows. As a measure of the degree of non-Arrhenius behavior we used the activation energy temperature index $I_{\Delta E}$ defined [56–58] as follows

$$I_{\Delta E}(T) = -\frac{d \ln(\Delta E(T))}{d \ln(T)}. \tag{6}$$

Here the activation energy $\Delta E(T)$ is defined by writing $f_{\max}(T) = f_0 \exp(-\Delta E(T)/k_B T)$ with $f_0 = 10^{14}$ Hz [57]. The temperature index $I_{\Delta E}$ reflects the degree of deviations from Arrhenius behavior at any given temperature. When evaluated at T_g the temperature index relates to m as follows: $m = 16(I_{\Delta E}(T_g) + 1)$ [58], where $16 = \log(\tau(T_g)/\tau_0)$ if $\tau(T_g) = 100$s and $\tau_0 = 10^{-14}$s. The advantage of using the temperature index for quantifying non-Arrhenius behavior comes from the fact that the index is defined at any temperature, whereas m is evaluated at the glass transition temperature and thus formally relates to the liquid's properties only here.

Figure 11(a) plots $I_{\Delta E}$ for all data sets. For liquids exhibiting approximate $\sqrt{t}$ relaxation there is little correlation between the approximate high-frequency power law and the degree of non-Arrhenius behavior. Even the very fragile liquid benzophenone (BP, cyan □) ($m = 125$ [59]) exhibits approximate $\sqrt{t}$ relaxation.

For liquids with $\alpha_{\min} > -0.4$ we likewise found poor correlation between $\alpha_{\min}$ and degree of non-Arrhenius behavior. Thus for DHIQ (red □) relaxation is characterized by $\alpha_{\min} \in [-0.25, -0.10]$), sorbitol (blue □), by
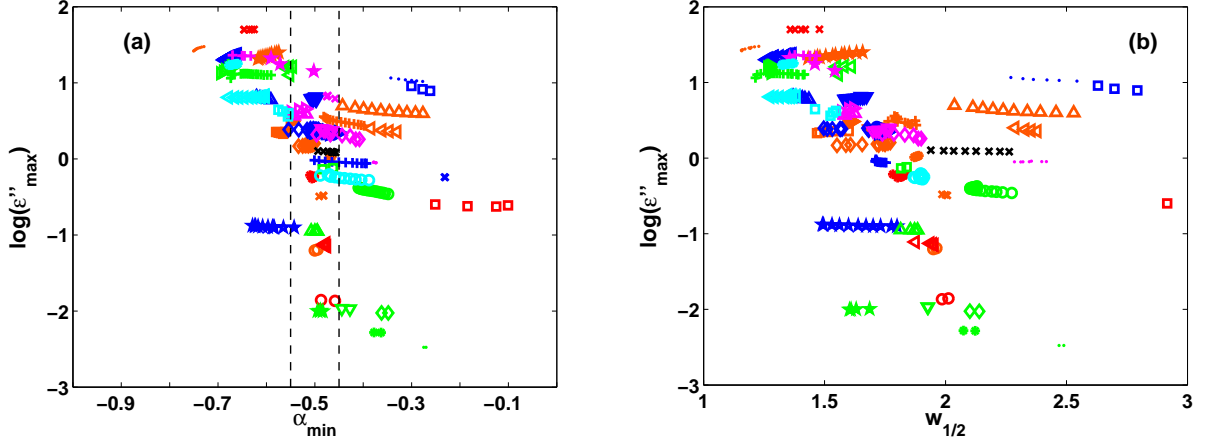
FIG. 12: (a) Maximum dielectric loss ε''_{max} versus α_{min} for all data sets. The liquids between the two dashed lines marking the interval $-0.55 < \alpha_{min} < -0.45$ have dielectric losses varying by more than a factor of 1,000. Large-loss liquids have minimum slopes that are numerically larger than 1/2; these liquids consistently disobey approximate $\sqrt{t}$ relaxation. (b) Maximum dielectric loss plotted versus width $w_{1/2}$. Glass formers with large dielectric loss consistently tend to be more Debye like as expected from (a).

$\alpha_{min} \in [-0.3, -0.26]$, and salicylsalicylic acid (SSA, blue $\times$), by $\alpha_{min} \cong -0.23$, whereas these three liquids have quite different temperature indices (Table 1). For these liquids fragilities reported in the literature are $m = 139$, $m = 100$, and $m = 31(45)$, respectively [60]. The lack of clear connection between the shape of the relaxation and the fragility is also clear in the plot $I_{\Delta E}$ versus $w_{1/2}$ in Figure 11 (b).

To summarize, liquids with approximate $\sqrt{t}$ relaxation exhibit a wide range of temperature indices (fragilities); there is no obvious correlation between the degree of non-Arrhenius temperature dependence of the loss peak frequency and the high-frequency decay of the loss.

Do minimum slopes correlate with dissipation magnitudes?

As a measure of dielectric strength one would prefer the overall loss $\Delta\varepsilon$, but since this quantity may be difficult to determine accurately we instead quantify the strength by the maximum loss. These two quantities are only strictly proportional for liquids with same relaxation function, of course, but this fact is not important here because the dielectric strengths span more than four decades.

As can be seen from Fig. 12 (a) there is little overall correlation between having $\sqrt{t}$ relaxation and the value of the maximum loss $\log(\varepsilon''_{max})$. However, liquids with large dielectric strength like PDE (cyan $\square$), PG (blue $\triangleleft$), PC (red $\times$), EG (magenta $+$), 1,3PD (orange $\bullet$), butyronitrile (green $+$), and DBAF (green $\triangleright$) consistently show minimum slopes that are numerically larger than 1/2. The corresponding α_{min} values are only weakly temperature dependent, which agrees with results for other hydrogen-bonding systems [61]. Liquids with $|\alpha_{min}| > 0.65$ tend to have Kirkwood correlation factors [62] significantly larger than unity, reflecting strong correlations between the motions of different dipoles. Higher Kirkwood correlation factors mean longer-range orientational and dynamical correlations, leading to spatial averaging of what might otherwise still be $\alpha_{min} = -1/2$ behavior (for Kirkwood correlation factors going to infinity one expects an approach to Debye relaxation because of the increasingly large degree of cooperativity). Figure 12 (b) shows loss-peak strength versus width. There is a clear tendency that large-strength liquids are more Debye like.

To summarize, liquids with approximate $\sqrt{t}$ relaxation span a wide range of dielectric losses. There is little overall correlation between loss strength and minimum slope. Liquids with large loss strengths, though, clearly have $|\alpha_{min}| > 1/2$.

CONCLUSIONS

The data compiled in this study suggest that – with the exception of large-loss liquids – $\sqrt{t}$ relaxation is generic to the α process of glass-forming liquids. This conclusion is not only based on the observed prevalence of $\sqrt{t}$ relaxation (Fig. 4), but also on our findings that:

- The better an inverse power law describes the high-frequency loss, the closer are minimum slopes to $-1/2$ (Fig. 5).

- The lower temperature is, the closer are minimum slopes to $-1/2$ (Fig. 6).

- The better TTS applies, the closer are minimum slopes to $-1/2$ (Fig. 7).

Intuitively, one would expect that interference from β processes can only explain minimum slopes that are numerically smaller than $1/2$. From measurements on liquids with a well-defined β process in the kHz range, however, we and other groups have repeatedly found that when the liquid is heated above the $\alpha\beta$ merging temperature, the high-frequency decay of the merged process has a minimum slope that is numerically larger than $1/2$ (and eventually converges to one upon further heating). Thus, since whenever there are very low-lying beta processes the liquid is above the $\alpha\beta$ merging temperature, $|\alpha_{\min}| > 1/2$ might well occur at the lowest attainable temperatures for some liquids. "Genuine" $\alpha_{\min} = -1/2$ behavior only appears when the system is significantly below the merging temperature, a situation that for several liquids is experimentally out of reach.

Liquids exhibiting approximate $\sqrt{t}$ relaxation have no particular loss peak widths, temperature indices (fragilities), or loss magnitudes.

A potential weakness of the analysis is that no objective criteria can be given for the selection of liquids included in the analysis. Thus there is the danger of unknowingly having a bias in the data. The data were gathered from leading groups in the field and supplemented by new or previously unpublished measurements. As detailed above, several data sets were discarded in the process because of having too much noise or other problems. The fact that we cannot report objective liquid selection criteria for the initial data pool makes, the analysis should be suplemented with data for other liquids before a firm conclusion can be drawn that approximate $\sqrt{t}$ relaxation is generic to the α relaxation process.

If $\sqrt{t}$ relaxation is confirmed as being generic for the α process (excluding high-loss liquids), the dynamics of glass-forming organic liquids is simpler than presently generally believed. That presents an important challenge to theory – although it should be noted again that there are already several theories predicting this [36, 38–43].

TABLE I: List of all liquids studied providing relevant references and information such as glass transition temperature, T_g, and intervals for quantities characterizing the data: the activation energy temperature index, $I_{\Delta E} \equiv |d\ln(\Delta E)/d\ln(T)|$; temperature T; maximum dielectric loss ilog(ε''_{max}); and minimum slopes of the log-log plot of the loss $|\alpha_{min}|$. The data listed bellow can be obtained from the "Glass and Time: Data repository", found online at http://glass.ruc.dk/data.

Liquid	Abbreviation	T_g (K)	Intervals				Symbol and ref.
			$I_{\Delta E}$	T (K)	$log\varepsilon''_{max}$	$|\alpha_{min}|$	
1,1'-bis (methoxyphenyl)-cyclohexane	BPC	212	3.67; 3.67	338; 362	0.258; 0.321	0.41; 0.5	◇ [84]
1,2-propanediol	PG	168 [73]	1.16; 1.56	180; 205	1.3; 1.375	0.66; 0.69	◁ this work
1,3-propane diol	13PD	167 [74]	0.73; 1.13	165; 189	1.419; 1.477	0.73; 0.75	● this work
2,3-dimethyl-pentane	2,3-DMP	87.5	1.78; 1.78	98; 99	−1.971; −1.967	0.43; 0.44	▽ [75]
2,3-epoxy-propyl-phenylether	23EPPPE	193	3.74; 3.79	196; 200	0.483; 0.522	0.55; 0.55	▷ this work
2,4,6-trimethyl-heptane	246TMH	123	2.51; 2.51	134; 135	−2.025; −2.024	0.35; 0.36	◇ [75]
2-methyl-pentane-2,4-diol	2MP24D	187	3.2; 3.5	210; 232	−0.28; −0.202	0.39; 0.49	○ this work
2-methyl-tetrahydrofuran	MTHF	91	2.77; 3.66	91; 103	0.776; 0.815	0.5; 0.51	▽ this work
2-phenyl-5-acetomethyl-5-ethyl- 1,3-dioxocyclo-hexane	APED	222 [76]	2.69; 3.23	220; 240	0.357; 0.397	0.46; 0.49	▽ this work
2-picoline	2pic	130	3.17; 3.26	135; 141	0.618; 0.658	0.52; 0.55	▷ [78]
3-fluoro-aniline	3FA	172 [22]	5.1; 5.1	235; 239	−0.135; −0.121	0.46; 0.48	□ [85]
3-methyl-heptane	3MH	97	1.78; 1.78	109; 110	−2.477; −2.477	0.27; 0.27	● [75]
3-methyl-pentane	3MP	79	1.97; 1.97	88; 89	−2.283; −2.281	0.36; 0.38	∗ [75]
4-methyl-heptane	4MH	99	1.63; 1.98	111; 114	−2.004; −1.995	0.48; 0.49	★ [75]
4-tertbuthyl-pyridine	4TBP	166	2.32; 13.79	164; 177	0.566; 0.602	0.52; 0.54	△ [86]
4,7,10-trioxatridecane-1,13- diamine	TOTDD	108	4.45; 4.45	177; 181	0.356; 0.401	0.33; 0.38	◁ this work
5-polyphenyl-ether	PPE	248	4.04; 4.24	252; 264	−0.258; −0.214	0.5; 0.51	∗ [35]
α-phenyl-o-cresol	PoC	219	4.01; 4.01	220; 228	0.011; 0.032	0.46; 0.47	∗ this work
benzophenone	BP	212	3.59; 3.66	215; 230	0.56; 0.647	0.55; 0.58	□ [59]
biphenyl-2yl-isobutylate	BP2BF	210 [76]	1.86; 2.03	190; 200	1.232; 1.253	0.66; 0.68	∗ this work
butyronitrile	But	95	1.91; 1.91	98; 116	1.061; 1.121	0.59; 0.67	+ [83]
decahydro-isoquinoline	DHIQ	180 [53]	7.13; 7.13	180; 185	−0.626; −0.599	0.1; 0.25	□ [35, 53]
dibutyl-ammonium-formide	DBAF	153	1.14; 2.22	162; 185	1.127; 1.218	0.67; 0.69	▷ [82]
dibutyl phthalate	DBP	177	2.6; 3.07	178; 192	0.301; 0.348	0.48; 0.51	∗ this work

TABLE I – continued from previous page

Liquid	Abbreviation	T_g (K)	Intervals				Symbol and ref.
			$I_{\Delta E}$	T (K)	$\log\varepsilon''_{max}$	$|\alpha_{min}|$	
di-*iso*-butyl phthalate	DisoBP	191 [22]	$1.65; 2.94$	$201; 221$	$-0.06; -0.016$	$0.39; 0.5$	$+$ this work
dicyclohexyl-methyl-2-methyl-succinate	DCMMS	220	$2.8; 3.41$	$224; 240$	$0.381; 0.411$	$0.49; 0.5$	∇ [77]
dicyclohexyl-2-methyl-succinate	DCHMS	222 [76]	$2.11; 2.64$	$218; 230$	$-0.05; -0.041$	$0.37; 0.38$	$\bullet$ this work
diethyl phthalate	DEP	187 [22]	$2.93; 2.93$	$183; 192$	$0.375; 0.412$	$0.49; 0.5$	$\circ$ this work
diglycidyl-ether of bisphenol A (epoxy-resin)	ER	259	$3.67; 3.67$	$338; 362$	$0.258; 0.321$	$0.41; 0.5$	$\diamond$ [79]
dioctyl phthalate	DOP	189 [63]	$1.35; 2.21$	$190; 220$	$0.168; 0.205$	$0.5; 0.53$	$\diamond$ this work
dipropylene-dimethyl-glycol-dimethylether	DPGDME	137 [64]	$3.52; 3.52$	$139; 151$	$0.327; 0.373$	$0.45; 0.48$	$\triangleright$ this work
ethylene glycol glycol	EG	152	$2.64; 2.64$	$158; 165$	$1.354; 1.364$	$0.63; 0.67$	$+$ [65]
glycerol	Gly	193 [74]	$1.29; 1.77$	$192; 236$	$1.317; 1.401$	$0.57; 0.62$	$\star$ [13]
isoeugenol		220	$2.85; 2.99$	$225; 248$	$0.085; 0.104$	$0.46; 0.49$	$\times$ this work
isopropyl-benzene (cumene)	Cumene	126	$3.01; 3.05$	$135; 139$	$-0.951; -0.948$	$0.49; 0.51$	$\triangle$ this work
methyl-m-toluate	MMT	165	$2.42; 2.6$	$173; 189$	$0.371; 0.397$	$0.49; 0.55$	$\diamond$ this work
n-ε-methyl-caprolactam	nMC	172 [51]	$1.45; 1.45$	$186; 196$	$0.778; 0.816$	$0.59; 0.62$	$\triangle$ this work
n-propyl-benzene	nPB	122 [22]	$2.05; 2.7$	$127; 137$	$-0.902; -0.878$	$0.54; 0.63$	$\star$ this work
phenol-phthalein-dimethylether	PDE	295 [66]	$3.61; 4.04$	$301; 325$	$0.808; 0.833$	$0.6; 0.68$	$\triangleleft$ [67]
phenylsalicate (salol)	Salol	215 [68]	$3.2; 4.53$	$177; 187$	$0.793; 0.834$	$0.46; 0.48$	$\times$ [78]
polypropylene-glycol 400	PPG	73	$1.9; 3.19$	$200; 226$	$0.436; 0.556$	$0.4; 0.48$	$+$ [13]
propylene carbonate	PC	160	$3.4; 4.22$	$162; 170$	$1.699; 1.703$	$0.63; 0.65$	$\times$ [69]
salicyl-salicylic acid	SSA	279 [81]	$3.1; 3.1$	$305; 308$	$-0.243; -0.238$	$0.23; 0.23$	$\times$ this work
sorbitol	Sor	268 [22]	$6.12; 6.12$	$268; 273$	$0.895; 0.959$	$0.26; 0.3$	$\square$ this work
sucrose-benzoate	SB	337	$2.47; 3.96$	$343; 373$	$-0.461; -0.373$	$0.35; 0.41$	$\circ$ [70]
tetraphenyl-tetramethyl-trisiloxane	DC704	211	$3.93; 3.93$	$211; 219$	$-1.148; -1.109$	$0.48; 0.48$	$\triangleleft$ [35]
tricresyl-phosphate	TCP	211	$2.5; 3.29$	$214; 236$	$0.33; 0.356$	$0.56; 0.58$	$\square$ [57]
trimethyl-pentaphenyl trisiloxane	DC705	230	$3.81; 3.81$	$233; 235$	$-1.203; -1.191$	$0.49; 0.5$	$\circ$ this work
trimethyl	3MPh	136	$2.7; 3.51$	$141; 150$	$1.104; 1.214$	$0.55; 0.56$	$\triangleleft$

TABLE I – continued from previous page

Liquid	Abbreviation	T_g (K)	Intervals				Symbol and ref.
			$I_{\Delta E}$	T (K)	$log\epsilon''_{max}$	$|\alpha_{min}|$	
phosphate							[86]
triphenyl phosphite	TPP	204	5.08; 5.08	204; 208	$-0.493; -0.479$	0.48; 0.49	$\times$ [13]
triphenyl-ethylene	TPE	249 [71]	3.72; 3.72	256; 258	$-1.866; -1.856$	0.46; 0.49	$\circ$ [35]
toluene-pyridine mixture	TolPyr	123 [72]	5.16; 6.1	126; 131	0.597; 0.698	0.28; 0.44	$\triangle$ [19]
xylitol	Xylitol	248 [22]	3.29; 3.98	254; 266	1.019; 1.065	0.28; 0.34	$\bullet$ this work

[1] I. Gutzow and J. Schmelzer, *The Vitreous State: Thermodynamics, Structure, Rheology, and Crystallization* (Springer, Berlin, 1995).
[2] M. D. Ediger, C. A. Angell, and S. R. Nagel, J. Phys. Chem. **100**, 13200 (1996).
[3] R. V. Chamberlin, Phase Transitions **65**, 169 (1999).
[4] C. A. Angell, K. L. Ngai, G. B. McKenna, P. F. McMillan, and S. W. Martin, J. Appl. Phys. **88**, 3113 (2000).
[5] E. Donth, *The Glass Transition* (Springer, Berlin, 2001).
[6] J. C. Dyre, Rev. Mod. Phys. **78**, 953 (2006).
[7] M. Doi and S. F. Edwards, *The Theory of Polymer Dynamics* (Oxford University Press, Oxford, 1986).
[8] L.-M. Wang, R. P. Liu, and W. H. Wang, J. Chem. Phys. **128**, 164503 (2008).
[9] W. Wernsdorfer and R. Sessoli, Science **284**, 133 (1999).
[10] W. Wernsdorfer, in *Advanced Magnetic Nanostructures*, edited by Sellmyer D. J. and Skomski R. (Springer, Berlin, 2006), p. 147.
[11] O. G. Bakunin, Chaos, Solitons & Fractals **23**, 1703 (2005).
[12] K. K. Mon and J. K. Percus, J. Chem. Phys. **117**, 2289 (2002).
[13] N. B. Olsen, T. Christensen, and J. C. Dyre, Phys. Rev. Lett. **86**, 1271 (2001).
[14] There may be several secondary β processes at various frequencies in the experimental frequency window.
[15] The boson peak is a faster process than the β process i.e. at higher frequencies, but they are not temperature dependend and they do not contain a significant information for the state.
[16] G. P. Johari and M. Goldstein, J. Phys. Chem. **74**, 2034 (1970).
[17] G. P. Johari and M. Goldstein, J. Chem. Phys. **55**, 4245 (1971).
[18] J. Jäckle, Rep. Prog. Phys. **49**, 171 (1986).
[19] N. B. Olsen, J. Non-Cryst. Solids **235**, 399 (1998).
[20] P. Lunkenheimer, R. Wehn, T. Riegger, and A. Loidl, J. Non-Cryst. Solids **307**, 336 (2002).
[21] T. Blochowicz, C. Gainaru, P. Medick, C. Tschirwitz, and E. A. Rössler, J. Chem. Phys. 124, 134503 (2006).
[22] L.-M. Wang and R. Richert, J. Phys. Chem. B **111**, 3201 (2007).
[23] J. C. Dyre and N. B. Olsen, Phys. Rev. Lett. **91**, 155703 (2003).
[24] S. Pawlus, M. Paluch, M. Sekula, K. L. Ngai, S. J. Rzoska, and J. Zioło, Phys. Rev. E **68**, 021503 (2003).
[25] S. Capaccioli, D. Prevosto, and K. Kessari, Philos. Mag. **87**, 681 (2007).
[26] S. Hensen-Bielówka, M. Paluch, and K. L. Ngai, J. Chem. Phys. **123**, 014502 (2005).
[27] R. Kohlrausch, Pogg. Ann. Phys. **91**, 179 (1854).
[28] G. Williams and D. C. Watts, Trans. Faraday Soc. **66**, 80 (1970).
[29] G. Williams, in *Dielectric and Related Molecular Processes*, edited by M. Davies (The Chemical Society, London, 1975), Vol. 2, p. 151.
[30] M. Cardona, R. V. Chamberlin, and W. Marx, Ann. der Physik **16**, 842 (2007).
[31] D. W. Davidson and R. H. Cole, J. Chem. Phys. **18**, 1417 (1950).
[32] D. W. Davidson and R. H. Cole, J. Chem. Phys. **19**, 1464 (1951).
[33] The two functions are not equivalent thus $\beta_{KWW} \neq \beta_{CD}$ for fit of the same data set [20].
[34] R. Böhmer, K. L. Ngai, C. A. Angell, D. J. Plazek, J. Chem. Phys. **99**, 4201 (1993).
[35] B. Jakobsen, K. Niss, and N. B. Olsen, J. Chem. Phys. **123**, 234511 (2005).
[36] J. C. Dyre, Phys. Rev. E **72**, 011501 (2005); J. C. Dyre, Phys. Rev. E **74**, 021502 (2006); J. C. Dyre, Phys. Rev. E **76**, 041508 (2007).
[37] J. C. Dyre, Europhys. Lett. **71**, 646 (2005).
[38] S. H. Glarum, J. Chem. Phys. **33**, 639 (1960).
[39] R. H. Doremus, J. Appl. Phys. **41**, 3366 (1970).
[40] P. Bordewijk, Chem. Phys. Lett. **32**, 592 (1975).
[41] M. A. Isakovich and I. A. Chaban, Zh. Eksp. Teor. Fiz. **50**, 1343 (1966) [Sov. Phys. JETP, **23**, 893 (1966)].
[42] A. J. Barlow, A. Erginsav, and J. Lamb, Proc. R. Soc. London, Ser. A **298**, 461 (1967).
[43] C. J. Montrose, and T. A. Litovitz, J. Acoust. Soc. Am. **47**, 1250 (1970).

[44] F. Kremer and A. Schönhals (Eds.), *Broadband Dielectric Spectroscopy* (Springer, Berlin, 2002).

[45] A. Kudlik, S. Benkhof, T. Blochowicz, T. Tschirwitz, and E. Rössler, J. Mol. Structure **479**, 201 (1999).

[46] C. M. Roland, S. Hensel-Bielowka, M. Paluch, and R. Casalini, Rep. Prog. Phys. **68**, 1405 (2005).

[47] H. Huth, L.-M. Wang, C. Schick, and R. Richert, J. Chem. Phys. **126**, 104503 (2007).

[48] B. Jakobsen, C. Maggi, T. Christensen, and J. C. Dyre, J. Chem. Phys. **129**, 184502 (2008).

[49] B. Igarashi, T. Christensen, E. H. Larsen, N. B. Olsen, I. H. Pedersen, T. Rasmussen, and J. C. Dyre, Rev. Sci. Instrum. **79**, 045106 (2008).

[50] R. Richert, Rev. Sci. Instrum. **67**, 3217 (1996).

[51] C. Hansen and R. Richert, J. Phys.: Condens. Matter **9**, 9661 (1997).

[52] W. Huang, S. Shahriari, and R. Richert, J. Chem. Phys. **123**, 164504 (2005).

[53] R. Richert, K. Duvvuri, and L.-T. Duong, J. Chem. Phys. **118**, 1828 (2003).

[54] R. Hilfer, Phys. Rev. E **65**, 061510 (2002).

[55] R. Böhmer and C. A. Angell in *Disorder Effects on Relaxational Processes*, edited by R. Richert and A. Blumen (Springer-Verlag, Berlin, 1994), p. 11.

[56] K. U. Schug, H. E. King, and R. Böhmer, J. Chem. Phys. **109**, 1472 (1998).

[57] T. Hecksher, A. I. Nielsen, N. B. Olsen, and J. C. Dyre, Nature Physics **4**, 737 (2008).

[58] J. C. Dyre and N. B. Olsen, Phys. Rev. E **69**, 042501 (2004).

[59] P. Lunkenheimer, L. C. Pardo, M. Koehler, and A. Loidl, Phys. Rev. E **77**, 031506 (2008).

[60] Moura Ramos et al.[80] determined the fragility by $m = \left| \frac{d \log(\tau(T))}{d \log(T)} \right|_{T=T_g} = \frac{E_a(T_g)}{2.303 R T_g} = 31$, obtained by the dielectric techniques of Thermally Stimulated Depolarization Currents (TSDC) but not from "standard" dielectric spectroscopy. From TSDC and calorimetric measurements should be expected a β-process but it is not to be seen neither in the dielectric frequency scans. In this work was not possible to estimate the fragility from the dielectric measurements because of the very high DC conductivity, that overrules the primary relaxation maximum at frequencies below 1 Hz. Thus in one series were not many relaxation times to provide a convincing estimate of fragility.

[61] L. De Francesco, M. Cutroni, and A. Mandanici, Philos. Mag. B **82**, 625 (2002).

[62] J. G. Kirkwood, J. Chem. Phys. **4**, 592 (1936); J. Chem. Phys. **7**, 911 (1939).

[63] E. Kaminska, K. Kaminski, M. Paluch, J. Ziolo, and K. L. Ngai, J. Chem. Phys. **126**, 174501 (2007).

[64] K. Grzybowska, S. Pawlus, M. Mierzwa, M. Paluch, and K. L. Ngai, J. Chem. Phys. **125**, 144507 (2006).

[65] T. Blochowicz, C. Tschirwitz, S. Benkhof, and E. A. Rössler, J. Chem. Phys. **118**, 7544 (2003).

[66] S. Sharifi, D. Prevosto, S. Capaccioli, M. Lucchesi, and M. Paluch, J. of Non-Crys. Sol. **353** 4313 (2007).

[67] S. Hensel-Bielowka and M. Paluch, Phys. Rev. Lett. **89**, 025704 (2002).

[68] M. Hatasea, M. Hanayab, and M. Oguni, J. Non-Cryst. Solids **333**, 129 (2004).

[69] L.-M. Wang, V. Velikov, and C. A. Angell, J. Chem. Phys. **117**, 10184 (2002).

[70] J. R. Rajesh, W. Huang, R. Richert, E. L. Quitevisa, J. Chem. Phys. **124**, 014510 (2006).

[71] K. Niss and B. Jakobsen, *Dielectric and Shear Mechanical Relaxation in Glass Forming Liquids – A thorough analysis and experimental test of the DiMarzio-Bishop model*, Master's thesis in physics (IMFUFA Tekst 424, Roskilde University) [http://milne.ruc.dk/imfufatekster/] (2003).

[72] N. B. Olsen, T. Christensen, and J. C. Dyre, Phys. Rev. E **62**, 4435 (2000).

[73] C. Leon, K. L. Ngai, and M. Roland, J. Chem. Phys. **110**, 11585 (1999).

[74] R. Richert and C. A. Angell, J. Chem. Phys. **108**, 9016 (1998).

[75] S. Shahriari, A. Mandanici, L.-M. Wang, and R. Richert, J. Chem. Phys. **121**, 8960 (2004).

[76] A. Garcia-Bernabé, private communication.

[77] R. Diaz-Calleja, A. Garcia-Bernabe, M. J. Sanchis, and L. F. del Castillo, Phys. Rev. E **72**, 051505 (2005).

[78] C. Gainaru, A. Rivera, S. Putselyk, G. Eska, and E. A. Rössler, Phys. Rev. B **72**, 174203 (2005).

[79] M. Mierzwa, S. Pawlus, M. Paluch, E. Kaminska, and K. L.Ngai, J. Chem. Phys. **128**, 044512 (2008).

[80] J. J. Moura Ramos, N. T. Correia, H. P. Diogo, C. Alvarez, and T. A. Ezquerra, J. Non-Cryst. Solids **351**, 3600 (2005).

[81] H. P. Diogo, S. S. Pinto, and J. J. Moura Ramos, J. Therm. Anal. Cal. **77**, 893 (2004).

[82] N. Ito, W. Huang, and R. Richert, J. Phys. Chem. B **110**, 4371 (2006).

[83] N. Ito, K. Duvvuri, D. V. Matyushov, and R. Richert, J. Chem. Phys. **125**, 024504 (2006).

[84] K. L. Ngai, and M. Paluch, J. Chem. Phys. **120**, 857 (2004).

[85] J. Wiedersich, T. Blochowicz, S. Benkhof, A. Kudlik, N. V. Surovtsev, C. Tschirwitz, V. N. Novikov, and E. A. Rössler, J. Phys.: Condens. Matter **11**, A147 (1999).

[86] T. Blochowicz, C. Gainaru, P. Medick, C. Tschirwitz, and E. A. Rössler, J. Chem. Phys. **124**, 134503 (2006).

Little evidence for dynamic divergences in ultraviscous molecular liquids

TINA HECKSHER, ALBENA I. NIELSEN, NIELS BOYE OLSEN AND JEPPE C. DYRE*

DNRF Centre 'Glass and Time', IMFUFA, Department of Sciences, Roskilde University, Postbox 260, DK-4000 Roskilde, Denmark
*e-mail: dyre@ruc.dk

The physics of the ultraviscous liquid phase preceding glass formation continues to pose major problems that remain unsolved. It is actively debated, for instance, whether the marked increase of the relaxation time reflects an underlying phase transition to a state of infinite relaxation time. To elucidate the empirical evidence for this intriguing scenario, some of the most accurate relaxation-time data available for any class of ultraviscous liquids—those obtained by dielectric relaxation experiments on organic liquids just above the glass transition—were compiled. Analysis of data for 42 liquids shows that there is no compelling evidence for the Vogel–Fulcher–Tammann (VFT) prediction that the relaxation time diverges at a finite temperature. We conclude that theories with a dynamic divergence of the VFT form lack a direct experimental basis.

All liquids may be supercooled. In some cases, the liquid crystallizes spontaneously. In other cases, a marked increase in viscosity and relaxation time is observed on continued cooling, and the liquid eventually solidifies into a glass—a frozen liquid. Which of the two scenarios that prevails depends on the cooling rate. The ultraviscous liquid phase preceding glass formation has universal physical properties, independent of the nature of the chemical bonds involved: metal bonds, ionic bonds, covalent bonds, van der Waals bonds or hydrogen bonds. The universalities and the lack of understanding of the basic phenomenology continue to make this research field attractive to physicists, chemists and materials scientists alike.

The universal features[1–7] that characterize ultraviscous supercooled liquids relate, in particular, to the time dependence of relaxation functions and to the temperature dependence of the relaxation time. The former is not our focus here; it is reflected in the fact that relaxation functions are generally well fitted by the so-called stretched exponential function. The focus below is on the relaxation time, which increases markedly on cooling into the ultraviscous phase, sometimes by more than a factor of ten when temperature is lowered by just 1%. Figure 1 shows the relaxation time as a function of temperature for some typical molecular liquids. This figure raises the question: Does the relaxation time diverge at finite temperatures or only as $T \to 0$?

The average relaxation time τ is generally non-Arrhenius. That is, on cooling, τ almost always increases faster than predicted by the well-known Arrhenius equation. This is the mathematical expression that characterizes, for example, the temperature dependence of a chemical reaction time in terms of an activation energy. For ultraviscous liquids, if the temperature-dependent activation energy $\Delta E(T)$ is defined by the Arrhenius expression

$$\tau(T) = \tau_0 \exp\left(\frac{\Delta E(T)}{k_B T}\right), \qquad (1)$$

it is generally found that $\Delta E(T)$ increases significantly on cooling. To the best of our knowledge, there are no liquids where ΔE decreases, which is in itself a striking fact.
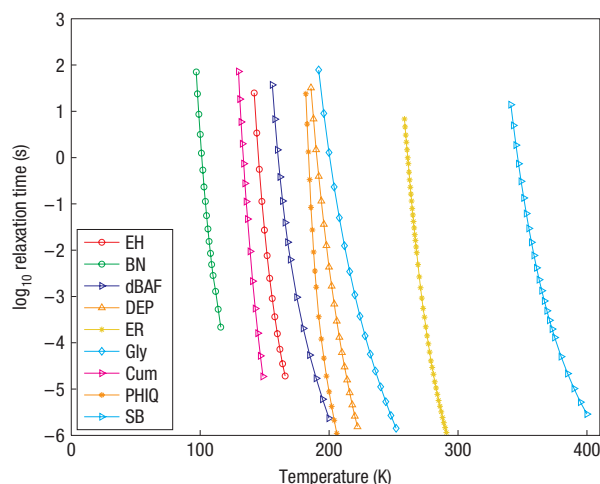
Figure 1 Relaxation time as a function of temperature for typical organic liquids supercooled into the ultraviscous phase. The relaxation time was determined as the inverse dielectric loss-peak frequency, identified by fitting data in a log–log plot around the maximum with a parabola. If a linear scale were used, the relaxation time would increase almost vertically on cooling; even on a log scale, the increase is marked. The question investigated in this article is whether or not there is reason to believe that the relaxation time diverges at some finite temperature. The full lines are drawn as guides to the eye. Table 1 explains the liquid abbreviations.

THE VFT EQUATION

The function most widely used to fit relaxation-time data is the Vogel–Fulcher–Tammann (VFT) equation dating back to the 1920s (refs 8–10):

$$\tau = \tau_0 \exp\left(\frac{A}{T - T_0}\right) \qquad (T_0 < T). \qquad (2)$$

1
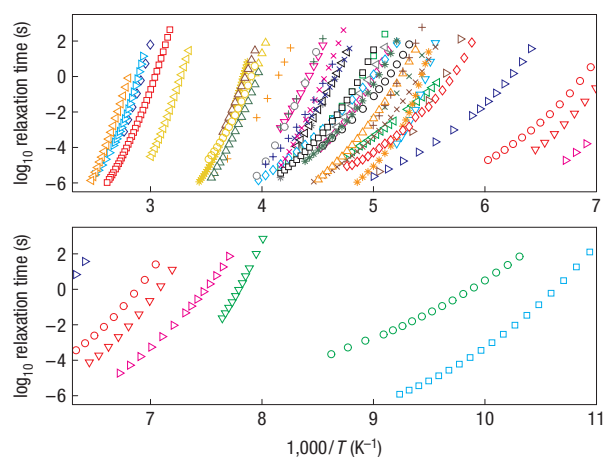
Figure 2 Relaxation time data identified from dielectric loss peaks for all of the 42 organic ultraviscous liquids used in the analysis. Both panels show the logarithm of the dielectric relaxation time as a function of inverse temperature. A straight line in this plot signals an Arrhenius temperature dependence. The liquids all exhibit the non-Arrhenius temperature dependence of the relaxation time that characterizes ultraviscous liquids. The symbols are explained in Table 1.

Table 1 Liquids included in the analysis. The name of each liquid, its abbreviation and the symbol used in the figures are listed. More details (including references, temperature, frequency intervals and some further information) are provided in the Supplementary Information.

Liquid	Abbreviation	Symbol
1,2-propandiol (propylene-glycol)	PG	◁
2-ethyl-hexylamine	EH	○
2-methyl-tetrahydrofurane	MTHF	□
2-phenyl-5-acetomethyl-5-ethyl-1,3-dioxocyclohexane	AFEH	▽
3,3,4,4-benzophenonetetracarboxylic dianhydride	BPC	◇
3-fluoro-aniline	FAN	▷
3-phenyl-1-propanol	3Ph1P	×
3-styrene	3Sty	+
5-polyphenyl-ether	5-PPE	△
benzophenone	BePh	✳
biphenyl-2yl-isobutylate	BP2lB	◁
butyronitrile	BN	○
cresolphthalein-dimethylether	KDE	□
decahydroisoquinoline	DHIQ	▽
di-iso-butyl-phtalate	dIBP	◇
dibutyl-ammonium-formide	dBAF	▷
dibutyl-phtalate	DBP	×
dicyclohexyl-methyl-2-methylsuccinate	DCHMMS	+
diethyl-phtalate	DEP	△
diglycidyl-ether-of-bisphenol A (epoxy-resin)	ER	✳
dimethyl-phtalate	DMP	◁
dioctyl-phtalate	DOP	○
dipropylene-glycol	DPG	□
dipropylene-glycol-dimethyl-ether	DPGDME	▽
glycerol	Gly	◇
isopropyl-benzene	Cum	▷
m-tricresyl-phosphate	mTCP	×
m-toluene	mTol	+
o-terphenyl	OTP	△
perhydroisoquinoline	PHIQ	✳
phenolphthalein-dimethylether	PDE	◁
phenyl-salicylate (salol)	Sal	○
polypropylene-glycol	PPG	□
pyridine–toluene mixture	PT	▽
squalane	Sqa	◇
sucrose-benzonate	SB	▷
tetraphenyl-tetramethyl-trisiloxane	DC704	×
tricresyl-phosphate	TCP	+
triphenyl-ethylene	TPE	△
tripropylene-glycol	TPG	✳
trisnaphthylbenzene	tNB	◁
xylitol	Xyl	○

This corresponds to an activation energy that increases on cooling as $\Delta E \propto T/(T - T_0)$. Although the VFT equation has few adjustable parameters, it generally gives quite good fits to data. The coefficients of the VFT equation were considered in the landmark paper published in 1955 by Williams, Landel and Ferry[11] that discussed the non-Arrhenius problem in terms of the free-volume model. In the 1970s, there were reports that the VFT equation breaks down at temperatures with long relaxation times (large viscosities)[12,13]. These 'early warnings' were to some extent forgotten or repressed, perhaps because probing the relaxation time accurately through viscosity measurements is difficult at high viscosities.

Experimentalists often regard the VFT equation as just a convenient fit to data[12]. Many theorists, on the other hand, were inspired by the VFT equation to develop theories predicting a phase transition at T_0 to a state with infinite relaxation time[14]. The first such approach was the famous Adam–Gibbs entropy model from 1965 predicting a second-order phase transition at $T = T_0$ to a state of zero configurational entropy and infinite relaxation time[15,16], a unique 'ideal glass'. A number of simplifying assumptions go into the Adam–Gibbs formalism, and in 1997 it was argued by DiMarzio and Yang[17] that even if the Adam–Gibbs idea of an underlying phase transition is accepted, the relaxation time remains finite at the transition temperature. Very recently, mathematically rigorous theorems derived by Eckmann and Procaccia[18] show that for two-dimensional soft-sphere mixtures, at least, the configurational entropy stays positive for $T > 0$.

Leading theorists such as Edwards[19,20], Anderson[21] and, more recently, Bouchaud and Biroli in 2004 (ref. 22) and Lubchenko and Wolynes in 2007 (ref. 23) have developed dynamic divergence scenarios far beyond Adam and Gibbs'. Although there are differing opinions from other famous theorists[24–27], it remains a popular idea that the marked slowing down on cooling reflects an underlying phase transition to a state of infinite relaxation time. The fact that data are usually well fitted by the VFT equation has reinforced this idea over many years[28]. Our aim is to provide an in-depth investigation of the evidence for dynamic divergences of the VFT form. Before detailing the data analysis, it should be noted that

support for the idea of a dynamic divergence traditionally came from several papers reporting near equality of the VFT fitting parameter T_0 and the Kauzmann temperature T_K, the temperature where the liquid phase entropy by extrapolation below the glass transition becomes identical to the crystal phase entropy[29–31]. In 2003, however, Tanaka presented a compilation of data showing that $T_0 = T_K$ is not confirmed by experiment[32].

As is evident from the above, an important question of contemporary glass science is the following: Is there experimental evidence for the dynamic divergence predicted by the VFT equation? Answering this is important, because if there is an underlying dynamic divergence, this obviously explains the marked relaxation-time increase on cooling. By its very nature the question is subtle, however, because if the equilibrium liquid relaxation time diverges at some finite temperature, it is impossible to equilibrate the liquid at or close to that temperature. This means that no experiment can conclusively prove the existence of a dynamic divergence. To cut this science–philosophical Gordian knot, we take the following pragmatic viewpoint: the conjecture of a diverging
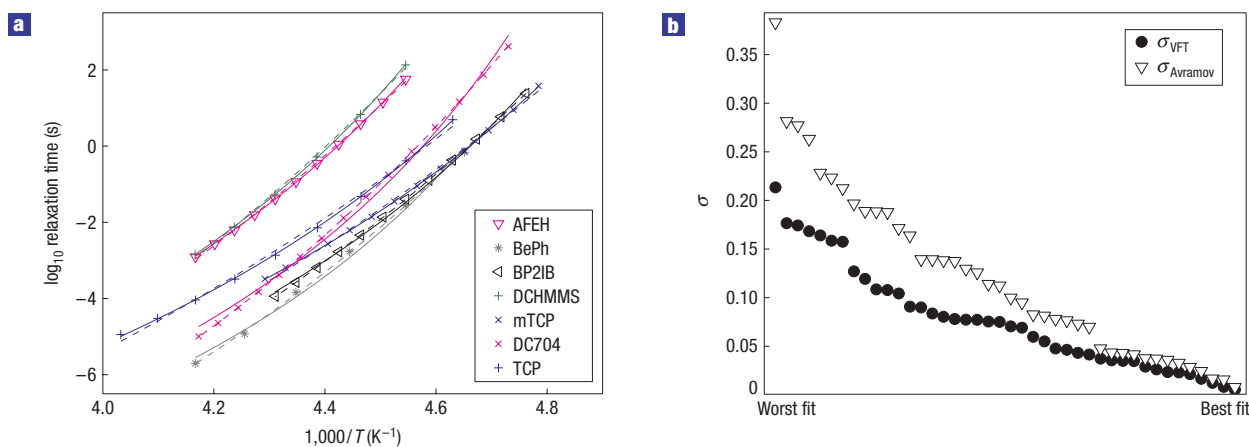
Figure 3 **The VFT and Avramov equations compared with data. a,** Examples of fits with the VFT equation (solid lines) and the Avramov equation (dashed lines). **b,** Standard deviation from fits to data of the two equations. The x axis represents the 42 liquids sorted in descending order of standard deviation for each of the two fitting functions; thus, a given position on the x axis generally corresponds to two different liquids. On average, the VFT equation fits data better than does the Avramov equation.

relaxation time of VFT form will be regarded as probably correct if—and only if—the VFT equation fits data considerably better than do other mathematically simple functions with the same number of fitting parameters and no dynamic divergence. To investigate this, data for a large number of liquids are needed.

DATA ANALYSIS

Accurate data are required to assess whether or not the VFT prediction of a diverging relaxation time is confirmed by experiment. Dielectric relaxation measurements give the most precise relaxation-time data, far more accurate than data from other relaxation processes or from viscosity measurements. For practical reasons, the best dielectric data for ultraviscous liquids are for organic liquids; such liquids are often easily supercooled and quite convenient to work with. Monoalcohols were omitted from the analysis because their dominant dielectric relaxation process does not relate to the calorimetric glass transition[33].

To quantify how well the VFT equation fits data, we compared the VFT equation with another popular fitting function[34–39] that is now known as the Avramov equation:

$$\tau(T) = \tau_0 \exp\left(\frac{B}{T^n}\right). \qquad (3)$$

Like the VFT equation, the Avramov equation has two parameters in addition to the prefactor τ_0, but it has no dynamic divergence. The prefactor is usually regarded as a free parameter, but we chose to fix it to $\tau_0 = 10^{-14}$ s (ref. 40). The below conclusions are not sensitive to the exact value of τ_0 if it is insisted that it should have a physically reasonable value, that is, be in (or just slightly outside) the range 10^{-14}–10^{-13} s.

At any given temperature, from the dielectric loss as a function of frequency, we define the liquid relaxation time τ as the inverse loss-peak frequency. The last of these is identified by fitting loss data as a function of log frequency close to the maximum loss with a parabola. Figure 2 shows all data analysed. All liquids exhibit the characteristic non-Arrhenius behaviour with a relaxation time that increases stronger on cooling than predicted by the Arrhenius equation (that is, equation (1) with temperature-independent activation energy). A list of all liquids included in the analysis and their corresponding symbols is given in Table 1; more details are provided in the Supplementary Information.

The fitting region was restricted to relaxation times between 1 µs and 1,000 s. This was done to avoid comparing different types of dynamic behaviour—otherwise there is the risk that we ultimately test the two equations' ability to interpolate between two different dynamics. The lower limit (1 µs) was chosen to ensure that the dynamics are well within the 'landscape dominated' domain[41,42]. The upper limit (1,000 s) was chosen to ensure that all data are true equilibrium data. A further requirement was that only data sets covering at least four decades in time measured at five or more temperatures were included in the analysis. Out of an initial collection of data for 62 liquids, 42 met these demands. The liquids represent some of the most commonly studied organic glass formers; their dielectric properties were measured by leading groups in the field. These data were supplemented by some new measurements of ours.

Equations (2) and (3) were fitted to data using the least-squares method. The procedures for selecting data and the subsequent fitting procedures were automated through MatLab routines. Examples of fits are shown in Fig. 3a with VFT fits as solid lines and Avramov fits as dashed lines. Both equations fit well with little visible difference. For a quantitative comparison of the two fitting functions, we used the standard deviation formula, $\sigma^2 = 1/(N - n) \sum_i (\log_{10}(\tau_{\text{fit,i}}) - \log_{10}(\tau_{\text{data,i}}))^2$, where N is the number of data points and $n = 2$ is the number of degrees of freedom. Figure 3b shows σ_{VFT} and σ_{Avramov} for all liquids, where the σ values for clarity are sorted in descending order for both fits. The VFT equation generally fits data better than does the Avramov equation.

Inspecting the fits closely—in Fig. 3a as well as those not shown—reveals that deviations are systematic. Thus, highly non-Arrhenius liquids, that is, data sets with large curvature, are generally poorly fitted by the Avramov equation. Apparently, the Avramov equation is not able to 'bend' enough to capture the curvature of these data sets. Is that a signal of the dynamic divergence predicted by the VFT equation? To investigate this possibility, we calculated how the activation energy changes with temperature using the temperature index defined[43] by

$$I = -\frac{\mathrm{d}\ln \Delta E}{\mathrm{d}\ln T}. \qquad (4)$$

The temperature index quantifies the activation-energy temperature dependence in a way that is independent of the
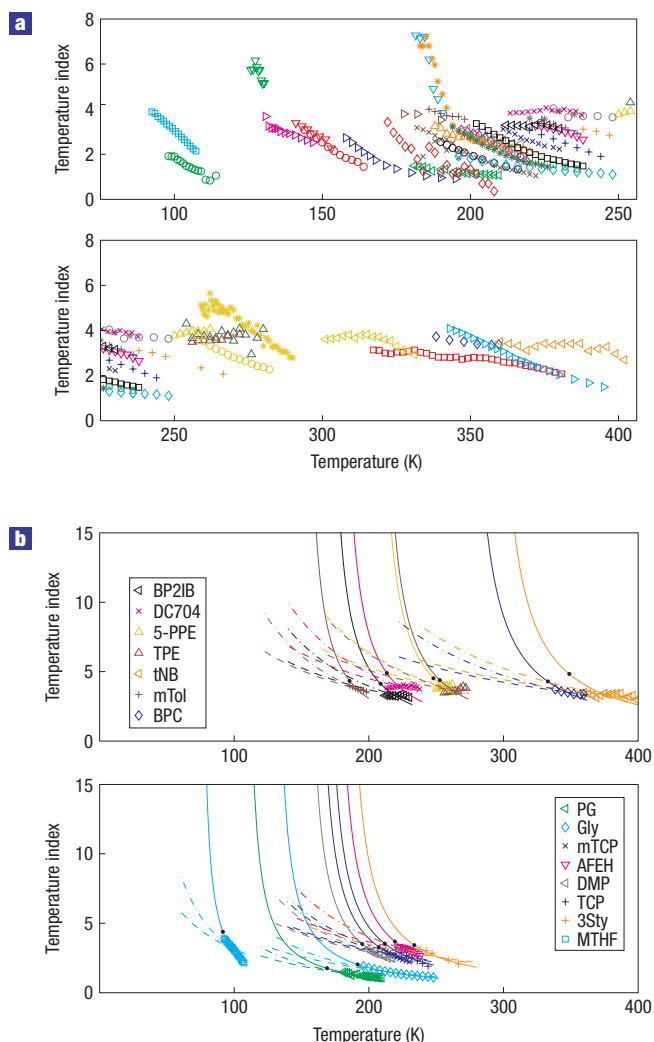
Figure 4 Temperature indices. This quantity (equation (4)) measures how fast the activation energy increases on cooling; it is plotted as a function of temperature. **a**, Temperature indices for all liquids. With few exceptions, the temperature index increases with decreasing temperature. This explains why the VFT equation fits data better than does the Avramov equation, which predicts a temperature-independent index. **b**, Temperature indices for the eight liquids where the Avramov equation (upper panel), respectively the VFT equation (lower panel), fits best. The full lines give the VFT-predicted temperature indices (equation (5)), the dashed–dotted and dashed lines, respectively, give the predictions of the two fitting functions FF1 and FF2 that do not have dynamic divergences (equations (6) and (7)). In both subfigures, the black circles mark the glass-transition temperature for each liquid.

unit system, like the Grüneisen parameter of solid-state physics quantifies the effects of thermal expansion. If for instance the temperature index is four, lowering the temperature by 1% leads to a 4% increase of the activation energy. If the glass transition temperature is defined by $\tau(T_g) = 100\,\mathrm{s}$, the temperature index is related to Angell's fragility $m \equiv \mathrm{d}\log_{10}(\tau)/\mathrm{d}(T_g/T)|_{T_g}$ by $m = c(1 + I(T_g))$, where $c = \log_{10}(\tau(T_g)/\tau_0) = 16$ (ref. 43).

For the Avramov equation, the temperature index is constant, $I_{\mathrm{Avramov}} = n - 1$. For the VFT equation, we find

$$I_{\mathrm{VFT}} = \frac{T_0}{T - T_0}. \qquad (5)$$
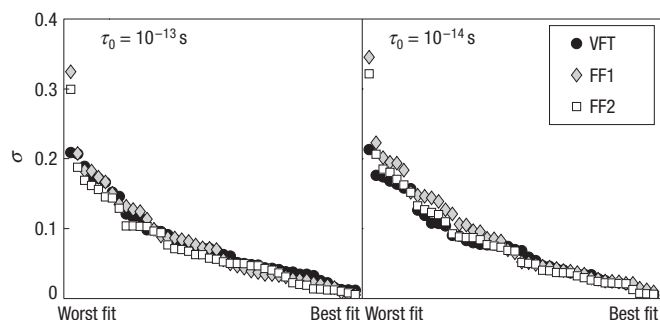
Figure 5 Standard deviation from fits to data of the VFT equation and two alternative fitting functions with the same number of parameters but no dynamic divergence, FF1 and FF2 of equations (6) and (7). The x axis represents the liquids sorted in descending order of standard deviation for each fitting function. For both choices of physically reasonable prefactors, the three functions fit equally well. The worst-fit outlier is perhydroisoquinoline, one of the most fragile (non-Arrhenius) liquids in the collection (compare Fig. 1).

Thus, the VFT temperature index increases on cooling and diverges at $T = T_0$. Figure 4a shows temperature indices for all 42 liquids as functions of temperature. For the vast majority of liquids, the temperature index increases with decreasing temperature. This explains why the VFT equation fits data better than the Avramov equation.

The temperature index is also useful for shedding light on how strong the evidence for a dynamic divergence is. Figure 4b (upper panel) shows the actual and the VFT-predicted temperature indices for the eight liquids that are best fitted by the Avramov equation; the lower panel shows those liquids that are best fitted by the VFT equation. The data are not inconsistent with the dynamic divergence predicted by the VFT equation, but we cannot reasonably say that there is compelling evidence for a divergent temperature index as predicted by the VFT equation. The dashed–dotted and dashed lines are the temperature indices of the two below fitting functions.

We proceed to compare the VFT function to two alternative fitting functions with temperature indices that increase on cooling, but without divergence at a non-zero temperature. Fitting functions one and two (FF1 and FF2) reflect the following temperature indices: $I = (T_1/T)^2$ and $I = (T_2 - T)/T$ $(T < T_2)$, respectively. Integrating these expressions via equation (4) leads to

$$\Delta E(T) \propto \exp\left[\frac{T_1^2}{2T^2}\right] \qquad (\mathrm{FF1}), \qquad (6)$$

$$\Delta E(T) \propto T \exp\left[\frac{T_2}{T}\right] \qquad (\mathrm{FF2}). \qquad (7)$$

Figure 5 shows the standard deviations from fitting these two functions to data compared with the VFT equation. The panels show results from two different prefactors, $\tau_0 = 10^{-13}\,\mathrm{s}$ and $\tau_0 = 10^{-14}\,\mathrm{s}$. In both cases the three functions fit equally well.

OUTLOOK

The analysis was limited to non-polymeric systems because the polymer glass transition may be fundamentally different from the liquid–glass transition. The VFT equation was often used also for the polymer glass transition, however, where it is generally

known as the Williams–Landel–Ferry equation[11]. A clever way to extend the range of relaxation times beyond those obtainable by linear relaxation experiments is to consider results from ageing experiments. Studies by McKenna, Simon, Plazek and co-workers mainly on polymeric systems show that the VFT prediction is not followed when systems are aged into equilibrium by annealing for sufficiently long time slightly below the glass-transition temperature[44–47]. Although the accuracy of these experiments is not comparable to that of dielectric relaxation experiments on the metastable equilibrium phase, it was nevertheless possible to conclude that the relaxation times deviate from the VFT equation by always increasing less markedly when lowering temperature than predicted by the VFT equation. These results are fully consistent with the above conclusion.

It is not possible to rule out that there is a dynamic divergence of the VFT form, but our findings give no indications of such a divergence. It is instructive to compare the situation to that of a second-order phase transition. This is associated with a dynamic divergence where the (maximum) relaxation time diverges as an inverse power law of the temperature distance to the transition temperature (critical slowing down). Thus, right at the phase transition, the relaxation time is infinite. Although it is not possible to experimentally definitively prove this dynamic divergence, nobody doubts it. This is because (1) the predicted mathematical form is supported by experiment, (2) the dynamic critical exponents fit theoretical predictions and (3) there is a fundamental understanding of what is going on and why relaxations slow down when the transition is approached. For ultraviscous liquids, there is no such generally agreed simple and universal model. Here, the logic was traditionally reversed. The observation that data are well fitted by the VFT equation was used to justify a search for models with a dynamic divergence. Our findings indicate that this is probably not a fruitful route. Thus, with Occam's razor in mind—'it is vain to do with more what can be done with fewer'—we suggest that in the search for the correct theory for ultraviscous liquid dynamics, theories not predicting a dynamic divergence of the VFT form should be focused on.

References

1. Brawer, S. *Relaxation in Viscous Liquids and Glasses* (American Ceramic Society, Columbus, 1985).
2. Debenedetti, P. G. *Metastable Liquids: Concepts and Principles* (Princeton Univ. Press, Princeton, 1996).
3. Ediger, M. D., Angell, C. A. & Nagel, S. R. Supercooled liquids and glasses. *J. Phys. Chem.* **100**, 13200–13212 (1996).
4. Angell, C. A., Ngai, K. L., McKenna, G. B., McMillan, P. F. & Martin, S. W. Relaxation in glassforming liquids and amorphous solids. *J. Appl. Phys.* **88**, 3113–3157 (2000).
5. Debenedetti, P. G. & Stillinger, F. H. Supercooled liquids and the glass transition. *Nature* **410**, 259–267 (2001).
6. Binder, K. & Kob, W. *Glassy Materials and Disordered Solids: An Introduction to their Statistical Mechanics* (World Scientific, Singapore, 2005).
7. Dyre, J. C. The glass transition and elastic models of glass-forming liquids. *Rev. Mod. Phys.* **78**, 953–972 (2006).
8. Vogel, H. Das Temperaturabhängigkeitsgesetz der Viskosität von Flüssigkeiten. *Phys. Zeit.* **22**, 645–646 (1921).
9. Fulcher, G. S. Analysis of recent measurements of the viscosity of glasses. *J. Am. Ceram. Soc.* **8**, 339–355 (1925).
10. Tammann, G. Glasses as supercooled liquids. *J. Soc. Glass Technol.* **9**, 166–185 (1925).
11. Williams, M. L., Landel, R. F. & Ferry, J. D. The temperature dependence of relaxation mechanisms in amorphous polymers and other glass-forming liquids. *J. Am. Chem. Soc.* **77**, 3701–3707 (1955).
12. Laughlin, W. T. & Uhlman, D. R. Viscous flow in simple organic liquids. *J. Phys. Chem.* **76**, 2317–2325 (1972).
13. Breitling, S. M. & Magill, J. H. A model for the Magill-Li viscosity-temperature relation. *J. Appl. Phys.* **45**, 4167–4171 (1974).
14. Angell, C. A. Oxide glasses in light of the ideal glass concept. I. Ideal and nonideal transitions and departures from ideality. *J. Am. Ceram. Soc.* **51**, 117–125 (1968).
15. Gibbs, J. H. & DiMarzio, E. A. Nature of the glass transition and the glassy state. *J. Chem. Phys.* **28**, 373–383 (1958).
16. Adams, G. & Gibbs, J. H. On the temperature dependence of cooperative relaxation properties in glass-forming liquids. *J. Chem. Phys.* **43**, 139–146 (1965).
17. DiMarzio, E. A. & Yang, A. J. M. Configurational entropy approach to the kinetics of glasses. *J. Res. Natl Inst. Stand. Technol.* **102**, 135–157 (1997).
18. Eckmann, J.-P. & Procaccia, I. Ergodicity and slowing down in glass-forming systems with soft potentials: No finite-temperature singularities. Preprint at <http://arxiv.org/abs/0802.4346> (2008).
19. Edwards, S. F. Theory of glasses. *Polymer* **17**, 933–937 (1976).
20. Edwards, S. F. The glass transition. *Int. J. Mod. Phys. B* **6**, 1587–1594 (1992).
21. Anderson, P. W. in *Ill-Condensed Matter* (eds Balian, R., Maynard, R. & Toulouse, G.) 159–261 (North-Holland, Amsterdam, 1979).
22. Bouchaud, J. P. & Biroli, G. On the Adam–Gibbs–Kirkpatrick–Thirumalai–Wolynes scenario for the viscosity increase in glasses. *J. Chem. Phys.* **121**, 7347–7354 (2004).
23. Lubchenko, V. & Wolynes, P. G. Theory of structural glasses and supercooled liquids. *Ann. Rev. Phys. Chem.* **58**, 235–266 (2007).
24. Götze, W. & Sjögren, L. Relaxation processes in supercooled liquids. *Rep. Prog. Phys.* **55**, 241–376 (1992).
25. Stillinger, F. H. Supercooled liquids, glass transition and the Kauzmann paradox. *J. Chem. Phys.* **88**, 7818–7825 (1988).
26. Kivelson, D., Tarjus, G., Zhao, X. & Kivelson, S. A. Fitting of viscosity: Distinguishing the temperature dependences predicted by various models of supercooled liquids. *Phys. Rev. E* **53**, 751–758 (1996).
27. Garrahan, J. P. & Chandler, D. Coarse-grained microscopic model of glass-formers. *Proc. Natl Acad. Sci.* **100**, 9710–9714 (2003).
28. Langer, J. S. The mysterious glass transition. *Phys. Today* 8–9 (February 2007).
29. Angell, C. A. & Smith, D. L. Test of the entropy basis of the Vogel–Tammann–Fulcher equation—dielectric relaxation of polyalcohols near T_G. *J. Phys. Chem.* **86**, 3845–3852 (1982).
30. Richert, R. & Angell, C. A. Dynamics of glass-forming liquids. V. On the link between molecular dynamics and configurational entropy. *J. Chem. Phys.* **108**, 9016–9026 (1998).
31. Angell, C. A. Entropy and fragility in supercooling liquids. *J. Res. Natl Inst. Stand. Technol.* **102**, 171–185 (1997).
32. Tanaka, H. Relation between thermodynamics and kinetics of glass-forming liquids. *Phys. Rev. Lett.* **90**, 055701 (2003).
33. Huth, H., Wang, L.-M., Schick, C. & Richert, R. Comparing calorimetric and dielectric polarization modes in viscous 2-ethyl-1-hexanol. *J. Chem. Phys.* **126**, 104503 (2007).
34. Harrison, G. *The Dynamic Properties of Supercooled Liquids* (Academic, New York, 1976).
35. Avramov, I. Viscosity in disordered media. *J. Non-Cryst. Solids* **351**, 3163–3173 (2005).
36. Bässler, H. Viscous flow in supercooled liquids analyzed in terms of transport theory for random media with energetic disorder. *Phys. Rev. Lett.* **58**, 767–770 (1987).
37. Litovitz, T. A. Temperature dependence of the viscosity of associated liquids. *J. Chem. Phys.* **7**, 1088–1089 (1952).
38. Barlow, A. J. & Lamb, J. The visco-elastic behaviour of lubricating oils under cyclic shearing stress. *Proc. R. Soc. A* **253**, 52–69 (1959).
39. Barlow, A. J., Lamb, J. & Matheson, A. J. Viscous behaviour of supercooled liquids. *Proc. R. Soc. A* **292**, 322–342 (1966).
40. Stickel, F., Fischer, E. W. & Richert, R. Dynamics of glass-forming liquids. I . Temperature-derivative analysis of dielectric data. *J. Chem. Phys.* **102**, 6251–6257 (1995).
41. Stillinger, F. H. A topographic view of supercooled liquid and glass formation. *Science* **267**, 1935–1939 (1995).
42. Schrøder, T. B., Sastry, S., Dyre, J. C. & Glotzer, S. C. Crossover to potential energy landscape dominated dynamics in a model glass-forming liquid. *J. Chem. Phys.* **22**, 9834–9840 (2000).
43. Dyre, J. C. & Olsen, N. B. Landscape equivalent of the shoving model. *Phys. Rev. B* **69**, 042501 (2004).
44. O'Connell, P. A. & McKenna, G. B. Arrhenius-like temperature dependence of the segmental relaxation below T_g. *J. Chem. Phys.* **110**, 11054–11060 (1999).
45. Shi, X. F., Mandanici, A. & McKenna, G. B. Shear stress relaxation and physical aging study on simple glass-forming materials. *J. Chem. Phys.* **125**, 174507 (2005).
46. Simon, S. L., Sobieski, J. W. & Plazek, D. J. Volume and enthalpy recovery of polystyrene. *Polymer* **42**, 2555–2567 (2001).
47. Echeverria, I., Kolek, P. L., Plazek, D. J. & Simon, S. L. Enthalpy recovery, creep and creep-recovery measurements during physical aging of amorphous selenium. *J. Non-Cryst. Solids* **324**, 242–255 (2003).

Author contributions

Project planning and data analysis were carried out by T.H. and J.C.D., experimental work by A.I.N. and N.B.O.

Little evidence for dynamic divergences in ultraviscous molecular liquids – Supplementary Information

By: Hecksher et al., [NPHYS-2008-02-00228]

A list of the liquids included in the analysis is given here. For each liquid is provided: Name, abbreviation, symbol used in the figures, temperature interval for which relaxation time data (i.e., dielectric loss peak data) are available, frequency interval for the dielectric loss measurements determining the relaxation times, temperature index interval, and reference. The term "this work" refers to new data obtained by the experimental set-up detailed in Refs. 21 and 22.

---

[1] Nielsen, A. I., Christensen, T., Jakobsen, B., Niss, K., Olsen, N. B., Richert, R. & Dyre, J. C. Approximate $\sqrt{t}$ relaxation in glass-forming liquids. *ArXiv* 0712.2827 (2008).

[2] Wang, L.-M. & Richert, R. Debye type relaxation and the glass transition of alcohols. *J. Phys. Chem. B* **109**, 11091-11094 (2005).

[3] Ngai, K. L. & Paluch, M. Classification of secondary relaxation in glass-formers based on dynamical properties. *J. Chem. Phys.* **120**, 857-873 (2004).

[4] Wiedersich, J., Blochowicz, T., Benkhof, S., Kudlik, A., Surovtsev, N. V., Tschirwitz, C., Novikov, V. N. & Rössler, E. A. Fast and slow relaxation processes in glasses. *J. Phys.: Condens. Matter* **11**, A147-A156 (1999).

[5] Blochowicz, T. *Broadband Dielectric Spectroscopy in Neat and Binary Molecular Glass Formers Frequency and Time Domain Spectroscopy, Non-Resonant Spectral Hole Burning*, Ph.D. thesis (Universität Bayreuth, 2003).

[6] Jakobsen, B., Niss, K. & Olsen, N. B. Dielectric and shear mechanical alpha and beta relaxations in seven glass-forming liquids. *J. Chem. Phys.* **123**, 234511 (2005).

[7] Lunkenheimer, P., Pardo, L. C., Koehler, M. & Loidl, A. Broadband dielectric spectroscopy on benzophenone: alpha relaxation, beta relaxation, and mode coupling theory. *Phys. Rev. E* **77**, 031506 (2008).

[8] Ito, N., Duvvuri, K., Matyushov, D. V. & Richert, R. Solvent response and dielectric relaxation in supercooled butyronitrile. *J. Chem. Phys.* **125**, 024504 (2006).

[9] Paluch, M., Ngai, K. L. & Hensel-Bielowka, S. Pressure and temperature dependence of the relaxation dynamics of cresolphthalein-dimethylether: Evidence of contributions from thermodynamics and molecular interactions. *J. Chem. Phys.* **114**, 10872-10883 (2001).

[10] Ito, N., Huang, W. & Richert, R. Dynamics of a supercooled ionic liquid studied by optical and

dielectric spectroscopy. *J. Phys. Chem. B* **110**, 4371-4377 (2006).

[11] Olsen, N. B., Christensen, T. & Dyre, J. C. Time-temperature superposition in viscous liquids. *Phys. Rev. Lett.* **86**, 1271-1274 (2001).

[12] Diaz-Calleja, R., Garcia-Bernabe, A., Sanchis, M. J. & del Castillo, L. F. Interconversion of mechanical and dielectrical relaxation measurements for dicyclohexylmethyl-2-methyl succinate. *Phys. Rev. E* **72**, 051505 (2005).

[13] Mierzwa, M., Pawlus, S., Paluch, M., Kaminska, E. & Ngai, K. L. Correlation between primary and secondary Johari-Goldstein relaxations in supercooled liquids: Invariance to changes in thermodynamic conditions. *J. Chem. Phys.* **128**, 044512 (2008).

[14] Blochowicz, T., Gainaru, C., Medick, P., Tschirwitz, C. & Rossler, E. A. The dynamic susceptibility in glass forming molecular liquids: The search for universal relaxation patterns II. *J. Chem. Phys.* **124**, 134503 (2006).

[15] Richert, R. On the dielectric susceptibility spectra of supercooled o-terphenyl. *J. Chem. Phys.* **123**, 154502 (2005).

[16] M. Paluch *et al.*, unpublished measurements.

[17] Hensel-Bielowka, S. & Paluch, M. Origin of the high-frequency contributions to the dielectric loss in supercooled liquids. *Phys. Rev. Lett.* **89**, 025704 (2002).

[18] Gainaru, C., Rivera, A., Putselyk, S., Eska, G. & Rössler, E. A. Low-temperature dielectric relaxation of molecular glasses: Crossover from the nearly constant loss to the tunneling regime. *Phys. Rev. B* **72**, 174203 (2005).

[19] Rajian, J. R., Huang, W., Richert, R. & Quitevis, E. L. Enhanced translational diffusion of rubrene in sucrose benzoate. *J. Chem. Phys.* **124**, 014510 (2006).

[20] Richert, R., Duvvuri, K. & Duong, L.-T. Dynamics of glass-forming liquids. VII. Dielectric relaxation of supercooled tris-naphthylbenzene, squalane and decahydroisoquinoline. *J. Chem. Phys.* **118**, 1828-1836 (2003).

[21] Igarashi, B., Christensen, T., Larsen, E. H., Olsen, N. B., Pedersen, I. H., Rasmussen, T. & Dyre, J. C. A cryostat and temperature control system optimized for measuring relaxations of glass-forming liquids. *Rev. Sci. Instrum.* **79**, 045105 (2008).

[22] Igarashi, B., Christensen, T., Larsen, E. H., Olsen, N. B., Pedersen, I. H., Rasmussen, T. & Dyre, J. C. An impedance-measurement setup optimized for measuring relaxations of glass-forming liquids. *Rev. Sci. Instrum.* **79**, 045106 (2008).

Liquid	Abr.	Symbol	Temp.int (K)	Freq.int.($\log_{10}\nu$)	Index int.	Reference
1,2-propandiol (propylene-glycol)	PG	◁	180 ; 211	0.34 ; 4.51	1.08 ; 1.49	[1]
2-ethyl-hexylamine	EH	○	142 ; 166	−1.4 ; 4.72	1.45 ; 3.08	[2]
2-methyl-tetrahydrofurane	MTHF	□	91 ; 108	−2.1 ; 5.92	2.14 ; 3.89	[1]
2-phenyl-5-acetomethyl-5-ethyl-1,3-dioxocyclohexane	AFEH	▽	220 ; 240	−1.75 ; 2.91	2.65 ; 3.27	[1]
3,3,4,4-benzophenonetetracarboxylic dianhydride	BPC	◇	334 ; 362	−1.79 ; 3.11	3.36 ; 3.73	[3]
3-fluoro-aniline	FAN	▷	173 ; 198	−2.11 ; 5.36	3.52 ; 3.79	[4]
3-phenyl-1-propanol	3Ph1P	×	180 ; 200	−1.89 ; 2.38	1.84 ; 2.57	this work
3-styrene	3Sty	+	235 ; 280	−1.61 ; 5.44	2.06 ; 3.1	[5]
5-polyphenyl-ether	5-PPE	△	248 ; 264	−1.9 ; 2.32	3.77 ; 4.07	[6]
benzophenone	BePh	∗	215 ; 240	0.16 ; 5.7	3.56 ; 3.91	[7]
biphenyl-2yl-isobutylate	BP2IB	◁	210 ; 232	−1.38 ; 3.94	3.14 ; 3.37	[1]
butyronitrile	BN	○	97 ; 116	−1.85 ; 3.66	0.83 ; 1.91	[8]
cresolphthalein-dimethylether	KDE	□	315 ; 383	−2.64 ; 5.98	2.08 ; 3.14	[9]
decahydroisoquinoline	DHIQ	▽	180 ; 192	−1.89 ; 3.78	3.83 ; 7.27	[6]
di-iso-butyl-phtalate	dIBP	◇	195 ; 221	−1.44 ; 4.02	1.72 ; 3.08	[1]
dibutyl-ammonium-formide	dBAF	▷	156 ; 200	−1.57 ; 5.63	0.91 ; 2.73	[10]
dibutyl-phtalate	DBP	×	180 ; 224	−1.67 ; 5.93	1.05 ; 3.18	[11]
dicyclohexyl-methyl-2-methylsuccinate	DCHMMS	+	220 ; 240	−2.13 ; 2.85	2.93 ; 3.54	[12]
diethyl-phtalate	DEP	△	186 ; 222	−1.51 ; 5.81	2.09 ; 3.24	this work
diglycidyl-ether-of-bisphenol A (epoxy-resin)	ER	∗	259 ; 291	−0.83 ; 5.94	2.79 ; 5.64	[13]
dimethyl-phtalate	DMP	◁	196 ; 220	−1.65 ; 3.87	2.48 ; 3.14	this work
dioctyl-phtalate	DOP	○	188 ; 220	−1.81 ; 3.9	1.33 ; 2.56	[1]
dipropylene-glycol	DPG	□	196 ; 240	−2.39 ; 5.13	1.34 ; 2.81	this work
dipropylene-glycol-dimethyl-e	DPGDME	▽	139 ; 155	−1.11 ; 4.12	2.26 ; 3.38	[1]

ther						
glycerol	Gly	◇	192 ; 252	-1.89 ; 5.85	1.1 ; 1.92	[11]
isopropyl-benzene	Cum	▷	130 ; 149	-1.86 ; 4.73	2.52 ; 3.68	[1]
m-tricresyl-phosphate	mTCP	×	209 ; 233	-1.58 ; 3.49	2.22 ; 3.11	[14]
m-toluene	mTol	+	184 ; 200	-2.77 ; 2.76	3.55 ; 4	this work
o-terphenyl	OTP	△	252 ; 282	-0.24 ; 5.71	2.94 ; 4.3	[15]
perhydroisoquinoline	PHIQ	∗	182 ; 206	-1.38 ; 5.96	2.57 ; 7.2	[16]
phenolphthalein-dimethylether	PDE	◁	299 ; 333	-1.47 ; 4.51	2.94 ; 3.81	[17]
phenyl-salicylate (salol)	Sal	○	223 ; 253	-1.38 ; 5.6	3.63 ; 4.04	[18]
polypropylene-glycol	PPG	□	200 ; 240	-1.51 ; 5.46	1.48 ; 3.36	[11]
pyridine-toluene	PT	▽	125 ; 131	-2.85 ; 1.63	5.13 ; 6.16	[11]
squalane	Sqa	◇	170 ; 210	-1.92 ; 5.05	0.36 ; 3.42	[6]
sucrose-benzonate	SB	▷	341 ; 400	-1.14 ; 5.54	1.5 ; 4.09	[19]
tetraphenyl-tetramethyl-trisi loxane	DC704	×	211 ; 240	-2.62 ; 5	3.73 ; 4.06	[6]
tricresyl-phosphate	TCP	+	216 ; 248	-0.69 ; 4.95	1.9 ; 3.06	this work
triphenyl-ethylene	TPE	△	254 ; 274	-1.47 ; 3.13	3.49 ; 3.91	[6]
tripropylene-glycol	TPG	∗	192 ; 228	-2.01 ; 4.78	1.44 ; 3.21	[11]
trisnaphthylbenzene	tNB	◁	357 ; 405	0.09 ; 5.86	2.7 ; 3.49	[20]
xylitol	Xyl	○	254 ; 284	-0.59 ; 4.66	2.27 ; 3.99	[1]